

Investigation of slow dynamic processes in amorphous and crystalline polymers by 1D-MAS NMR spectroscopy

Dissertation

zur Erlangung des akademischen Grades
doktor rerum naturalium (Dr. rer. nat.)

vorgelegt der

Mathematisch-Naturwissenschaftlich-Technischen Fakultät
(mathematisch-naturwissenschaftlicher Bereich)
der Martin-Luther-Universität Halle-Wittenberg

von Herrn Ovidiu F. Pascui
geb. am: 29.8.1976 in Oradea, Rumänien

Gutachter:

1. Priv.-Doz. Dr. D. Reichert
2. Prof. T. J. Bonagamba
3. Prof. D. E. Demco

Halle(Saale)

den 5 Februar 2003

urn:nbn:de:gbv:3-000004823

[<http://nbn-resolving.de/urn/resolver.pl?urn=nbn%3Ade%3Agbv%3A3-000004823>]

Summary:

page

<u>Introduction</u>	1
1. <u>Short review of other methods than NMR, used to investigate polymer dynamics.</u>	3
2. <u>2D and 1D-MAS exchange experiments in NMR spectroscopy</u>	9
2.1 A simple NMR-MAS experiment	9
2.2 2D-MAS NMR exchange	15
2.3 1D-MAS NMR exchange	22
2.3.1 ODESSA	24
2.3.2 trODESSA	28
2.3.3 PASS, PASS+trODESSA (PATROS)	33
2.3.4 CODEX	39
3. <u>Data processing and spin diffusion correction</u>	46
3.1 Spin diffusion in exchange experiments	46
3.2 Kinetic parameters. Spin diffusion correction. Data normalization	48
4. <u>Investigations of molecular dynamics using 1D-MAS NMR methods</u>	59
4.1 Investigation of molecular exchange in poly-n-alkyl methacrylates	59
4.1.1 Exchange in PnBMA	60
4.1.2 Investigation of exchange processes in PnHMA	69
4.2 Investigation of exchange processes in semicrystalline polymers	78
<u>Conclusions</u>	92
<u>Reference</u>	96
<u>Appendix A</u>	100
<u>Appendix B</u>	101
<u>Appendix C</u>	102

Introduction

The investigation of structure (orientations, molecular distances) and dynamics (molecular reorientations) represents the basis for the understanding of molecular processes and their correlation with the macroscopic properties in solids and polymers. While in the past, the structure of interesting substances like polymers, was the aim, nowadays, the dynamics plays a more important role. In the last decades, a fast development of the NMR (Nuclear Magnetic Resonance) techniques has produced new methods useful for the investigation of polymer behavior in the glass transition region. The fact that the NMR methods use to probe the nuclear moment of the nuclei, makes the applicability of this type of investigation possible for each nucleus with a nuclear spin different from zero.

The investigation of slow molecular dynamics in several polymers (amorphous and semicrystalline) by 1D-MAS exchange NMR methods, was the aim of this work.

Nowadays, when NMR spectrometers with MAS (Magic Angle Spinning) capable probes are not a rarity and after 2D-NMR exchange techniques proved their power in the characterization of the dynamics in various substances [KSR94], new methods based on 1D-MAS exchange experiments are developed and used to gain a detailed overview of the slow dynamics in polymers, in a shorter experimental time. The advantage of the NMR methods, especially 1D-MAS exchange methods, over those involving other techniques (see next chapter), is that we can assign specific parts of the polymers (side or main chain, etc.) to specific processes in the glass transition region. Like any experimental method, also the NMR techniques have their advantages and disadvantages. One of the disadvantages comes from the fact that they are useful only in a limited frequency range, which limits the accessible experimental window to, sometimes, temperatures for which no interesting dynamics occurs. Another disadvantage would be the fact that NMR exchange experiments are usually very time consuming; for example, to obtain a detailed Arrhenius diagram of a polymer several hundreds of hours of measurement are necessary. To overcome these problems, several 1D-MAS exchange methods were proposed, their aim being to provide the same information as the 2D-MAS experiments but in a shorter experimental time and with a better resolution.

In this work, new 1D-MAS exchange experiments are described together with the results obtained, for polymers, ranging from amorphous to semicrystalline polymers. For the relevance of the results obtained with these methods, the experimental data were always correlated with those obtained from other experimental techniques like dielectric spectroscopy, mechanical relaxation, DSC, HCS, etc. Despite the fact that usually a good correlation of the experimental results from different investigation methods is hard to achieve, this work proves that the 1D-MAS NMR exchange

techniques provide reliable results, which are in good agreement with those obtained from other techniques.

In the chapters presenting the theory behind the NMR methods used, a detailed description of the NMR-MAS exchange methods like 2D-MAS, trODESSA, CODEX and PATROS is provided. All these methods detect the molecular dynamics by observing the changes in the chemical shift anisotropy CSA (see chapter II). A comparison between different experiments is available, so that the reader could easily distinguish between the advantages and disadvantages of each particular method. Special attention is attributed to the proper data processing routine of the acquired experimental data. One of the chapters shows that an improper processing routine, which would not consider the correction of the acquired exchange decays by spin diffusion and T_1 relaxation, would lead to erroneous results. Also a proper conversion between the correlation times obtained from NMR MAS exchange experiments to those obtained from other investigation methods is necessary in order to allow an exact comparison between different experimental methods. Experimental results presented in fourth chapter, offer a detailed description of the experimental data obtained from NMR methods for different polymers (PnBMA - chapter 4.1.1, PnHMA - chapter 4.1.2 and i-P4M1P -chapter 4.2) and their comparison with similar data available in the literature from other experimental techniques. The conclusions resulted from these extensive investigations are given in the last chapter.

CHAPTER I

Short review of experimental methods used to investigate the polymer dynamics

The knowledge of the dynamic behavior of polymers in the glass transition region, especially the characterization of the slow dynamic processes with correlation times τ_c in the milliseconds range, plays an important role for understanding their macroscopic properties. In a general way, the glass transition is the transition of an undercooled liquid from the liquid, viscoelastic phase to the amorphous, solid state. This transition happens on a temperature interval of several degrees around the assigned glass transition temperature T_g . The glass transition is not specific only for polymers; glassy states were obtained also in other substances (ice, water, metallic glasses, silicate glasses, salt melts, polar liquids, liquid and plastic crystals) by quenching (fast cooling) [Donth92]. In glass-forming substances the characteristic length of the interest to structure and dynamics are of order of one nanometer [Donth92]. The different scales of molecular motion are put in order by a general scaling principle: the larger the typical length, the larger the typical relaxation time. Usually the thermal glass transition is thermoreversible, but that does not mean that the process is an reversible cycle. Any cycle with freezing-in parts is seen like an irreversible cycle.

The experimental basis for polymer relaxation was found by Tobolski and Ferry in the 40's and 50's; the results were crowned by the scaled representation with the aid of the famous WLF equation (**W**illiams, **L**andel, **F**erry) [Williams66], a relation in the $\ln\omega-T$ or $\ln\tau-T$ diagram. WLF means a set of curves that guides the frequencies of maxima, inflection points, etc. of different activities in their dependence on temperature [Donth92].

The reason for the universality of the leading traces in the $\ln\omega-T$ diagram and their connection to the numerous activities led by them are the central problems of the dynamic glass transition. The behavior of polymer chains in the glass transition region are tempted to be explained with frequent terms like activation energy, Rouse (or normal) modes and reptation [Doi88].

The barrier model (or Arrhenius mechanism) is based on the idea of two positions (energy minima) separated by a barrier of height ϵ_A (*activation energy*) it is used to describe the linear behavior of the relaxation β -process shown in figure 1. A particle in one of the valleys (energy minima) is described by a potential $\phi(x)$, where the x coordinate could be an angle describing a conformation change of the polymer chain. Considering a Boltzmann distribution of energies, the ratio success/attempt to overcome the barrier is described by such an equation:

$$\ln v = \ln v_0 - \frac{\epsilon_A}{kT} \quad (1.1)$$

where v, v_0 denotes an success respectively attempt of the particle to overcome the barrier. A process which obeys the equation (1.1) is called an Arrhenius mechanism. In the Arrhenius diagram this will be a straight line with the intercept v_0 for $T^{-1} = 0$ ($T = \infty$) and the slope ϵ_A/k (see fig.1, LM or β -process).

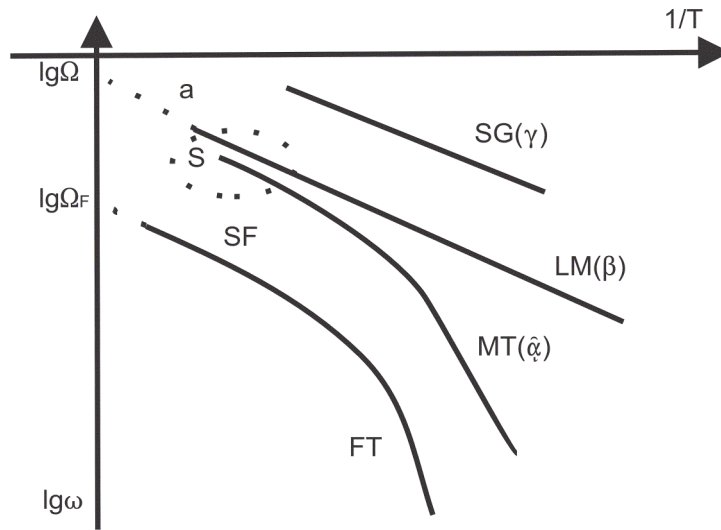


Fig.1 Arrhenius diagram of an amorphous polymer. *S* represents the splitting or crossover region, *FT* flow transition, *MT* main transition, *SG* side groups relaxations, *LM* local modes, *SF* breakdown of scaling, α, β, γ conventional labels for amorphous polymers (decreasing relaxation temperatures for a given frequency) [Donth92]

The approximate values for the activation energy are between 20 kJ and 60 kJ in polymer systems with different concentrations. For polymer solutions, the barrier height is estimated to come 50% from conformational barrier and 50% from the influence of the environment (viscosity). In polymers, the parts of the dynamics which are described by an Arrhenius mechanism are the so-called secondary relaxations **SR** (for example the motion of the side groups **SG** or the local modes **LM** of the chain itself, possibly with a mutual influence of both). The activation model is a simple model that can explain the secondary relaxations but not the so-called main transition **MT** or flow transition **FT** (figure 1). These processes are represented by a strong non-Arrhenius behavior, that may be parametrized in a good approximation by the WLF equation with asymptotic temperatures ($T_{\infty} > 0$ $T_{\infty F} > 0$, the Vogel temperatures for MT and FT). Adam and Gibbs have introduced the

concept [Adam, 1965] of cooperatively rearranging regions **CRR** for the cooperativity volume and particle number V_a, N_a . The point is, that the size of the CRR is assumed to increase with decreasing temperature and that its increase is connected to the curvature in an Arrhenius plot. Using this idea one can understand the main **MT** and flow **FT** transitions like being cooperative processes while the secondary relaxations are expected to be more or less localized processes.

At a closer inspection of the figure 1 we notice the multiplicity of the dynamic glass transition in amorphous polymers. The $\{a, \alpha\}$ trace represents the dynamic glass transition which is characterized by a non-Arrhenius behavior. It is assumed to have a fine structure with three different regions [Beiner96]. The calorimetric measurements also show an activity (an entropy change at the dynamic glass transition) being a prove of the cooperativity of the process. Usually the processes in the $\{a, \alpha\}$ trace, are described by a stretched exponential, so-called **Kohlrausch Williams Watts** (KWW) function (equation 1.2), and not by a simple Debye process ($\beta^{KWW} = 1$):

$$\Phi(t) = \exp \left[- \left(\frac{t}{\tau_0} \right)^{\beta_{KWW}} \right] \quad (1.2)$$

where the parameter $0 < \beta_{KWW} < 1$ is a non-dimensional relaxation parameter which is inversely proportional to the relaxation-time-distribution width. Typical values of β_{KWW} for the α -process are between 0.5 and 1. Smaller values of the β_{KWW} means a broader distribution of the relaxation times. Usually to characterize the detected dynamics we will use the notion of correlation time which describes the decay of the correlation functions defining the process. In some cases a mean correlation time have to is defined using:

$$\langle \tau_c \rangle = \frac{\tau_0}{\beta^{KWW}} \Gamma \left(\frac{1}{\beta^{KWW}} \right) \quad (1.2')$$

If we consider the frequency domain, another function describing the $\{a, \alpha\}$ process, is the Havriliak-Negami function:

$$\varepsilon^*(\omega) = \frac{\Delta\varepsilon}{\left[1 + \left(i\omega\tau_{HN}\right)^\beta\right]^\gamma} + \varepsilon_\infty \quad (1.3)$$

In case that $\beta = \gamma = 1$ we obtain a Debye relaxation and when $\beta < 1$ $\gamma = 1$ we are in the case of Cole-Davidson function. In the main glass transition region, the polymers obey the rules of the WLF equation:

$$\lg\left(\frac{\omega}{\omega_0}\right) = \frac{C_1^0(T-T_0)}{C_2^0 + (T-T_0)} \quad (1.4)$$

where typical values of the WLF constants for the α -process are for temperatures $T_0 = T_g$:

$$\begin{aligned} C_1^0 &= 17 \pm 3 \\ C_2^0 &= 50 \pm 25 \text{ (K)} \end{aligned} \quad (1.5)$$

A formally identical equation is used in the case of a supercooled liquid, where the temperature dependence is described by the Vogel-Tamman-Fulcher equation [Ediger96] :

$$\lg\omega = \lg\Omega - \frac{B}{T - T_\infty} \quad (1.6)$$

where the Vogel temperature T_∞ is defined like as low temperature asymptote.

The flow transition FT is separated from the main transition MT, by the rubbery *plateau zone* (the name comes from the fact that this region is common for rubbers). This process is a result of the entanglements in polymer melts with high molecular weight.

The secondary relaxation SR or in amorphous polymers β -relaxation (Johari-Goldstein process [Johari70]) is a process described by an Arrhenius activation mechanism, eq. (1.1). Secondary relaxations are not specific only for polymers, they are observed also in other glass formers like inorganic glasses or plastic crystals. Polymer relaxations which are not related to the main transition (γ, δ , etc.) are often interpreted by relatively isolated motions of the side groups or isolated molecules [Beiner01]. The spectrum of a secondary relaxation is usually broad, up to four logarithmic

decades; a large spatial variation of local environments in thermokinetic or amorphous structure must be considered to imply a large spatial variation of activation energies [Beiner99].

The S region in the figure 1 is *splitting* region or *crossover* region where one finds the minimal size of the cooperativity. It is considered that the temperature T_S where the minimal cooperativity is reached is the *splitting point* for the glass transition and local modes.

The thermal glass transition or freezing-in is considered to be the process where the modes successively become too slow for the cooling experiment. The multiplicity of the glass transition makes possible the existence of several glass temperatures: T_F the temperature for the flow transition, T_g for the main transition, T_γ , T_β , T_δ for the secondary relaxations.

The β -relaxations are considered to be local modes or shared side group motions for other polymers and the γ -relaxation is usually related to the side group motions [Beiner99]. In the homologue series of alkyl methacrylate polymers, it is shown that increasing the size of the alkyl group has an influence on the β relaxation (as we shall see in this work in the particular case of PnBMA and PnHMA an important difference exists), mainly by shifting the splitting region to lower frequency and producing the internal softening of the material.

There are several investigation methods well established in the last five decades which are used to investigate the dynamic glass transition in polymers. The dielectric spectroscopy is based on the existence of the dipole moment in polymers; fluctuations of the dipole moment due to various factors like molecular dynamics or the effect of an electric field would produce a variation of the complex dielectric function $\epsilon^*(\omega)$ which depends on the circular frequency (see also eq. (1.3)). The fact that the dielectric spectroscopy detects the molecular electric dipole moment, represents the power and at the same time the weakness of this method. In large polymers, the relaxation data obtained from dielectric spectroscopy characterize only the part of the polymer which contains the dipole moments and sometimes its vicinities. Therefore, parts of the polymers which are far from the functional groups with a dipole moment remains unexplored, and as we will observe in this work (especially amorphous polymers from the poly-acrylates family) alone the dynamics of the group containing the dipole moment is not significant for the behavior of the entire polymer in the glass transition region. The typical frequency range covered by the dielectric measurements is between $10^{11} - 10^{-5} Hz$ [Haarer95].

The DSC (*Differential Scanning Calorimetry*) is based on the material property to store energy in form of thermal motion [Munk89]. This motion is different in several substances: simple translations of molecules in gases and liquids, oscillations of the crystalline lattice, rotations of the molecules or reorientations of the segments in polymers. Every change in the state of the system is accompanied by a change in the energy which may be expressed in terms of heat capacity. The

magnitude of the heat capacity depends on the nature of molecular movement and therefore it is large when many modes are implied and small for frozen systems. Thus, heat capacity is small for glassy and crystalline polymers and changes approximately abruptly close to the glass transition temperature. Usually all phase transitions are accompanied by a change of heat with the environment. In the DSC scans, the glass transition is characterized by three more or less linear sections corresponding to glass transition, unfreezing of the segmental motion and a zone specific for rubbers. These methods are usually used to investigate the dynamic properties of the polymers in the glass transition region.

Another frequently used method is HCS (*Heat Capacity Spectroscopy*) [Schwarzl90], which allows the determination of the complex heat capacity, $c_p^* = c_p'(\omega) - ic_p''(\omega)$, dynamic glass transition α (which is the only calorimetric active process), in equilibrium [Beiner96]. HCS probes the time scale and intensity of internal entropy fluctuations of a sample by means of the entropy response to an external temperature perturbation, namely, $c_p^*(\omega)$ is the equilibrium entropy compliance [Beiner96]. Above T_g in HCS experiments, the frequency dependence of the complex product $(\rho kc_p(\omega))^*$ between mass density (ρ), heat conductivity (k) and heat capacity ($c_p(\omega)$) is measured at equilibrium. The dynamic glass transition shows up in the isotherm plots of the real part $\rho kc_p'$ as a characteristic step to whom in the frequency dependence of the imaginary part $\rho kc_p''$ a loss peak is corresponding. All isothermal representations can be approximated with a Havriliak-Negami function (eq.(1.3)). In the scheme of linear response, the experimental value ρkc_p^* is proportional to the disturbance temperature amplitude and it is interpreted as a susceptibility: c_p^* is an entropy compliance related to the natural entropy fluctuation by the FDT [Beiner96]. Experimental results from the above reference have shown that the dynamic entropy compliance c_p^* behaves similarly to the dielectric compliance ϵ^* at the dynamic glass transition. The techniques described above usually provides informations about the time scale of the relaxation processes or their type. In order to obtain informations about the typical length of structures present, techniques based on scattering of light, neutrons or X-rays are used.

CHAPTER II

In this chapter we shall introduce the basic notions of NMR exchange experiments, which were used to investigate the molecular dynamics in different polymers. First we present a simple NMR experiment performed under MAS conditions (**M**agic **A**ngle **S**pinning) and then we introduce some advanced NMR-exchange methods with which the reader should be familiar before looking at the experimental results. The **N**uclear **M**agnetic **R**esonance (NMR), discovered in the 40's by Bloch and Purcell, is based on the interaction between the nuclear spin of a nucleus placed in an external magnetic field with an applied *radio-frequency* (rf) field. The use of the NMR techniques is restricted to nuclei with a nuclear spin $I \neq 0$. The so called gyromagnetic ratio γ defines the magnetic moment of a spin, $\mu_i = \gamma_i I$, and is specific to each nucleus. Different isotopes of a some species of nucleus have different abundances, making it an important criteria to choose them for certain investigations. The ^1H is the most abundant specie with a nuclear spin different from zero and therefore ^1H -NMR experiments are very common. The fact that usually all the organic substances contains several C atoms correlated with the abundance of the ^{13}C isotope makes the ^{13}C a good candidate for NMR investigations in different organic substances. Under the influence of the external magnetic field, the magnetization of each type of nuclei will precess with the Larmor frequency (or resonance frequency) $\omega_0 = \gamma B_0$. It is clear that each type of nuclei will have it's own resonance frequency, making the selective excitation of the desired species possible.

Considering the lower abundance of the ^{13}C as compared with that of the protons, cross-polarization techniques were used in most of the experiments.

2.1. A simple NMR-MAS experiment

Let's consider a simple NMR experiment which usually consists of an excitation pulse, in this case an $\frac{\pi}{2}$ pulse. After applying this excitation, the magnetization of the nuclei in the sample will start to evolve producing the so called **F**ree **I**nduction **D**ecay (FID). The FID can be viewed like an amortized oscillation in which the magnetization decays under the influence of interactions between

the neighboring nuclei or with the entire network considered. In this case we can write the function which describe the time evolution of the signal like:

$$FID(t) = e^{-\frac{t}{T_2}} e^{i\omega t} \quad (2.1)$$

where T_2 describes several effects. One of them is the spin-spin relaxation which occurs because of the loss of coherence during the precession due to interactions between the neighboring spins. By applying a Fourier transformation (FT) to equation (2.1) we obtain a spectrum which contains an absorption part $A(\omega)$ and a dispersion part $D(\omega)$, the whole signal being:

$$f(t) = A(\omega) + iD(\omega) \quad (2.2)$$

In liquid-state NMR, the result of such a simple excitation pulse is a spectrum in which each line corresponds to a chemical identity, namely the chemical shift isotropy (CSI) σ_{iso} . In solids, because of the strong interactions between the spins and because of the anisotropic interactions, the spectra are characterized by the presence of broad lines (fig. 2.1) which in the case of a substance with many non-equivalent nuclei produces an overlapping of the lines to such an extent that no reliable information can be extracted anymore. In this case the precession frequency of the spins can be written [KSR94] as:

$$\omega(\theta, \phi) = \omega_{iso} + \delta \frac{1}{2} (3\cos^2\theta - 1 - \eta \sin^2\theta \cos(2\phi)) \quad (2.3)$$

where η is the asymmetry parameter, δ is the anisotropy parameter and θ, ϕ are the polar and also Euler angles which describe the transformation of the principal axis system (PAS) into the laboratory frame. The third Euler angle, corresponding to a rotation around $\overline{B_0}$ axis, is not relevant to the frequency, since the secular interactions are invariant under a rotation around $\overline{B_0}$ [KSR94]. The anisotropy and asymmetry parameters from eq. (2.3) are given in the following equations, where σ_{ij} are the elements of the chemical shift anisotropy tensor (CSA) in principal axis system (PAS):

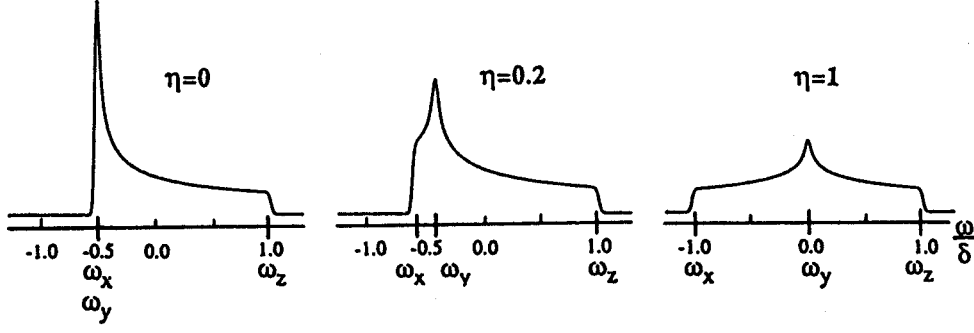


Fig.2.1 Examples of powder static spectra for different asymmetry parameters [KSR94]

$$\eta := \frac{\sigma_y - \sigma_x}{\sigma_z} = \frac{\omega_y - \omega_x}{\omega_z} \quad \delta := \omega_z$$

$$\sigma_{iso} = \frac{1}{3}(\sigma_{xx}^{PAS} + \sigma_{yy}^{PAS} + \sigma_{zz}^{PAS})$$

$$\sigma_i := \sigma_{ii}^{PAS} - \sigma_{iso} \quad \omega_i := -\omega_0 \sigma_i \quad (2.4)$$

The term $(3\cos^2\theta - 1)$ from eq. (2.3) represents the second Legendre polynomial and here one can act in order to eliminate the broadening effect in NMR solids spectra. The solution to overcome this impediment in solid-state NMR is to find a method which by mean of a similar effect to the Brownian motion in liquids to average out the second Legendre polynomial. Such a method is the Magic Angle Spinning (MAS) in which the probe tilted to an angle (called ‘‘magic angle’’) for which the term considered above become irrelevant, is spun around this axis, and it is this rotation that makes the Hamiltonian of the system time-dependent producing the averaging of the interactions between the spins. Under MAS conditions the FID changes from form described in eq. (2.1) to [Mehring76]:

$$\begin{aligned} FID(t) &= e^{-\frac{t}{T_2}} e^{i\omega_0 \sigma_{iso} t} e^{i \int_0^t \omega(\tau) d\tau} \\ &= e^{-\frac{t}{T_2}} e^{i\omega_0 \sigma_{iso} t} e^{i\Phi(t)} e^{-i\Phi(0)} \\ &= e^{-\frac{t}{T_2}} e^{i\omega_0 \sigma_{iso} t} f(\omega_R t + \gamma) f^*(\gamma) \end{aligned} \quad (2.5)$$

The time-dependent resonance frequency becomes then [Mehring76; Luz92]:

$$\omega(t) = \omega_0 \sigma_{iso} + C_1 \cos(\omega_R t + \gamma) + S_1 \sin(\omega_R t + \gamma) + C_2 \cos(2\omega_R t + 2\gamma) + S_2 \sin(2\omega_R t + 2\gamma) \quad (2.6)$$

where the terms C_1 , C_2 , S_1 , S_2 are given in eq. (2.7); α , β , γ are the Euler angles describing the orientation of the molecular system axis relative to the MAS rotor system (fig. 2.2) :

$$\begin{aligned}
 C_1 &= \frac{\sqrt{2}}{3} \left\{ -\frac{3}{2}(\sigma_{33} - \sigma_{\text{iso}}) \sin 2\beta - \left[\frac{1}{2}(\sigma_{22} - \sigma_{11}) \cos 2\alpha - \sigma_{12} \sin 2\alpha \right] \sin 2\beta + 2(\sigma_{13} \cos \alpha + \sigma_{23} \sin \alpha) \cos 2\beta \right\} \\
 S_1 &= \frac{2\sqrt{2}}{3} \left\{ \left[\frac{1}{2}(\sigma_{22} - \sigma_{11}) \sin 2\alpha + \sigma_{12} \cos 2\alpha \right] \sin \beta - (\sigma_{13} \sin \alpha - \sigma_{23} \cos \alpha) \cos \beta \right\} \\
 C_2 &= \frac{1}{3} \left\{ \frac{3}{2}(\sigma_{33} - \sigma_{\text{iso}}) \sin^2 \beta - \frac{1}{2} \left[\frac{1}{2}(\sigma_{22} - \sigma_{11}) \cos 2\alpha - \sigma_{12} \sin 2\alpha \right] (\cos 2\beta + 3) - (\sigma_{13} \cos \alpha + \sigma_{23} \sin \alpha) \sin 2\beta \right\} \\
 S_2 &= \frac{2}{3} \left\{ \left[\frac{1}{2}(\sigma_{22} - \sigma_{11}) \sin 2\alpha + \sigma_{12} \cos 2\alpha \right] \cos \beta + (\sigma_{13} \sin \alpha - \sigma_{23} \cos \alpha) \sin \beta \right\}
 \end{aligned}
 \tag{2.7}$$

The representation of the NMR signal with the help of f -function (2.5) was first introduced by Mehring [Mehring76] and it has proved to be valuable in the theoretical description of MAS exchange experiments in the $\tau_c \gg T_2$ regime. In the argument of the f -function only the angle γ and the dependence of the spinning rate $\omega_R t$ are present. In the case of an isotropic powder, the averaging over the Euler angles (α, β, γ) is still necessary.

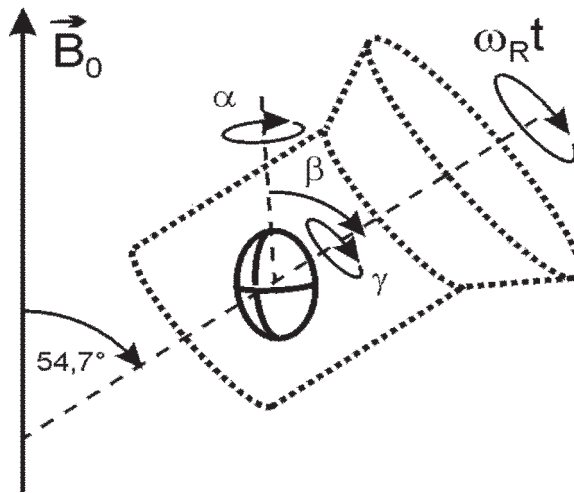


Fig.2.2 Relation between external magnetic field, MAS rotor and CSA tensors

From equations (2.5, 2.6, 2.7) it is obvious that the f -function is periodic (dependence on the MAS frequency) and complex exponential functions [idem]:

$$\begin{aligned} f(2\pi N + \xi) &= f(\xi) \\ f(\xi)f^*(\xi) &= 1 \end{aligned} \quad (2.8)$$

Considering also the properties of a δ -function:

$$\begin{aligned} f(\xi) &= \frac{1}{2\pi} \int_0^{2\pi} d\theta \delta(\theta - \xi) f(\theta) \\ \frac{1}{2\pi} \int_0^{2\pi} d\theta \delta(\theta - \xi) &= 1 \\ \delta(\theta - \xi) &= \sum_N e^{-iN(\theta - \xi)} \end{aligned} \quad (2.9)$$

then we can write the signal recorded after a simple MAS experiment like:

$$\begin{aligned} M^{MAS}(t) &= e^{-\frac{t}{T_2}} e^{i\omega_0 \sigma_{iso} t} e^{i \int_0^t \omega(\tau) d\tau} \cong e^{-\frac{t}{T_2}} e^{i\omega_0 \sigma_{iso} t} f^*(\gamma) f(\omega_R t + \gamma) \\ &= e^{-\frac{t}{T_2}} e^{i\omega_0 \sigma_{iso} t} f^*(\gamma) \int d\theta \delta(\theta - \omega_R t - \gamma) f(\theta) \\ &= e^{-\frac{t}{T_2}} e^{i\omega_0 \sigma_{iso} t} f^*(\gamma) \int d\theta \sum_M e^{-iM\theta} e^{iM\omega_R t} e^{iM\gamma} f(\theta) \end{aligned} \quad (2.10)$$

The term 2π from eq. (2.9) was dropped in eq. (2.10). In order to obtain the final form of the NMR-MAS signal from all the crystallites from the rotor we have to perform the powder averaging, which in a first step is an integration over the γ angle. From the mathematical point of view, this is identic to the integration over the θ angle from the f -functions, which here has no physical relevance.

$$\begin{aligned}
\frac{d\gamma}{dt} \rightarrow M^{MAS}(t) &= e^{-\frac{t}{T_2}} e^{i\omega_0\sigma_{iso}t} \sum_M e^{iM\omega_R t} \int d\gamma e^{iM\gamma} f^*(\gamma) \int d\theta e^{-iM\theta} f(\theta) \\
&= e^{-\frac{t}{T_2}} e^{i\omega_0\sigma_{iso}t} \sum_M e^{iM\omega_R t} F_M F_M^* \\
&= e^{-\frac{t}{T_2}} e^{i\omega_0\sigma_{iso}t} \sum_M e^{iM\omega_R t} I_M^{MAS}
\end{aligned} \tag{2.11}$$

For an exact form of the signal (especially when it comes to simulate the intensities of the lines from a spectrum) we have to perform also the averaging over the other angles: α, β , but for the qualitative discussion this plays no role. As we mentioned before, by spinning the sample at the magic angle, we introduce a time-dependence of system's Hamiltonian, which will result in a periodicity of the signal recorded. Because the signal eq. (2.11) is periodic with $t_R = \frac{2\pi}{\omega_R}$, according to the harmonic time dependences in equation (2.6), intensity can only appear at ω_R and its harmonics $N\omega_R$ (referenced to the isotropic resonance frequency) [KSR94]. The coefficients of $I_M^{MAS}(\alpha, \beta, \gamma)$ are usually complex, and rotor-synchronized spectra of single crystals can, therefore, contain negative and dispersive sidebands. In the above phrase was mentioned the existence of the rotor-synchronized experiments. These are experiments where the delays in pulse sequence are an integer number of rotation period or they deviate from that value by definite values. For powder samples, equation (2.11) shows that the spinning sidebands (ssb) are all real and positive like one can see in figure 2.3. That means that the MAS spectrum of a powder sample can be phase corrected until we obtain an absorption spectrum, in this case $I_M^{MAS}(\alpha, \beta, \gamma)$ being a real number.

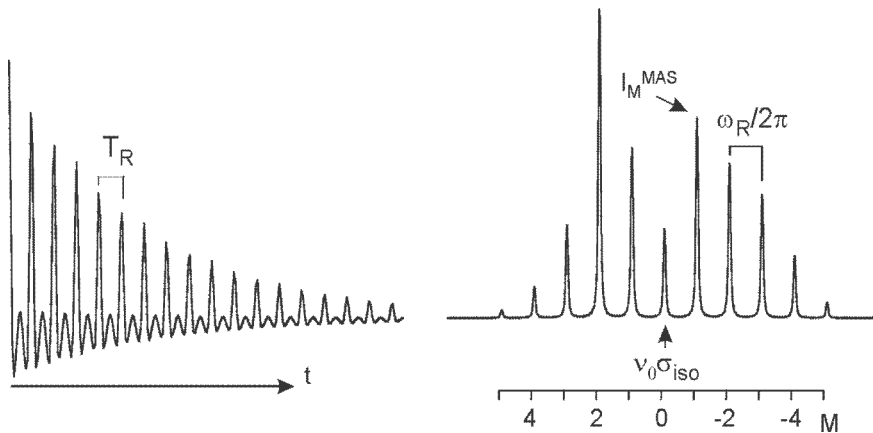


Fig.2.3 Representation of a FID (left) and MAS-spectrum (right) with ssb's

At a closer inspection of figure 2.3 (right part) we notice the presence of spinning sidebands (ssb), which are the distinctive mark of an NMR-MAS spectrum. Following the application of a $\frac{\pi}{2}$ pulse in a MAS experiment the spin system evolves under the influence of MAS Hamiltonian. When the spin rate is smaller than the width of the CSA ($\omega_R < \Delta\sigma$), the local field experienced by each spin packet changes due to mechanical rotation and the different spin packets dephase quickly, leading to a rapid decrease of FID. But because the local field experienced by a certain spin does not fluctuate (as it would under the influence of dipolar homonuclear coupling [Raleigh88]), the spins rephase at the end of each rotor period and a rotational echo is produced. The decay envelope of the entire echo train is related to the linewidth of each spinning sideband, while the shape of the rotational echoes govern the envelope of the sidebands intensities. The sidebands intensities contain information on the anisotropic chemical shift (CSA) and the line width of ssb is proportional with $\frac{1}{\pi T_2}$, the effects described by the T_2 -relaxation being responsible for the loss of coherence during the precession of the magnetization. For isotropic samples ('powders'), the spectra can be characterized by three parameters: the isotropic chemical shift σ_{iso} , which is well known from the position of the central band, the anisotropy parameter δ , and the asymmetry parameter η . To determine the last two parameters, specific methods are needed; one of the methods is a graphical one [Herzfeld80] and others are based on computer simulations and iterative fittings. Sometimes, when we deal with substances with many chemical shift isotropies, the presence of ssb can disturb and different techniques may be applied to remove the ssb. A trivial technique is based on the fact that the signal can be improved by spinning at higher spin rates $\omega_R \gg \Delta\sigma$ when all the spinning sidebands of order $N \neq 0$ disappear. In the following paragraphs we shall use the term I_M^{MAS} to describe the intensity of a 1D-MAS experiment [Herzfeld80].

2.2 2D-MAS exchange

Molecular dynamics represents an important aspect of solid polymers which influences many macroscopic materials properties and is the aim of application of NMR methods in polymers investigations. Multidimensional exchange NMR can be applied to characterize molecular details of the dynamical ($\alpha, \beta, \gamma, \dots$) processes when the correlation times range between $10^{-3} \div 10^2$ seconds [KSR94].

The basic principle of exchange NMR [Jeener79] is the measurement of the NMR frequency of one and the same molecular segment at two different times (see fig. 2.4) and the detection of slow dynamics through a change in NMR frequency.

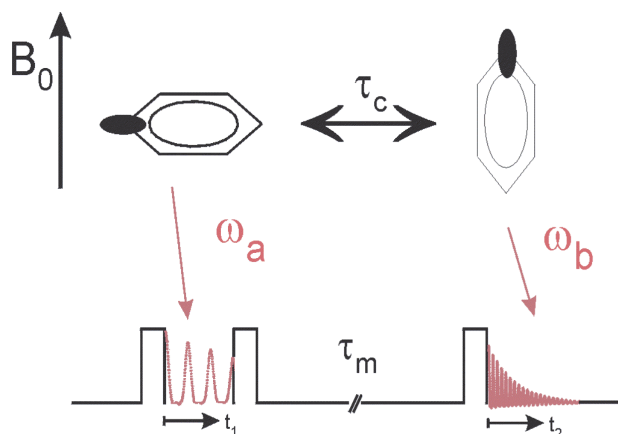


Fig.2.4. Schematic representation of an NMR-exchange experiment.

The change in the orientation of the molecular segment produces a modification in the NMR frequency which can be recorded at the end of the experiment.

In the general context of exchange NMR spectroscopy, the dynamics can be understood beside a change in the molecular orientation (only the CSA is changing), also like an chemical exchange (both CSI and CSA are changing), spin diffusion (or 'spin dynamics'). In this work we shall refer to the exchange in the sense of molecular reorientation of segments and in some particular cases, which will be discussed further in more detail, like a spin diffusion.

We shall return to figure 2.4 and mention that in case that no reorientation of the molecular segments occurs, then there will be no change in the NMR frequency and so the recorded spectrum will show no dynamics. Usually the exchange experiment is viewed like an 2D-MAS experiment and because of this, we shall try first to make a short review of this type of experiment to a better understanding of the methods further described in this chapter.

The schematic representation of a 2D-MAS exchange experiment is given in figure 2.5, all the pulses represents the pulses applied on the ^{13}C channel. On the ^1H channel will be applied a $\pi/2$ pulse, the cross-polarization pulse, [Pines72; Pines73] and the decoupling irradiation which must be turned off during the mixing time period. For a better understanding of the resulting signal we shall treat the effect of such pulse sequence using the f -functions formalism [Mehring76], briefly described in the first paragraph. Considering the moment immediately after the CP (cross-polarization) pulse, the magnetization is transferred from protons to the carbons in the xy -plane and

during the first evolution time t_1 it will precess with a certain resonance frequency. During the mixing time period τ_m , which can vary from several microseconds up to tens of seconds, some parts of the molecule can change their orientations such that after the last pulse in the detection period t_2 we shall detect a resonance frequency determined by the orientation at that time.

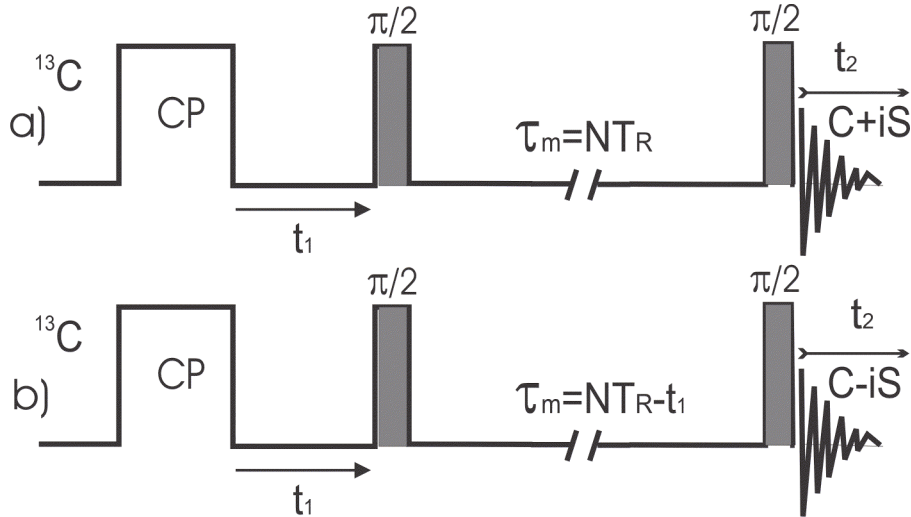


Fig.2.5. Representation of a 2D-MAS experiment

a) rotor-synchronized experiment

b) "time-reversed" experiment

Here we have to point out that the mixing time periods must be synchronized with the MAS rotation (see previous subchapter) such that the eventual change in the frequency comes only from the change in the orientation of the molecular segment and not from the different positions of the MAS rotor (sample) during the pulse sequence. During the phase cycle used to avoid the artifacts, the phase of the two 90° pulses is chosen such that different components of the signal, real part - cos (C) or imaginary part - sine (S) can be acquired. This, together with the phase of the receiver allows us to record different combinations of the magnetization components such anti-echo (C+iS) or echo (C-iS).

a) Considering first type of experiments in figure (2.5-a) by recording the C+iS combination of data sets we obtain [Hagemeyer89]:

$$M^{2D/RS,ij}(t_1, t_2) = e^{-\frac{t_1+t_2}{T_2}} \left[e^{i\omega_0 \sigma_{iso}^j t_1} f^{*j}(\gamma) f^j(\omega_R t_1 + \gamma) \right] \times \left[e^{i\omega_0 \sigma_{iso}^i t_2} f^{*i}(\omega_R t_1 + \omega_R \tau_m + \gamma) f^i(\omega_R t_1 + \omega_R \tau_m + \omega_R t_2 + \gamma) \right] \quad (2.12)$$

where (\times) marks the separation between the signal before and after the mixing time and i, j describe the system before and after the mixing time. The first term in eq. (2.12) represents the loss of signal due to spin-spin relaxation during the evolution and detection period, then we have the signal before and after the mixing time. Considering the fact that the mixing time is rotor-synchronized and the expansion in Fourier series we obtain from eq. (2.12):

$$\begin{aligned}
M^{2D/RS,ij}(t_1, t_2) &\xrightarrow{RS: \omega_R \tau_m = 2\pi N} \\
&= e^{-\frac{t_1+t_2}{T_2}} e^{i\omega_0 \sigma_{iso}^j t_1} f^{*j}(\gamma) f^j(\omega_R t_1 + \gamma) \times e^{i\omega_0 \sigma_{iso}^i t_2} f^{*i}(\omega_R t_1 + \gamma) f^i(\omega_R t_1 + \omega_R t_2 + \gamma) \\
&= e^{-\frac{t_1+t_2}{T_2}} e^{i\omega_0 \sigma_{iso}^j t_1} e^{i\omega_0 \sigma_{iso}^i t_2} f^{*j}(\gamma) \int d\theta \delta(\theta - \omega_R t_1 - \gamma) f^j(\theta) f^{*i}(\theta) f^i(\theta + \omega_R t_2) \\
&= e^{-\frac{t_1+t_2}{T_2}} e^{i\omega_0 \sigma_{iso}^j t_1} e^{i\omega_0 \sigma_{iso}^i t_2} f^{*j}(\gamma) \int d\theta \delta(\theta - \omega_R t_1 - \gamma) f^j(\theta) f^{*i}(\theta) \int d\phi \delta(\phi - \theta - \omega_R t_2) f^i(\phi) \\
&= e^{-\frac{t_1+t_2}{T_2}} e^{i\omega_0 \sigma_{iso}^j t_1} e^{i\omega_0 \sigma_{iso}^i t_2} f^{*j}(\gamma) \int d\theta \sum_M e^{-iM\theta} e^{iM\omega_R t_1} e^{iM\gamma} f^j(\theta) f^{*i}(\theta) \int d\phi \sum_N e^{-iN\phi} e^{iN\theta} e^{iN\omega_R t_2} f^i(\phi) \quad (2.13)
\end{aligned}$$

which by integrating over the angle γ (powder averaging) becomes:

$$\begin{aligned}
M^{2D/RS,ij}(t_1, t_2) &= e^{-\frac{t_1+t_2}{T_2}} e^{i\omega_0 \sigma_{iso}^j t_1} e^{i\omega_0 \sigma_{iso}^i t_2} \sum_{M,N} e^{iM\omega_R t_1} e^{iN\omega_R t_2} \int d\gamma e^{iM\gamma} f^{*j}(\gamma) \int d\theta e^{-i(M-N)\theta} f^j(\theta) f^{*i}(\theta) \int d\phi e^{-iN\phi} f^i(\phi) \\
&= e^{-\frac{t_1+t_2}{T_2}} e^{i\omega_0 \sigma_{iso}^j t_1} e^{i\omega_0 \sigma_{iso}^i t_2} \sum_{M,N} e^{iM\omega_R t_1} e^{iN\omega_R t_2} F_M^j F_{M-N}^{ij} F_N^{*i} \quad (2.14)
\end{aligned}$$

A 2D-MAS exchange spectrum consist of 2D-NMR lines positioned in the intersection points of the chemical shift anisotropies and several multiples of MAS frequency in both dimensions. It can be shown that the spectrum of a powder sample can be phased to pure absorption, that means the lines intensities are real [Hagemayer89], The question: what is in fact the effect of the exchange process on the lines intensities and what is happening when no exchange occurs, arise. Considering the latter case, no exchange occurs during the mixing time ($i = j$), it can be shown that [idem] :

$$\begin{aligned}
&\xrightarrow{i=j} F_{M-N}^{ij} = \int d\theta e^{-i(M-N)\theta} f^j(\theta) f^{*i}(\theta) = \int d\theta e^{-i(M-N)\theta} = \delta_{MN} \\
&\sum_{M,N} F_M^j F_N^{*i} \delta_{MN} = \sum_M F_M^j F_M^{*i} \quad (2.15')
\end{aligned}$$

$$M^{2D-MAS,ij}(t_1, t_2) = e^{-\frac{t_1+t_2}{T_2}} e^{i\omega_0\sigma_{iso}^j t_1} e^{i\omega_0\sigma_{iso}^i t_2} \sum_M e^{iM\omega_R t_1} e^{iN\omega_R t_2} I_M^{MAS} \quad (2.15)$$

This means, that in the case of no exchange $i=j$, there is only intensity along the main diagonal and the peaks intensity is identical with that of a 1D-MAS experiment.

In a 2D-MAS exchange spectrum the presence of the crosspeaks distributed on both sides of the main diagonal, reveals the existence of an exchange process. The question now is how to obtain the correlation times of the dynamics detected in a 2D-MAS exchange spectrum? The answer is simple: we have to plot the intensities of the crosspeaks versus mixing time and we obtain a curve (the correlation function) which describes the dynamics of each particular site in the sample (see eq(2.31)). Besides the information about dynamics, the 2D-MAS exchange spectrum provides information also about the exchange pathways just by analyzing the origin of the crosspeaks in the spectrum. Sometimes the origin of the crosspeaks is not the molecular reorientation but the so called chemical exchange. As we see in figure 2.6, in a 2D-MAS exchange spectrum one can clearly see the difference between crosspeaks (exchange) originating in a reorientation process (circle symbols) and those who occur in an chemical exchange process (square symbols).

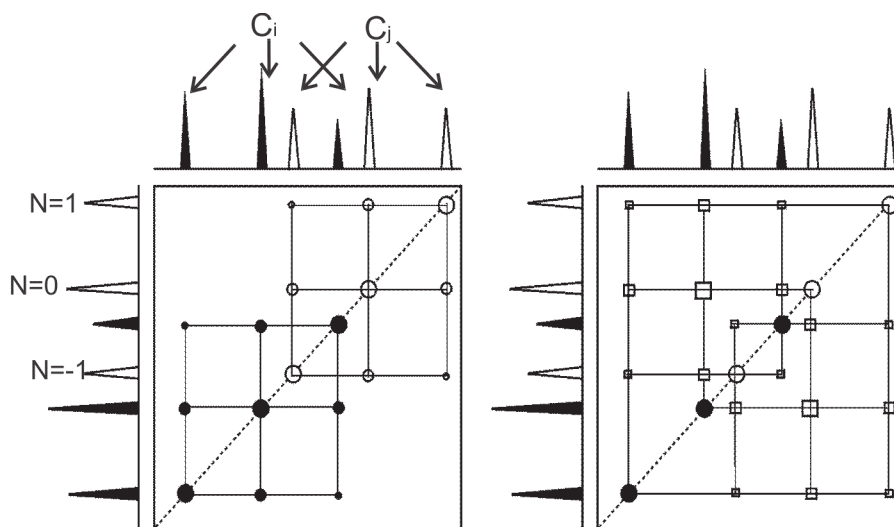


Fig.2.6 Schematic representation of auto- (left) and hetero- (right) crosspeaks between two ssb families

The chemical exchange process produces crosspeaks only between spinning sidebands belonging to different atoms (hetero-crosspeaks), while those describing a molecular reorientation or a spin diffusion (SD) process occur between the spinning sidebands belonging to the same atom (auto-crosspeaks). One may observe that in the case of a 2D-FID the simple 2D-FT (Fourier

Transform) does not produce a purely absorption spectrum, and the application of States-Haberhorn procedure [Reichert, hab] is not possible anymore because of the fact that both evolution and detection times are in argument. A solution to obtain just real separated data sets, could be to generate an analog signal according to eq. (2.14), but with the negative time variable t_1 . In this case the addition and subtraction of signals would provide the desired data sets. But, the above equations show that simple echo combination of both real data sets produces useless data.

b) The problem was solved by Hagemeyer [Hagemeyer89], who introduced the so called "time-reversed" experiment. The idea is that from mixing time which before was a multiple of rotation periods we subtract the evolution time t_1 and we record a combination of C-iS (echo) data sets. The schematic representation of the pulse sequence is given in figure (2.5-b).

Considering the time-reversed 2D-MAS exchange experiment, we expect at the end of detection period a signal with the following form:

$$\begin{aligned}
M^{2D/TR,ij}(t_1,t_2) &= e^{-\frac{t_1+t_2}{T_2}} e^{-i\omega_0\sigma_{iso}^j t_1} f^j(\gamma) f^{*j}(\omega_R t_1 + \gamma) \times e^{i\omega_0\sigma_{iso}^i t_2} f^{*i}(\omega_R t_1 + \omega_R \tau_m + \gamma) f^i(\omega_R t_1 + \omega_R \tau_m + \omega_R t_2 + \gamma) \\
&\xrightarrow{TR:\omega_R \tau_m = 2\pi N - \omega_R t_1} e^{-\frac{t_1+t_2}{T_2}} e^{-i\omega_0\sigma_{iso}^j t_1} f^j(\gamma) f^{*j}(\omega_R t_1 + \gamma) \times e^{i\omega_0\sigma_{iso}^i t_2} f^{*i}(\gamma) f^i(\omega_R t_2 + \gamma)
\end{aligned} \tag{2.16}$$

Here we make the following substitution $\gamma' = \gamma + \omega_R t_1$ and eq. (2.16) becomes:

$$\begin{aligned}
&M^{2D/TR,ij}(t_1,t_2) \\
&= e^{-\frac{t_1+t_2}{T_2}} e^{-i\omega_0\sigma_{iso}^j t_1} f^j(\gamma' - \omega_R t_1) f^{*j}(\gamma') \times e^{i\omega_0\sigma_{iso}^i t_2} f^{*i}(\gamma' - \omega_R t_1) f^i(\omega_R t_2 + \gamma' - \omega_R t_1) \\
&= e^{-\frac{t_1+t_2}{T_2}} e^{-i\omega_0\sigma_{iso}^j t_1} e^{i\omega_0\sigma_{iso}^i t_2} f^{*j}(\gamma') \int d\theta \delta(\theta - \gamma' + \omega_R t_1) f^j(\theta) f^{*i}(\theta) f^i(\theta + \omega_R t_2) \\
&= e^{-\frac{t_1+t_2}{T_2}} e^{-i\omega_0\sigma_{iso}^j t_1} e^{i\omega_0\sigma_{iso}^i t_2} f^{*j}(\gamma') \int d\theta \delta(\theta - \gamma' + \omega_R t_1) f^j(\theta) f^{*i}(\theta) \int d\phi \delta(\phi - \theta - \omega_R t_2) f^i(\phi) \\
&= e^{-\frac{t_1+t_2}{T_2}} e^{-i\omega_0\sigma_{iso}^j t_1} e^{i\omega_0\sigma_{iso}^i t_2} f^{*j}(\gamma') \int d\theta \sum_M e^{-i\theta M} e^{iM\gamma'} e^{-iM\omega_R t_1} f^j(\theta) f^{*i}(\theta) \int d\phi \sum_N e^{-iN\phi} e^{iN\theta} e^{iN\omega_R t_2} f^i(\phi) \tag{2.17}
\end{aligned}$$

Now we still have to perform the integration over the γ angle:

$$\begin{aligned}
& M^{2D/TR,ij}(t_1, t_2) \\
&= e^{-\frac{t_1+t_2}{T_2}} e^{-i\omega_0\sigma_{iso}^j t_1} e^{i\omega_0\sigma_{iso}^i t_2} \int e^{iM\gamma} d\gamma f^{*j}(\gamma) \int d\theta \sum_M e^{-i\theta(M-N)} e^{-iM\omega_R t_1} f^j(\theta) f^{*i}(\theta) \int d\phi \sum_N e^{-iN\phi} e^{iN\omega_R t_2} f^i(\phi) \\
&= e^{-\frac{t_1+t_2}{T_2}} e^{-i\omega_0\sigma_{iso}^j t_1} e^{i\omega_0\sigma_{iso}^i t_2} \sum_{M,N} e^{-iM\omega_R t_1} e^{iN\omega_R t_2} F_M^j F_{M-N}^{ij} F_N^{*j} \\
&= e^{-\frac{t_1+t_2}{T_2}} e^{-i\omega_0\sigma_{iso}^j t_1} e^{i\omega_0\sigma_{iso}^i t_2} \sum_{M,N} e^{-iM\omega_R t_1} e^{iN\omega_R t_2} I_{MN}^{2D-MAS}
\end{aligned} \tag{2.18}$$

Evaluating the equations (2.14) and (2.18) we see that the NMR signals have a similar form, the only difference consisting in the opposite sign of the term concerning the evolution period t_1 , from where it comes also the name of "time-reversed" experiment. The physical meaning of this change is the fact that now we can record purely absorption spectra by combining the two data sets.

We can say that the 2D-MAS NMR exchange experiments provide the desired information about the exchange process but from the experimental point of view they are very demanding. The base of a 2D experiment is the incrementation of the evolution time t_1 , an increased number of increments providing narrow lines with a better signal-to-noise ratio, making the experiment time consuming. Considering that, in order to obtain the information about the time scale of the exchange process we need to perform the experiment for several values of the mixing time (at least 10), extending the total acquisition time to several days. Considering the hardware instability and available machine time, this is not desired. On the other hand, despite the fact that the States-Haberkmorn procedure allow recording absorption spectra some unwanted factors (like an improper synchronization of the pulse sequence with the rotor period, [Reichert99]) may produce additional artifacts, their cause can be difficult to prove and eliminate. From here came the idea of using the principle of the 2D-MAS experiment to create an 1D exchange experiment with the same sensitivity regarding the exchange process, but which, due to reduced dimension, to provide a better signal-to-noise ratio within the same amount of experimental time.

2.3 1D-MAS NMR exchange

For a 1D-NMR experiment we can describe the signal like:

$$s(t) = s^e(t)e^{i\omega t} \quad (2.19)$$

where $s^e(t)$ is the envelope function which is responsible for the peak shape in the resulting spectrum [Ernst87]. Usually the signal is multiplied with an weighting function $h(t)$ and therefore we must define an averaged of the weighted time-domain signal envelope like:

$$\overline{sh} = \frac{1}{t^{\max}} \int_0^{t^{\max}} s^e(t)h(t)dt \quad (2.20)$$

With the help of equation 2.20, the signal-to-noise ratio for a 1D-NMR experiment can be written as:

$$S/N = \frac{nM\overline{sh}}{2\sigma_N} \quad (2.21)$$

where the product between the number of FID's which have to be summed n , the weighted time-domain signal envelope \overline{sh} , and the M equidistant samples is the peak height S in the frequency domain and the term to the nominator represents the noise. Considering the average signal power in the sampling window as:

$$\overline{s^2} = \frac{1}{t^{\max}} \int_0^{t^{\max}} s^e(t)^2 dt \quad (2.22)$$

then we can compare the sensitivities of the 1D and 2D-NMR experiments in the case when we consider that the same resolution must be achieved in the ω_2 -domain as in the 1D experiment as:

$$\frac{2D}{1D} = \frac{\left[\overline{s^2(2D)} \right]^{\frac{1}{2}}}{\left[\overline{s^2(1D)} \right]^{\frac{1}{2}}} = \left[\frac{1}{t_1^{\max}} \int_0^{t_1^{\max}} dt_1 s_1^e(t_1)^2 \right]^{\frac{1}{2}} \quad (2.23)$$

A closer inspection of equation (2.23) allows us to observe that the sensitivity is only determined by the average signal power given by the root mean square signal envelope in the two experiments [Ernst87]. Equation (2.23) indicates that the same sensitivity can be obtained in the two experiments if:

- i) $s_1^e(t_1)$ is equal to unity, i.e. transverse relaxation and the inhomogeneous decay in the evolution period t_1 can be neglected
- ii) the instrumental stability is sufficient to allow us to neglect the t_1 -noise
- iii) the number of peaks in the two experiments is the same (the intensity of a line in the 1D spectrum is not distributed among several peaks in the 2D spectrum)

The first condition implies low resolution in t_1 , therefore, in cases where high resolution in t_1 must be achieved (large number of increments), a small sensitivity loss in 2D spectroscopy must be considered. The third condition is not fulfilled in the case of 2D exchange experiments, and therefore additional sensitivity loss must be taken into account as compared with 1D experiments. Therefore, for exchange NMR experiments in which the sensitivity is very important, it is preferable to have a 1D experiment instead of a 2D, despite the potential loss of information.

The idea of a reduced MAS exchange experiment is based on the assumption that we can avoid the time consuming procedure of correlation of the resonance frequency of the nucleus before and after the mixing time in a 2D-MAS exchange experiment by creating a specific state of the spin system that the exchange process may disturb. In this way we shall measure a different state of the spin system if the exchange take place. In the process in which we are interested, the molecular re-orientation has, in most of the cases, no influence on the chemical shift isotropy (CSI), it only change the orientation of the chemical shift anisotropy (CSA) tensors. In the limit case of the slow-MAS $\omega_R/2\pi < \Delta\sigma$ the reduction of the 2D-MAS experiment would mean that we have to produce a magnetization gradient between the spinning sidebands of the observed nucleus. But it is not possible to apply directly the idea of a magnetization transfer because this would mean to treat the MAS spinning sidebands like normal NMR lines like in the case of a static NMR experiment or for different isotropic lines in MAS experiments, so there must be other ways to reduce the exchange experiment.

2.3.1 One Dimensional Exchange Spectroscopy (ODESSA)

The idea behind the ODESSA [Gerar96] experiment is that in the case of the 1D-MAS experiment by starting the acquisition at the rotor echo we can create a specific state of the spin system so that all the spinning sidebands can be phased. If the acquisition is delayed with a multiple of rotation period, then all the spinning sidebands of N-th order would experience the same phase shift $e^{i2\pi N}$ as it is obvious from the f -function formalism. From equation (2.10) we know the form of a MAS signal. If we consider that the acquisition is done only after a time $t' = t + xT_R$ ($1 \geq x \geq 0$) then the MAS signal would have the following expression:

$$\begin{aligned}
 M^{MAS}(t') &= e^{-\frac{t'}{T_2}} e^{-i\omega_0 \sigma_{iso} t'} f^*(\gamma) f(\omega_R t' + \gamma) \\
 &= e^{-\frac{t'}{T_2}} e^{-i\omega_0 \sigma_{iso} t'} f^*(\gamma) f(\omega_R t + \omega_R x T_R + \gamma) \\
 &= e^{-\frac{t'}{T_2}} e^{-i\omega_0 \sigma_{iso} t'} f^*(\gamma) f(\omega_R t + 2\pi x + \gamma)
 \end{aligned} \tag{2.24}$$

Following the procedure similar to that used to obtain equation (2.11), from equation (2.24) we obtain:

$$\begin{aligned}
 M^{MAS}(t') &= e^{-\frac{t'}{T_2}} e^{-i\omega_0 \sigma_{iso} t'} f^*(\gamma) \int d\theta \delta(\theta - \omega_R t - 2\pi x - \gamma) f(\theta) \\
 &= e^{-\frac{t'}{T_2}} e^{-i\omega_0 \sigma_{iso} t'} f^*(\gamma) \int d\theta \sum_M e^{-iM\theta} e^{iM\omega_R t} e^{i2\pi x M} e^{i\gamma M} f(\theta)
 \end{aligned} \tag{2.25}$$

which after integration $\int d\gamma$ becomes:

$$M^{MAS}(t') = e^{-\frac{t'}{T_2}} e^{-i\omega_0 \sigma_{iso} t'} \sum_M e^{iM\omega_R t} e^{i2\pi x M} I_M^{MAS} \tag{2.26}$$

In case that $x=0.5$, that means the acquisition starts in the middle of two rotation echoes, will result an additional phase shift:

$$\Psi^N = e^{iN\pi} = (-1)^N \tag{2.27}$$

This means that all even spinning sidebands have the same phase while the odd ones are in antiphase. In this manner a specific state of the spin system is produced, which by a dynamic process may be destroyed. Like the experiments showed [Reichert, hab], this method is useful just in cases when we deal with a simple substance with only few chemical shift isotropies well separated. In the case of polymers, like the ones in which we are interested, the high number of non-equivalent nuclei makes the application of ODESSA impossible. Despite this, we should have a look to the method because represents the base of another method used in this work. The effect of the different chemical shift isotropies can be seen in the following equation:

$$\Psi^{N,i} = e^{iN\pi} e^{i\omega_0\sigma_{iso}^i \frac{T_R}{2}} = (-1)^N e^{i\omega_0\sigma_{iso}^i \frac{T_R}{2}} \quad (2.28)$$

which means that only the spinning sidebands belonging to the same chemical shift isotropy have the same phase and can be phased correctly. By using this approach in a 1D-MAS exchange experiment the ODESSA (**O**ne **D**imensional **E**xchange Spectroscopy by **S**ideband **A**lternation) was born [Gerar96]. The basic of the pulse sequence is given in figure 2.7.

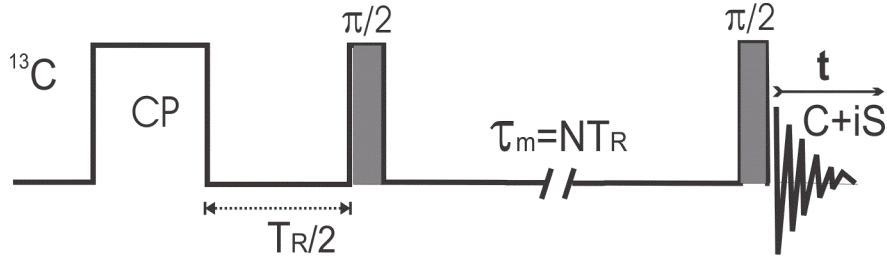


Fig.2.7 Schematic representation of ODESSA experiment

Using again the f -function formalism, in the case of ODESSA where the evolution time is chosen to be half of the rotor period ($t_1 = T_R/2 \leftrightarrow \omega_R t_1 = \pi$), we obtain:

$$\begin{aligned} M^{ODESSA,ij}(t) &= e^{-\frac{T_R/2}{T_2}} e^{i\sigma_{iso}^j \omega_0 \frac{T_R}{2}} f^{*j}(\gamma) f^j(\pi + \gamma) \times e^{-\frac{t}{T_2}} e^{i\sigma_{iso}^i \omega_0 t} f^{*i}(\gamma + \pi + \omega_R \tau_m) f^i(\gamma + \pi + \omega_R \tau_m + \omega_R t) \\ &= e^{-\frac{T_R/2+t}{T_2}} e^{i\sigma_{iso}^j \omega_0 \frac{T_R}{2}} f^{*j}(\gamma) f^j(\pi + \gamma) \times e^{i\sigma_{iso}^i \omega_0 t} f^{*i}(\gamma + \pi) f^i(\gamma + \pi + \omega_R t) \\ &= e^{-\frac{T_R/2+t}{T_2}} e^{i\sigma_{iso}^j \omega_0 \frac{T_R}{2}} e^{i\sigma_{iso}^i \omega_0 t} f^{*j}(\gamma) \int d\theta \delta(\theta - \pi - \gamma) f^j(\theta) f^{*i}(\theta) \int d\phi \delta(\phi - \theta - \omega_R t) f^i(\phi) \\ &= e^{-\frac{T_R/2+t}{T_2}} e^{i\sigma_{iso}^j \omega_0 \frac{T_R}{2}} e^{i\sigma_{iso}^i \omega_0 t} f^{*j}(\gamma) \int d\theta \sum_M e^{-iM\theta} e^{iM\pi} e^{iM\gamma} f^j(\theta) f^{*i}(\theta) \int d\phi \sum_N e^{-iN\phi} e^{iN\theta} e^{iN\omega_R t} f^i(\phi) \end{aligned} \quad (2.29)$$

Now, performing the powder averaging over γ and taking into account that $e^{iM\pi} = (-1)^M$ we obtain from equation (2.29) the following form for the ODESSA signal:

$$\begin{aligned}
M^{ODESSA,ij}(t) &= e^{-\frac{T_R/2+t}{T_2}} e^{i\sigma_{iso}^j \omega_0 \frac{T_R}{2}} e^{i\sigma_{iso}^i \omega_0 t} \sum_{M,N} (-1)^M e^{iN\omega_R t} \int d\gamma e^{iM\gamma} f^{*j}(\gamma) \int d\theta e^{-i(M-N)\theta} f^i(\theta) \int d\phi e^{-iN\phi} f^j(\phi) \\
&= e^{-\frac{T_R/2+t}{T_2}} e^{i\sigma_{iso}^j \omega_0 \frac{T_R}{2}} e^{i\sigma_{iso}^i \omega_0 t} \sum_N e^{iN\omega_R t} \sum_M (-1)^M I_{MN}^{2D-MAS,ij}
\end{aligned} \tag{2.30}$$

Equation (2.30) shows that the 1D-ODESSA spectrum is in fact a projection of a 2D-MAS spectrum in which all odd spinning sidebands are inverted (fig. 2.8). In the case that no exchange occurs, the ODESSA spectrum is a MAS spectrum with the odd spinning sidebands inverted; on the other hand when exchange happens, the intensities of the different spinning sidebands are reduced with a different factor which may be calculated as shown in figure 2.9, for different lines. Another aspect here is the fact that in the ODESSA experiment at longer mixing times the intensity does not decay to 0, rather to a plateau zone which is determined by the spin rate ω_R , the main values of the chemical shift anisotropy tensors σ_{ii} and the topology of the process, which depends on the non-diagonal elements of the chemical shift anisotropy tensors σ_{ij} .

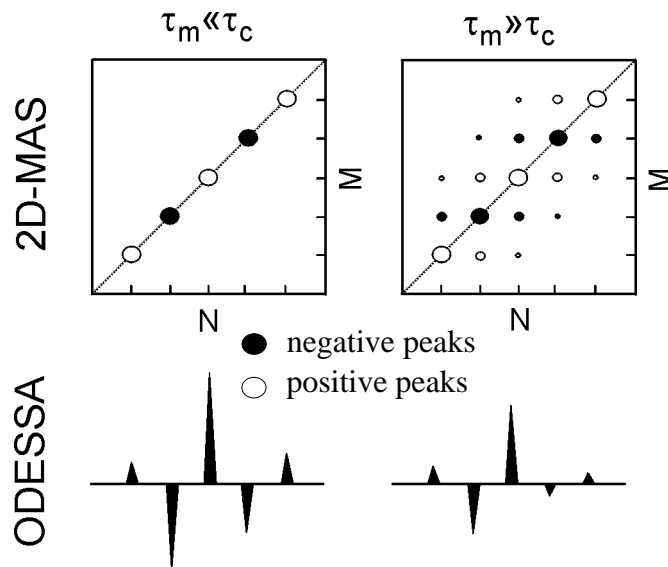


Fig.2.8 ODESSA spectrum as projection of a 2D-MAS spectrum

In the following we discuss the behavior of ODESSA intensities $I_N^{ODESSA} = \sum_N (-1)^M I_{MN}^{2D-MAS}$

in the case of an exchange process involving a two sites jump, like it is in the case of the Dimethyl sulfone (DMS, fig. 2.9).

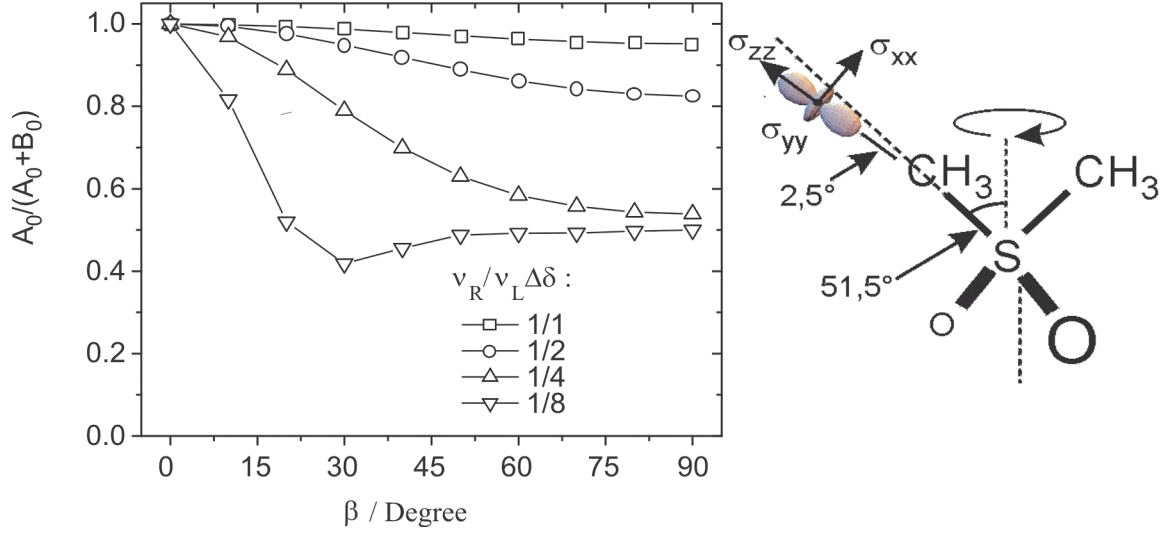


Fig.2.9 Sensitivity of the ODESSA decay to exchange process in DMS for several $v_R/\Delta\sigma$ ratios (left) and CSA tensors orientations (right)

In a crystal, DMS molecules perform slow twofold π -flips around their individual C_2 symmetry axes, which exchange the positions of each pair of chemically equivalent methyl groups. The reorientation angle found in this case is close to 108° [Favre98].

In this case the ODESSA decay can be described in the following manner:

$$\begin{aligned}
 I_N^{ODESSA}(\tau_m) &= (A_N + B_N e^{-2k\tau_m}) e^{-\frac{\tau_m}{T_1}} \\
 A_N &= \frac{1}{2}(I_N^{11} + I_N^{12}) & B_N &= \frac{1}{2}(I_N^{11} - I_N^{12}) \\
 I_N^{11} &= I_N^{22} & I_N^{12} &= I_N^{21} \\
 I_N^{ij} &= \sum_M (-1)^M F_M^j F_N^{*i} F_{M-N}^{ij}
 \end{aligned} \tag{2.31}$$

where the terms in the last equation in (2.31) were already defined in previous paragraphs. More about the origin of the equation (2.31) one can find in the next chapter. As we can see the ODESSA

decay is influenced by the T_1 relaxation and for larger mixing times ($\tau_m \geq 5T_1$) disappears. From the ODESSA decay we can obtain the correlation time τ_c or the jump rate k of the molecular process. Usually it is sufficient to have the ODESSA decay for the spinning sidebands of order 0 to obtain the correlation time of the molecular process. As we mentioned at the beginning of this section the different phase of the different chemical shift isotropies limits the application of this method to substances with one or few chemical shift isotropies. In figure 2.8 we show schematically the ODESSA spectrum as a projection in the indirect dimension of a 2D-MAS spectrum. The left part, shows the shape of both types of spectra in the case of no exchange ($\tau_m < \tau_c$); we see that for the 2D case this means that only peaks on the main diagonal appears while for the ODESSA case we obtain a typical ODESSA spectrum with inverted odd spinning sidebands with a certain intensity. If we consider the case when the exchange process took place ($\tau_c < \tau_m$) in a 2D-MAS spectrum this means that we have beside the main diagonal peaks also the so called crosspeaks which can be positive (circle symbols) or negative (filled circles), while for the ODESSA we obtain a similar spectrum like in the first case. The only difference, and the crucial one, is that the intensities of the different spinning sidebands are decreased due to the fact that the molecular dynamics altered the system state considered before the mixing time. In both cases we see that by projecting the positive or negative (black marking) peaks from the 2D-MAS spectrum we obtain in the indirect dimension the ODESSA spectrum with positive even and inverted odd ssb's. In the case of exchange (right part) the alternance of positive and negative peaks in the 2D spectrum makes by addition along the indirect dimension the reduced intensities of the ssb from ODESSA spectrum.

In the ODESSA experiment the sensitivity in detecting the molecular reorientations is strongly dependent of the B_N part from equation (2.31) which describes the ODESSA decay. This is dependent besides the topology of the process also from the spinning rate. Simulations regarding this problem (fig. 2.9) shows that the best sensitivity is reached in the case when the spinning rate is $\nu_R \cong \Delta\sigma / 4$ of the width of chemical shift anisotropy [Reichert, hab].

2.3.2 Time Reversed ODESSA (tr-ODESSA)

As demonstrated above, the 1D-MAS exchange experiment can be an alternative to the time consuming 2D-MAS exchange experiments. The problem encountered in the application of ODESSA is the different phase of spinning sidebands belonging to different atoms. This is the big

obstacle in using ODESSA in NMR investigation of molecular reorientations in natural abundance samples. In the following we show how this impediment was eliminated [Reichert97]. The term responsible for the phase distortion in the ODESSA experiment is the one describing the evolution of chemical shift isotropy during the preparation period $\frac{T_R}{2}$. An easy way to solve the problem would be to refocus this evolution during the preparation period. There are several ways to do this: one would be to apply a π pulse in the middle of the evolution time like in the case of a Hahn-echo, but this beside the NMR interactions will also refocus the evolution of the chemical shift anisotropy and would spoil the MAS spectrum. Another way, as proposed by Hagemeyer for the 2D-MAS "time-reversed" experiment, is to apply before the acquisition another delay and to choose the appropriate combination of data sets (C-iS) to reverse the effect of the disturbing term. This was the method applied by Reichert in developing the tr-ODESSA experiment. The nomenclature "time-reversed" comes from the similarities with Hagemeyer's experiment. Here care must be taken, while changing the start of the acquisition can destroy the MAS synchronization necessary for recording the desired molecular reorientation. That's why the mixing time must be changed accordingly: if we add an additional $\frac{T_R}{2}$ delay before acquisition we also must subtract it from the mixing time so that the position of the rotor before and after the mixing time to be the same. In this way for the tr-ODESSA experiment the mixing time must be set to $\tau_m = (N-1/2)T_R$ and so avoiding undesired artifacts in the spectrum.

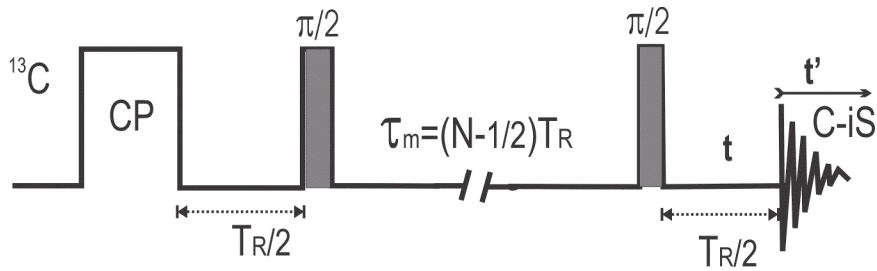


Fig.2.10 *trODESSA pulse sequence*

The acquired tr-ODESSA signal after applying the pulse sequence from figure 2.10 is described in the following equations:

$$\begin{aligned}
 & M^{trODESSA,ij}(t) \\
 &= e^{-\frac{T_R/2}{T_2}} e^{-i\omega_0\sigma_{iso}^j \frac{T_R}{2}} f^j(\gamma) f^{*j}(\gamma + \pi) \times e^{-\frac{t}{T_2}} e^{i\omega_0\sigma_{iso}^i t} f^{*i}(\omega_R\tau_m + \gamma + \pi) f^i(\omega_R\tau_m + \gamma + \pi + \omega_R t) \quad (2.32)
 \end{aligned}$$

Considering that for trODESSA we have:

$$\begin{aligned}\omega_R \tau_m &= 2\pi \left(N - \frac{1}{2}\right) & t = \frac{T_R}{2} + t' \leftrightarrow \omega_R t &= \pi + \omega_R t' \\ \gamma' &= \gamma + \pi\end{aligned}\tag{2.33}$$

we obtain for the trODESSA signal:

$$\begin{aligned}M^{trODESSA,ij}(t) &= e^{-\frac{T_R+t'}{T_2}} e^{i\omega_0 \left(\sigma_{iso}^i - \sigma_{iso}^j\right) \frac{T_R}{2}} e^{i\omega_0 \sigma_{iso}^i t'} f^j(\gamma) f^{*j}(\gamma + \pi) \times f^{*i}(\gamma) f^i(\gamma + \pi + \omega_R t') \\ &= e^{-\frac{T_R+t'}{T_2}} e^{i\omega_0 \left(\sigma_{iso}^i - \sigma_{iso}^j\right) \frac{T_R}{2}} e^{i\omega_0 \sigma_{iso}^i t'} f^{*j}(\gamma) \int d\theta \delta(\theta - \gamma + \pi) f^j(\theta) f^{*i}(\theta) \int d\phi \delta(\phi - \theta - \pi - \omega_R t') f^i(\phi) \\ &= e^{-\frac{T_R+t'}{T_2}} e^{i\omega_0 \left(\sigma_{iso}^i - \sigma_{iso}^j\right) \frac{T_R}{2}} e^{i\omega_0 \sigma_{iso}^i t'} f^{*j}(\gamma) \int d\theta \sum_M e^{-i(M-N)\theta} e^{iM\gamma} e^{-i(M-N)\pi} f^j(\theta) f^{*i}(\theta) \int d\phi \sum_N e^{-iN\phi} e^{iN\omega_R t'} f^i(\phi)\end{aligned}\tag{2.34}$$

We need again to perform the integration $\int d\gamma$ and knowing that $e^{-i(M-N)\pi} = (-1)^{(M-N)}$ we obtain for the trODESSA signal:

$$\begin{aligned}M^{trODESSA,ij}(t) &= e^{-\frac{T_R+t'}{T_2}} e^{i\omega_0 \left(\sigma_{iso}^i - \sigma_{iso}^j\right) \frac{T_R}{2}} e^{i\omega_0 \sigma_{iso}^i t'} \sum_{M,N} e^{-i(M-N)\pi} e^{iN\omega_R t'} \int d\gamma e^{iM\gamma} f^{*j}(\gamma) \int d\theta e^{-i(M-N)\theta} f^j(\theta) f^{*i}(\theta) \int d\phi e^{-iN\phi} f^i(\phi) \\ &= e^{-\frac{T_R+t'}{T_2}} e^{i\omega_0 \left(\sigma_{iso}^i - \sigma_{iso}^j\right) \frac{T_R}{2}} e^{i\omega_0 \sigma_{iso}^i t'} \sum_N e^{iN\omega_R t'} \sum_M (-1)^{(M-N)} I_{MN}^{2D-MAS,ij}\end{aligned}\tag{2.35}$$

The last equation proves that using the "time-reversed" approach we annihilate the disturbing phase term from the ODESSA experiment, in case that the molecular process does not change the chemical shift isotropy. The delay introduced before the acquisition contributes also to the evolution of

the chemical shift anisotropies by adding a $(-1)^{(M-N)}$ phase to each spinning sideband. That in fact

means that all the spinning sidebands would be positive and for short mixing times the trODESSA spectrum is identical with a normal 1D-MAS spectrum. Following the same approach like in description of ODESSA method, also here we remark that the trODESSA spectrum is a projection along the indirect dimension of a 2D-MAS exchange experiment (fig. 2.11).

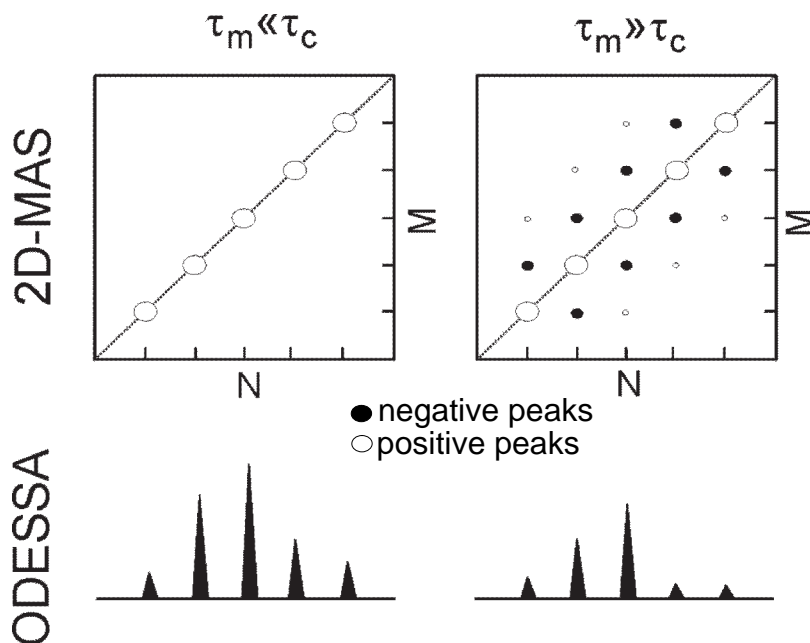


Fig.2.11 trODESSA spectrum as a projection of a 2D-MAS spectrum

One may notice that also in trODESSA experiment, the existence of an exchange process is confirmed by the reduction of spinning sidebands intensities with increasing mixing times (fig. 2.12). Again, as the equation (2.35) and figure 2.11 proves, trODESSA spectrum is seen like a projection in the indirect dimension of a 2D-MAS experiment, so provides the same type of information like last one but due to reduced dimension in shorter experimental time. When the exchange process involves only exchange between equivalent nuclei, no phase twist occurs in the spectrum, while dealing with an exchange between non-equivalent sites a phase twist or "phase transfer" is

present as revealed by the term $e^{i\omega_0(\sigma_{iso}^i - \sigma_{iso}^j)\frac{T_R}{2}}$ in equation (2.35). One may think that this is a major impediment, but as proposed in the literature [Luz02] this could be turned into an advantage by considering the phase twist as an additional parameter to characterize the dynamic process.

Both ODESSA and trODESSA experiments are characterized by the same so called ODESSA decay (eq. (2.31)), from which we may obtain the correlation time of the molecular dynamics. The major difference between the two methods is the addition of the delay before the acquisition in trODESSA experiment, which forces the modification of the mixing time and has as result a MAS spectrum with positive lines which can be easily phased.

The experiments, as mentioned in literature [Reichert, hab], performed on the DMS provide identical values for the correlation times obtained from ODESSA and trODESSA. We must mention that as expected, at longer mixing times the effect of the spin-lattice relaxation, together with the spin diffusion (which would be discussed later in this work) become the major contributors to ODESSA decay and further treatment of the acquired data must be done (see next chapter).

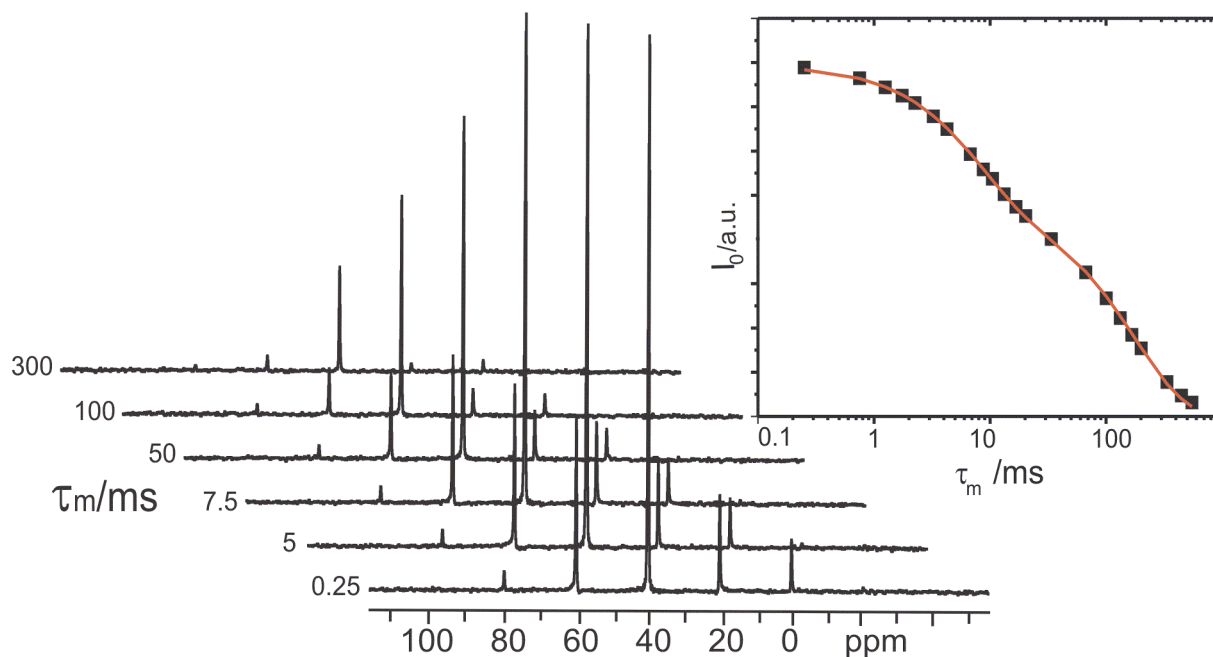


Fig.2.12 *trODESSA decay (right) and spectra (left) of DMS*

An alternative way to solve the phase problem from ODESSA experiment, is to combine it with a SELDOM experiment [Kolbert90, Tekely98] so that at the beginning of the mixing time period all the spinning sidebands families, except the one selected to be saturated. This would mean that if more than the selected spins are involved in the exchange process, new spinning sidebands would appear in the spectrum. The advantage of this method is the simplicity of the resulted spectrum, but due to the fact that it detects the hetero-processes and to the loss of signal during the SELDOM pulse sequence, we decided not to apply it in our investigations.

2.3.3 PASS, PATROS

We saw that the additional delay in the trODESSA experiment helps us to overcome the phase disturbing effect from ODESSA, when we deal with substances with more than one chemical shift isotropy, like in the case of polymers and other interesting substances. Also we mentioned that the sensitivity of the ODESSA/trODESSA experiments in detecting the molecular reorientations is strongly dependent of the ratio between spinning rate and the chemical shift anisotropy of the inquired site (see fig. 2.9). That means that in a substance with a large distribution of chemical shift anisotropies, there may be the case that those values are so different that a spinning rate chosen to fulfill the condition for sensitivity for one site is no more valid for all the lines present in the spectrum. This is the case of our polymers (PnBMA, PnHMA), where the carboxyl group COO, is separated from the signals coming from the main- and side chain (fig. 2.13). That in fact means, that the sensitivity condition for ODESSA/trODESSA experiment can not be fulfilled simultaneously for the COO and other resonances.

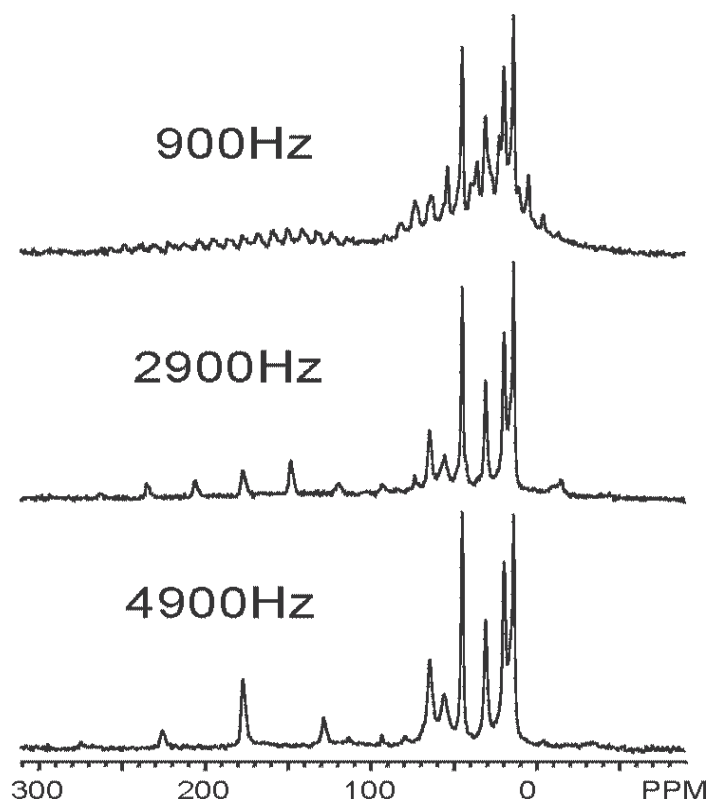


Fig.2.13 MAS spectra of PnBMA at different spinning rates.

In our experiments, to investigate the dynamic of the COO group, a spinning rate of 4 kHz for a Larmor frequency of 200 MHz would be sufficient, knowing that the width of the CSA for this

group is about 150 ppm. At this spinning rate, the other carbons in the spectrum features few or no spinning sidebands and therefore they are not sensitive to the exchange between equivalent sites. For the other lines, considering their smaller CSA, a lower spinning rate would be necessary.

But as we discussed previously (chapter 2.1), a lower rotation frequency implies more spinning sidebands, which, considering the neighbored resonances, would result in a crowded spectrum, where different ssb from different sites would overlap (fig. 2.13), so that no useful information can be extracted anymore. From here would emerge the need to combine the trODESSA experiment with other pulse sequence in order to be able to separate the spinning sidebands from a crowded spectrum for different resonances.

There are several methods, extended used in NMR-MAS experiments which deal with the separation of the spinning sidebands, but because we used specifically one of them we should restrict ourselves to this one. The PASS (*P*hase *A*justed *S*pinning *S*idebands) experiment [Dixon82] consist of a sequence of π pulses with defined intervals and ends with a delay which leads to a Hahn echo. The timing in the pulse sequence is such that the result is a spectrum in which the spinning sidebands are separated by a phase shift proportional to their order, called ‘‘pitch‘‘. In our investigation we used a slightly modified PASS sequence consisting of five π pulses [Antzugin95,94], which avoids the problems of differential transverse relaxation by using the same overall duration, independent of the sideband phase shift. The PASS experiment is in essence similar with a 2D--MAS experiment in which instead to increment the preparation time we increment the phase pitch Θ so that the phase of a spinning sideband of N-th order will be $N\Theta$.

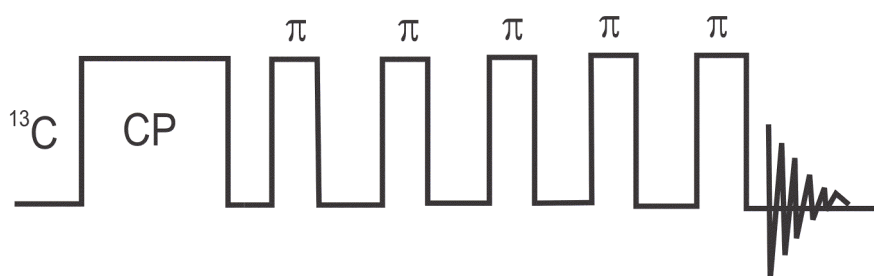


Fig.2.14 *The basics of the PASS sequence*

The PASS sequence (fig. 2.14) does not provide information about the exchange process, therefore it must be combined with another method sensitive to the exchange. In our case PASS was used together with trODESSA and the new born pulse sequence was named PATROS (*P*ASS+*tr*ODESSA) [Reichert00]. Before going into details about PATROS we should see the effect of the PASS sequence on the signal, using again the f -functions formalism.

The FID acquired in a PASS sequence would have the form:

$$M^{PASS}(t) = e^{-\frac{T^{PASS}+t}{T_2}} e^{i\omega_0\sigma_{iso}t} f^*(\Theta + \gamma) f(\omega_R t + \gamma) \quad (2.36)$$

Using the change of variable $\gamma' = \gamma + \Theta$ we can write the equation (2.31) as:

$$\begin{aligned} M^{PASS}(t) &= e^{-\frac{T^{PASS}+t}{T_2}} e^{i\omega_0\sigma_{iso}t} f^*(\gamma') f(\omega_R t + \gamma' - \Theta) \\ &= e^{-\frac{T^{PASS}+t}{T_2}} e^{i\omega_0\sigma_{iso}t} f^*(\gamma') \int d\theta \delta(\theta - \omega_R t - \gamma' + \Theta) f(\theta) \\ &= e^{-\frac{T^{PASS}+t}{T_2}} e^{i\omega_0\sigma_{iso}t} f^*(\gamma') \int d\theta \sum_M e^{-iM\theta} e^{iM\omega_R t} e^{iM\gamma'} e^{-iM\Theta} f(\theta) \end{aligned} \quad (2.37)$$

After the integration $\int d\gamma'$ we have:

$$\begin{aligned} M^{PASS}(t) &= e^{-\frac{T^{PASS}+t}{T_2}} e^{i\omega_0\sigma_{iso}t} \sum_M e^{iM\omega_R t} e^{-iM\Theta} \int d\gamma' e^{iM\gamma'} f^*(\gamma') \int d\theta e^{-iM\theta} f(\theta) \\ &= e^{-\frac{T^{PASS}+t}{T_2}} e^{i\omega_0\sigma_{iso}t} \sum_M e^{iM\omega_R t} e^{-iM\Theta} F_M F_M^* \\ &= e^{-\frac{T^{PASS}+t}{T_2}} e^{i\omega_0\sigma_{iso}t} \sum_M e^{iM\omega_R t} e^{-iM\Theta} I_M^{MAS} \end{aligned} \quad (2.38)$$

A closer inspection of equation (2.38) allows us to see that the PASS signal corresponds to a MAS spectrum in which each spinning sideband is dephased with a factor $M\Theta$, where M is the order of the spinning sideband. The pulse sequence is repeated n times incrementing the phase "pitch", and after a 2D-FT we obtain a 2D spectrum consisting in n discrete frequency slices, each corresponding to a specific spinning sideband order M . In fact, one may consider the PASS experiment like a reduced 2D-MAS experiment because the number n of necessary increments is much smaller (16 to 32) than in a normal 2D experiment (see also the discussion about the signal/noise in case of a 2D and 1D experiment). Figure 2.15, shows the effect of the PASS sequence on the spectrum after each increment of the phase, by performing only a 1D-FT and the resulted spectrum after a 2D-FT .

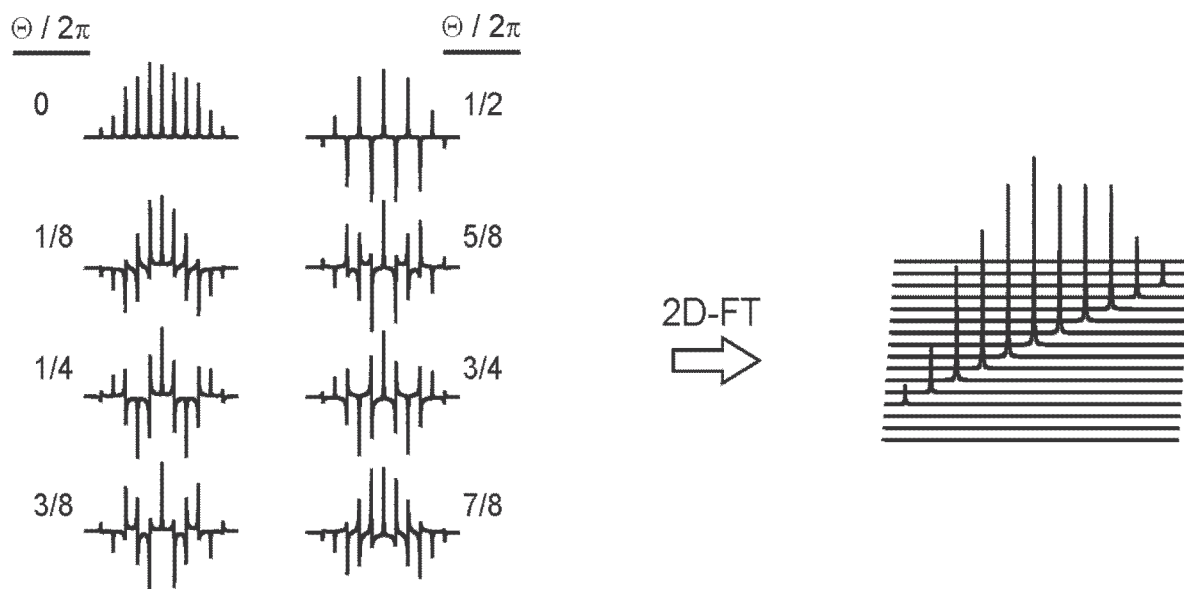


Fig.2.15 PASS spectra after 1D-FT (left) and 2D-FT (right)

Let's now return to the PATROS pulse sequence in which trODESSA and PASS are combined. The pulse sequence is presented in the figure 2.16. There were several attempts to add the PASS sequence in trODESSA and the one which proved to be the correct one is the one in which the train of π pulses are inserted immediately after the reading pulse, before the $\frac{T_R}{2}$ delay before the acquisition (fig. 2.16). As one may see in the following calculations, the mixing time must be again modified for correct performance.

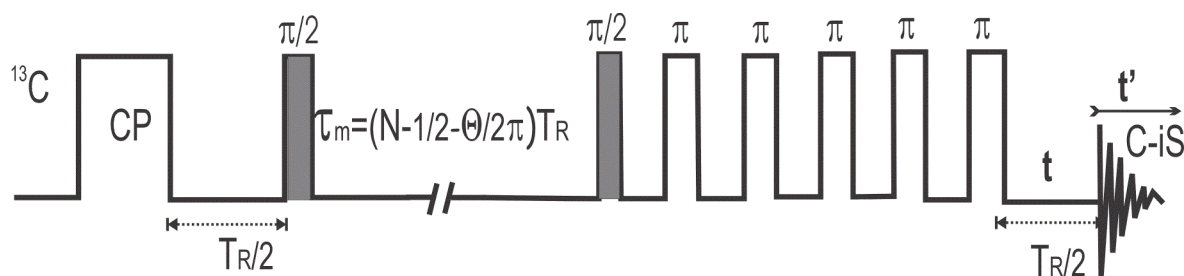


Fig. 2.16 PATROS pulse sequence

The signal recorded in the PATROS experiment has the following features:

$$M^{PATROS,ij}(t) = e^{-\frac{T_R/2}{T_2}} e^{-i\omega_0\sigma_{iso}^i \frac{T_R}{2}} f^j(\gamma) f^{*j}(\gamma + \pi) \times e^{-\frac{T^{PASS} + t}{T_2}} e^{i\omega_0\sigma_{iso}^i f^{*i}(\gamma + \pi + \omega_R \tau_m + \Theta)} f^i(\gamma + \pi + \omega_R \tau_m + \omega_R t) \quad (2.39')$$

which after the transformation: $t = \frac{T_R}{2} + t' \leftrightarrow \omega_R t = \omega_R t' + \pi$ becomes:

$$M^{PATROS,ij}(t) = e^{-\frac{T^{PASS}_{+t+T_R}}{T_2}} e^{i\omega_0 \sigma_{iso}^i t'} e^{i\omega_0 (\sigma_{iso}^i - \sigma_{iso}^j) \frac{T_R}{2}} f^j(\gamma) f^{*j}(\gamma + \pi) \times f^{*i}(\gamma + \pi + \omega_R \tau_m + \Theta) f^i(\gamma + 2\pi + \omega_R \tau_m + \omega_R t') \quad (2.39)$$

Here, as we mentioned above, we have to modify the value of the mixing time which in this case will be:

$$\tau_m = T_R \left(N - \frac{1}{2} - \frac{\Theta}{2\pi} \right) \quad (2.40)$$

where the last term was introduced to compensate the effect of the phase pitch from the PASS sequence. Considering that:

$$\begin{aligned} \omega_R \tau_m &= 2\pi N - \pi - \Theta \\ \gamma' &= \gamma + \pi \end{aligned} \quad (2.41)$$

we obtain for the acquired PATROS signal:

$$M^{PATROS,ij}(t) = e^{-\frac{T^{PASS}_{+t+T_R}}{T_2}} e^{i\omega_0 (\sigma_{iso}^i - \sigma_{iso}^j) \frac{T_R}{2}} e^{i\omega_0 \sigma_{iso}^i t'} f^j(\gamma) f^{*j}(\gamma + \pi) \times f^{*i}(\gamma) f^i(\gamma - \Theta + \pi + \omega_R t') \quad (2.42)$$

Again the integration $\int d\gamma$ is necessary to obtain the signal in the final form:

$$\begin{aligned} M^{PATROS,ij}(t) &= e^{-\frac{T^{PASS}_{+t+T_R}}{T_2}} e^{i\omega_0 (\sigma_{iso}^i - \sigma_{iso}^j) \frac{T_R}{2}} e^{i\omega_0 \sigma_{iso}^i t'} \\ &\sum_{M,N} e^{-i(M-N)\pi} e^{-iN\Theta} e^{iN\omega_R t'} \int d\gamma e^{iM\gamma} f^{*j}(\gamma) \int d\theta f^j e^{-i(M-N)\theta} (\theta) f^{*i}(\theta) \int d\phi e^{-iN\phi} f^i(\phi) \\ &= e^{-\frac{T^{PASS}_{+t+T_R}}{T_2}} e^{i\omega_0 (\sigma_{iso}^i - \sigma_{iso}^j) \frac{T_R}{2}} e^{i\omega_0 \sigma_{iso}^i t'} \sum_N e^{-iN\Theta} e^{iN\omega_R t'} \sum_M (-1)^{(M-N)} F_M^j F_{M-N}^{ij} F_N^{*i} \\ &= e^{-\frac{T^{PASS}_{+t+T_R}}{T_2}} e^{i\omega_0 (\sigma_{iso}^i - \sigma_{iso}^j) \frac{T_R}{2}} e^{i\omega_0 \sigma_{iso}^i t'} \sum_N e^{-iN\Theta} e^{iN\omega_R t'} \sum_M (-1)^{(M-N)} I_{MN}^{2D-MAS,ij} \end{aligned} \quad (2.43)$$

As one may think, we return from trODESSA to a 2D-MAS experiment, but this is not quite true. The PATROS signal using the PASS pulses uses only a small number of increments compared with the classical 2D-MAS exchange experiment. Also in PATROS we have no signal decay in the second dimension and in principle the signal to noise should be equal to that of trODESSA experiment, but in reality we have a small loss of the signal due to the pulse imperfections and the T_2 decay during the long PASS part of the pulse sequence. One should remark in equation (2.43) that only a correct adjustment of the mixing time period, by subtraction of the term regarding the phase pitch, produces the desired spectrum. If we do not consider this term, a corrupt spectrum with mixed order of the spinning sidebands will be produced.

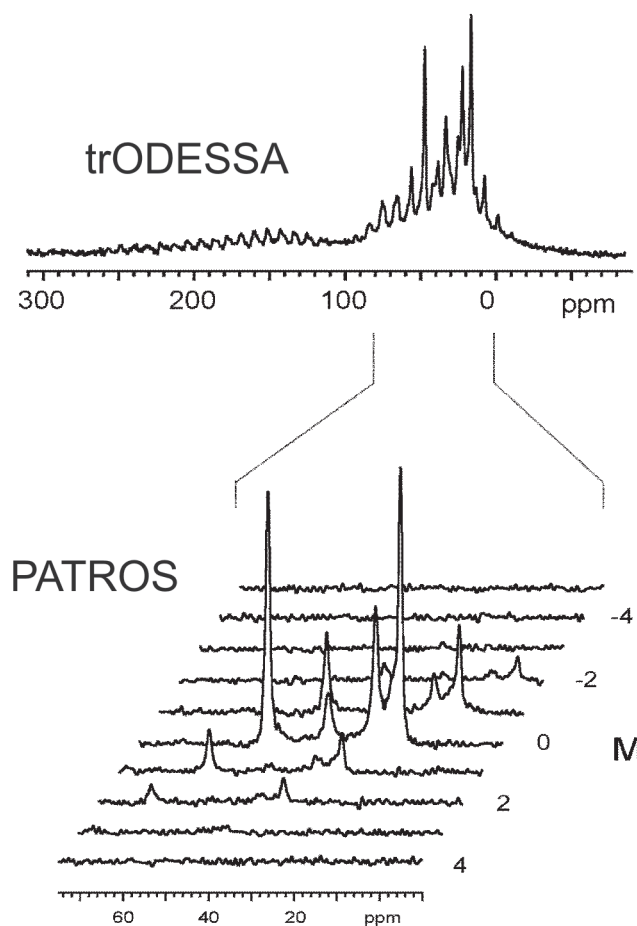


Fig.2.17 PATROS (bottom) and trODESSA (top) spectra of PnBMA

The PATROS spectrum (fig. 2.17) shows a clear separation of the different signals in our polymer (PnBMA). The signal corresponding to the COO group does not show up in the spectrum due to the slow spinning rate required to apply the PASS sequence and the T_2 relaxation during the

pulses and the $\frac{T_R}{2}$ delay. By plotting the intensity of the N=0 order of each spinning sideband, we get the PATROS decay which like in trODESSA case contains information about molecular exchange and T_1 relaxation.

2.3.4 CODEX (Centerband-Only Detection of EXchange)

As demonstrated in the previous paragraphs (2.2-2.3) the sensitivity of ODESSA-like experiments to the dynamic and magnetic parameters depends on the spinning frequency ω_R . By rotating at higher spinning rates the intensity and number of the spinning sidebands are reduced and therefore the change in the intensities during the mixing time τ_m and the accuracy of the results are also reduced. As we know the best condition to run ODESSA/trODESSA experiments is when $\omega_R \cong \frac{\Delta\sigma}{4}$ which sometimes, as we remarked on paragraph 2.3.3, is not convenient.

This impediment may be avoided by the CODEX experiment [de Azevedo99; de Azevedo00] which can be performed efficiently even at higher spinning rates. In the following we shall see that performing two short series of 1D-MAS spectra, the correlation function, correlation time, and motional amplitude can be determined for each site with a resolved line in the MAS spectrum. The recoupling efficiency (which characterize the degree of reintroduction of the CSA) depends only on the total time of recoupling (NT_R) and can be easily adjusted for different spinning rates.

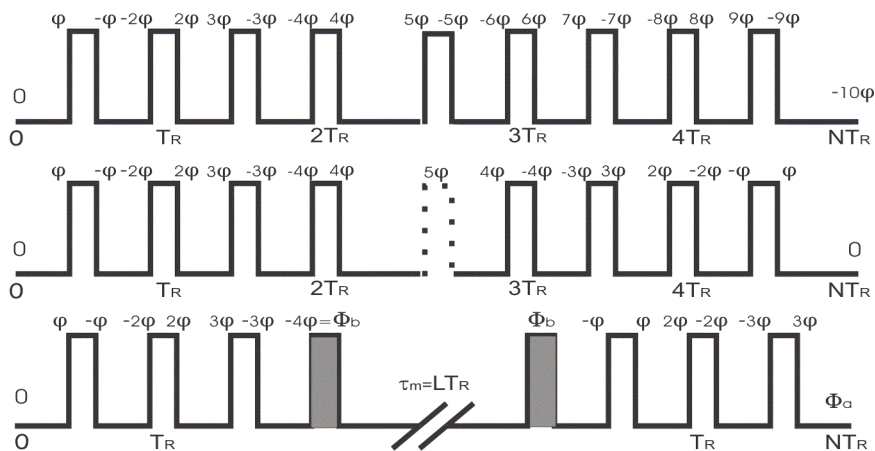


Fig. 2.18 The effect of the π pulses on the phase in a MAS experiment

In the CODEX experiment one use a train of π pulses separated by a $\frac{T_R}{2}$ period before and after the mixing time. Again the mixing time is chosen to be an integer number of rotation period T_R . The $\frac{\pi}{2}$ store pulse before the mixing time is set along $-y$ or x direction. After the mixing time, another $\frac{\pi}{2}$ is applied and again the train of π pulses identical with the one from the evolution period (fig. 2.18).

Before going into details about the signal generated in a CODEX experiment we should have a look at the effect of applying π pulses in a MAS experiment (fig. 2.18). If one apply a π pulse at half of the rotor period in a MAS experiment at the end of the rotation period the phase change introduced by the π pulse will be :

$$\Phi(T_R) = -\int_0^{\frac{T_R}{2}} \omega(t) dt + \int_{\frac{T_R}{2}}^{T_R} \omega(t) dt = -\int_0^{\frac{T_R}{2}} \omega(t) dt + \left(\int_0^{T_R} \omega(t) dt - \int_0^{\frac{T_R}{2}} \omega(t) dt \right) = -2 \int_0^{\frac{T_R}{2}} \omega(t) dt \quad (2.45)$$

If $N\pi$ are applied after each half of rotation period, the phase will be:

$$\Phi(NT_R) = -N \left(\int_0^{\frac{T_R}{2}} \omega(t) dt - \int_{\frac{T_R}{2}}^{T_R} \omega(t) dt \right) = -2N \int_0^{\frac{T_R}{2}} \omega(t) dt \quad (2.46)$$

In case that during one rotor period a π is omitted the total phase will be zero, as one can see in figure 2.18 (middle). Again, if instead of the omitted π pulse we insert two $\frac{\pi}{2}$ pulses separated by a mixing time period the total phase accumulated after applying the train of π pulses synchronized with the rotor period will have the following form:

$$\Phi(NT_R) = -2\frac{N}{2}\Phi^b + 2\frac{N}{2}\Phi^a = N(\Phi^a - \Phi^b) \quad (2.47)$$

Equation (2.47) describes the effect of the π pulses from the CODEX pulse sequence; between the pulses a dephasing factor $\Phi(0, \frac{T_R}{2})$ due to the chemical shift anisotropy will be created.

Before the mixing time this dephasing effect is accumulated so that even that Φ is small with a considerable number of π pulses a significant dephase may be achieved. If the echo combination of cosine and sine sets of data is performed, rephasing will be achieved after the mixing time, so that in case that no exchange occurs ($i=j$) cancellation of the dephasing will be complete. If during the mixing time period an exchange process occurs ($i \neq j$), the phase acquired during the second train of π pulses will be different and therefore, the rephasing will not be complete and therefore the intensities in the spinning sideband spectrum will be reduced. The resulted CODEX spectrum will provide informations about kinetic and chemical shift parameters, like the ODESSA/trODESSA spectrum.

After the first $\frac{T_R}{2}$ rotor period the transverse magnetization will be $e^{-i\omega_0\sigma_{iso}^j \frac{T_R}{2}} f^j(\gamma) f^{*j}(\gamma + \omega_R \frac{T_R}{2})$.

The next π pulse along the x direction, flips the magnetization which will become $e^{i\omega_0\sigma_{iso}^j \frac{T_R}{2}} f^{*j}(\gamma) f^j(\gamma + \omega_R \frac{T_R}{2})$. Now, knowing that the dephasing in the second half of the rotor period is identical with the one after the first half, after one full rotor period this yields:

$e^{-i\omega_0\sigma_{iso}^j \frac{T_R}{2}} f^j(\gamma) f^{*j}(\gamma + \omega_R \frac{T_R}{2}) \times e^{i\omega_0\sigma_{iso}^j \frac{T_R}{2}} f^{*j}(\gamma) f^j(\gamma + \omega_R \frac{T_R}{2}) \xrightarrow{\omega_R \frac{T_R}{2} = \pi} [f^{*j}(\gamma) f^j(\gamma + \pi)]^2$. In CODEX experi-

ment this is repeated for n rotor cycles so that the transverse magnetization becomes [Luz02] $[f^{*j}(\gamma) f^j(\gamma + \pi)]^{2n}$. Here one must bear in mind that by applying the train of π pulses, the dephasing due to chemical shift isotropy is canceled, while the dephasing due to the chemical shift anisotropy is accumulated. As one can see in figure 2.19, now a $\frac{\pi}{2}$ pulse will store one component of the transverse magnetization along the z -direction, and after a rotor synchronized mixing time period another $\frac{\pi}{2}$ pulse bring it back to the transverse plane. Before acquiring the signal with a combination of C-iS of data sets, another train of π pulses is applied, its effect being now:

$[f^i(\gamma + \omega_R \tau_m) f^{*i}(\gamma + \omega_R \tau_m + \pi)]^{2n} \xrightarrow{\omega_R \tau_m = \omega_R L T_R = 2\pi L} [f^i(\gamma) f^{*i}(\gamma + \pi)]^{2n}$.

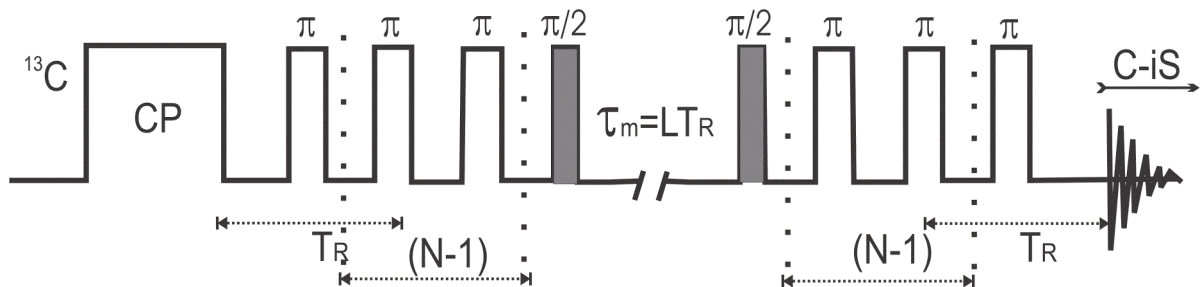


Fig. 2.19 CODEX pulse sequence

Considering again the f -function formalism, the acquired CODEX signal will have the following characteristics:

$$\begin{aligned}
M^{CODEX,ij}(nT_R, \tau_m, t) &= e^{-\frac{t+2nT_R}{T_2}} \left[f^{*j}(\gamma) f^j(\gamma + \pi) f^i(\gamma) f^{*i}(\gamma + \pi) \right]^{2n} e^{-i\omega_0 \sigma_{iso}^i t} f^{*i}(\gamma) f^i(\gamma + \omega_R t) \\
&= e^{-\frac{t+2nT_R}{T_2}} e^{-i\omega_0 \sigma_{iso}^i t} f^{*i}(\gamma) \left[f^{*j}(\gamma) f^j(\gamma) \right]^{2n} \left[f^j(\gamma + \pi) f^{*i}(\gamma + \pi) \right]^{2n} f^i(\gamma + \pi + \omega_R t - \pi) \\
&= e^{-\frac{t+2nT_R}{T_2}} e^{-i\omega_0 \sigma_{iso}^i t} f^{*i}(\gamma) \left[f^{*j}(\gamma) f^j(\gamma) \right]^{2n} \int d\theta \delta(\theta - \gamma - \pi) \left[f^j(\theta) f^{*i}(\theta) \right]^{2n} f^i(\theta + \omega_R t - \pi) \\
&= e^{-\frac{t+2nT_R}{T_2}} e^{-i\omega_0 \sigma_{iso}^i t} f^{*i}(\gamma) \left[f^{*j}(\gamma) f^j(\gamma) \right]^{2n} \int d\theta \sum_M e^{-iM\theta} e^{iM\gamma} e^{iM\pi} \left[f^j(\theta) f^{*i}(\theta) \right]^{2n} \int d\phi \delta(\phi - \omega_R t + \pi) f^i(\phi) \\
&= e^{-\frac{t+2nT_R}{T_2}} e^{-i\omega_0 \sigma_{iso}^i t} f^{*i}(\gamma) \left[f^{*j}(\gamma) f^j(\gamma) \right]^{2n} e^{iM\gamma} \int d\theta \sum_M e^{-iM\theta} e^{iM\pi} \left[f^j(\theta) f^{*i}(\theta) \right]^{2n} \int d\phi \sum_N e^{-iN\phi} e^{iN\omega_R t} e^{-iN\pi} f^i(\phi)
\end{aligned} \tag{2.48}$$

Again the integration $\int d\gamma$ must be performed and the result yields:

$$M^{CODEX,ij}(nT_R, \tau_m, t) = e^{-\frac{t+2nT_R}{T_2}} e^{i\omega_0 \sigma_{iso}^i t} \sum_N e^{iN\omega_R t} C_N^{CODEX,ij} \tag{2.49}$$

where the term which gives the spinning sidebands intensities in the CODEX spectrum is:

$$C_N^{CODEX,ij} = \sum_{M,N} e^{i(M-N)\pi} \int d\gamma e^{iM\gamma} f^{*i}(\gamma) \left[f^{*j}(\gamma) f^j(\gamma) \right]^{2n} \int d\theta e^{-i(M-N)\theta} \left[f^j(\theta) f^{*i}(\theta) \right]^{2n} \int d\phi e^{-iN\phi} f^i(\phi) \tag{2.50}$$

In the particular case when no reorientation of the molecular segments occurs ($i=j$), the equation (2.49) becomes much simpler:

$$M^{CODEX,ij}(nT_R, \tau_m, t) = e^{-\frac{t+2nT_R}{T_2}} e^{i\omega_0 \sigma_{iso}^i t} \sum_N e^{iN\omega_R t} F_N^j F_N^{*j} \tag{2.51}$$

which represents in fact a normal MAS spectrum.

We must mention here that in all the expressions describing the signal of MAS exchange spectrum we deliberately omitted to insert the term $e^{-\frac{\tau_m}{T_1}}$ which describes the loss of the signal due to the spin-lattice relaxation during the mixing time period. Therefore, to have an exact description of spectrum intensity this term must be added to all equations describing an exchange experiment together with additional integration over the rest of the Euler angles (α, β). We shall discuss in the next chapter how the effect of the T_1 relaxation must be subtracted from the exchange decay. Now we shall say that the CODEX experiment (like normalized-trODESSA or REDOR [Guillon89]) can do this in a relative simple manner. In this work we used a modified [deAzevedo99] CODEX pulse sequence, in which a second mixing time τ_z is used after the second train of π pulses (fig. 2.20).

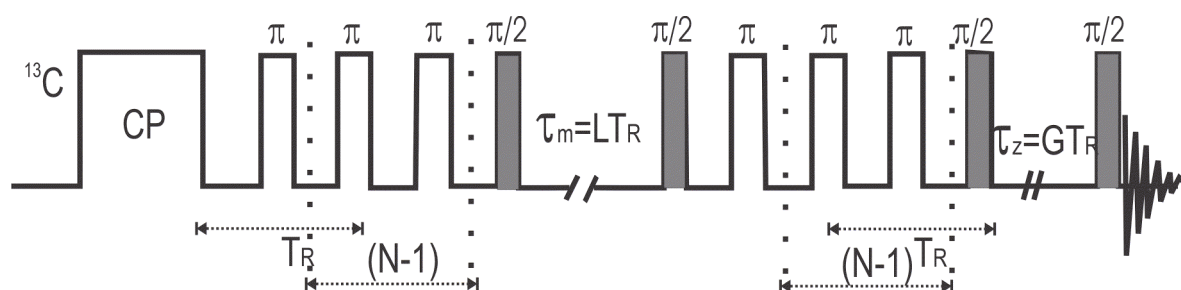


Fig.2.20 Schematic representation of CODEX pulse sequence with z -filter

The second mixing time period acts as a z -filter and it is sensitive only to the loss of the signal due to T_1 relaxation. To run such sort of CODEX experiments one has to set the first mixing time to the desired values while keeping the length of the z -filter as short as possible (usually one rotor period); in this way one gets a signal (let's call it S) which probes exchange, spin diffusion and T_1 relaxation. In the second part of the experiment one must set the value of the first mixing time very short (one rotor period) while giving the desired values of the mixing time to the z -filter. This yields a signal (let's call it S_0) which because it is sensitive only to the T_1 relaxation and not the exchange, we call it "reference". In this manner, allocating the desired values of the mixing time alternatively to the τ_m and τ_z , we acquire for each mixing time value two experiments: the "exchange" and the "reference". The condition that must be fulfilled is that $\tau_m + \tau_z = \text{const}$. By plotting the ratio S/S_0 versus the mixing time values, we obtain the CODEX decay which is influenced only by exchange process and spin diffusion and provides information about the correlation times and the amplitude of the motion.

Also one have to mention that there are two ways in which a CODEX experiment can be run. On one hand, we can choose an array of mixing time and in this case we acquire a CODEX spectrum in which by plotting the ratio S/S_0 versus the mixing time (fig. 2.21 left) we obtain informations about the correlation time τ_c , and some hints about the number of sites involved or the mobile fraction, that means the number of the nuclei which actually participate in the exchange process. On the other hand one may array the other parameter from the CODEX sequence, namely the recoupling period NT_R or the number of rotor cycles, and obtaining a CODEX decay which provides information about the reorientation angle (fig. 2.21, right).

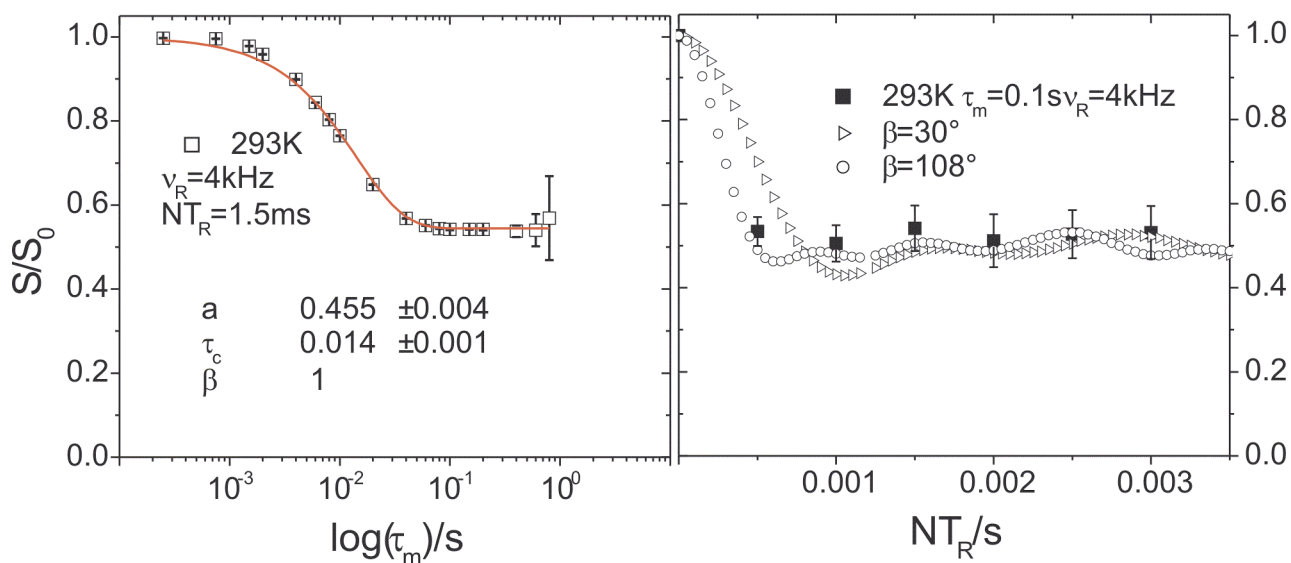


Fig.2.21 DMS, mixing time (left) and NT_R (right) CODEX dependence

One must be careful about assigning the number of sites of the reorientation motion, the best results being obtained when the 4-times-CODEX pulse sequence is used. Usually, if one consider that all the spins participate in the exchange process, for a jump involving two sites, the CODEX decay reaches a plateau at an asymptotic value $a = 1 - 1/n = 0.5$, where n means the number of sites. The long-time exchange intensity ($E_\infty = 1 - a = f_m(1 - 1/n)$), which depends also on the number of equivalent orientational sites accessible in the exchange process, provides information about the number of segments directly involved in the exchange (mobile fraction f_m). In the case of a two-site process, like for DMS, this would mean that at least a fraction $1/n$ of the mobile species will be found in the originally selected site [Bonagamba01]. a values higher than 0.5 would mean an increased number of sites involved in the exchange process and/or a change in the mobile fraction. Sometimes, due to the fact that only small fractions of the spins participate in the exchange, the

plateau is reached at a value for which from the normal CODEX experiments we can not say exactly how many sites are involved. In this case, it is better to use the 4-times-CODEX variant of the method. Also there are cases when the asymptotic plateau is reached for a value of 0.5 but this does not necessarily indicates the existence of a two site jump, but the fact that the detected process fits good in our experimental window.

Figure 2.21 shows an example of CODEX data for DMS obtained from an mixing time dependence, and NT_R -dependence. In the right part, besides the experimental points acquired from CODEX NT_R dependence experiments, some simulations are showed to illustrate how different jump angles of the exchange process may affect the slope and the shape of the CODEX decay. In the case of DMS, we know that the motion involves jumps with a 108° angle of the two equivalent methyl groups (see figure 2.9), therefore the experimental points are best fitted with the simulated curve indicating a 108° jump. From the mixing time dependence, we obtain, as mentioned before, information about the correlation time τ_c and its distribution width β . After fitting the experimental points with a KWW function (figure 2.21 left), we obtain $a=0.45$, which means that at this temperature the detected process in the middle of our experimental window. Increasing or decreasing the temperature, this value will change, which means that the process is shifted or the mobile fraction changes.

As one observe, it is trivial to explain the behavior of the curve from the right side of the figure by the existence of an exchange process involving two sites (see also fig. 2.9). To correlate the results from both type of experiments one must run the recoupling period dependence at a mixing time for which the exchange is done, so that we are in a plateau, otherwise the results may lead to wrong conclusions. The experiments and also the simulations [Luz02] show that the sensitivity of the CODEX experiment compared to the ODESSA/trODESSA is better only in the cases where high spinning frequency are required, but in a slow-MAS experiment, the CODEX performed with a small recoupling period has the same sensitivity like trODESSA.

CHAPTER III

3.1 Spin diffusion in exchange experiments

As we saw in the previous chapters, NMR exchange experiments are based on the detection of a change in the resonance frequency after a mixing time period τ_m . This frequency change may occur due to the molecular reorientations of the different segments or could appear also as a result of the spin diffusion. The term spin diffusion refers to the transfer of magnetization by means of dipolar interactions between spins. The dipolar magnetization transfer depends on the spin species involved, specially on their abundance and strength of the dipolar couplings between them. Due to the fact that the 1H is the most abundant spin species, the spin diffusion processes involving protons are most relevant in polymers. But samples, as polymers, contains ^{13}C and in exchange experiments with mixing times comparable to the inverse of the dipolar decoupling strength (ω_D^{-1}) the spin diffusion becomes relevant also for these nuclei (the ^{13}C - ^{13}C dipolar couplings have a strength of 15 Hz for average internuclear distances of 7 Å). For 1H spin diffusion in polymers, the proton-proton dipolar coupling is the dominating interaction (for 1H - 1H coupling strength is 40000 Hz) and therefore makes the spin diffusion process very efficient [KSR94]. The ^{13}C "proton driven" spin diffusion, is determined by the powerful 1H - ^{13}C couplings (20000 Hz) . The latest theory and results in NMR experiments have demonstrated that the term "spin diffusion" should not be understood in the classical way of a diffusion process. Due to its nature of a dipolar transfer of magnetization the nomenclature of "dipolar magnetization transfer" should be a more appropriate name. However, the experimental data for protons show an initial $\tau_m^{1/2}$ dependence typical for diffusive processes [KSR94].

If we consider the effect of both spin diffusion and relaxation, the evolution of z -magnetization is described by the following equation:

$$\frac{dM_z(r,t)}{dt} = DM_z(r,t) - \frac{M_z(r,t) - M_\infty}{T_1(r)} \quad (3.1)$$

which in case that the T_1 is independent of r , has the following solution:

$$M_z^d(r, \tau_m) = M_z^d{}_{diffus}(r, \tau_m) e^{-\frac{\tau_m}{T_1}} \quad (3.2)$$

the term $M_z^d{}_{diffus}(r, \tau_m)$ being the solution in case that the T_1 relaxation is not present.

The effect of dipolar transfer of magnetization is the base for several types of experiments like Goldman-Shen (1966) or 2D-WISE experiment (1992), which investigate the molecular (crystal-line) structure in organic solids. On the other hand, the spin diffusion process (SD) can become a concurrent process for molecular exchange, while the exchange experiment detects only the frequencies of the investigated spins and does not provide information about the state of the system during the mixing time and therefore can not distinguish between different dynamic processes. Therefore it is expected that in exchange spectra information about molecular exchange, spin diffusion, and also T_1 relaxation is contained.

To restrict these effects, the maximal range of the mixing times must be limited to 1 to 10 seconds. Therefore the question about how we can retain from our results only the part referring to the molecular exchange must be raised.

In the following, we shall consider the presence of the spin diffusion as "proton driven" process, in this case the SD-rate between two ^{13}C nuclei is [Abragam61]:

$$k_{ij} = \frac{\pi}{2} g_{ij}(0) \omega_D^{ij2} \quad (3.3)$$

where the dipolar coupling is:

$$\omega_D^{ij} = \frac{\gamma_C^2 h}{2\pi r_{ij}^3} \frac{1}{2} (1 - 3\cos^2\theta_{ij}) \quad (3.4)$$

The spin diffusion rate depends on the 6-th power of the distance r_{ij} between the nuclei and the angle θ_{ij} that this vector makes with the external magnetic field. Function $g_{ij}(0)$ represents the intensity of the ^1H zero-quantum transition at the frequency difference between the ^{13}C resonances and gives the probability for two carbon resonances to have the same resonance frequency. In good approximation, this can be considered as an overlapping signal of proton coupled line shapes:

$$g_{ij}(0) = \int g_i(\omega) g_j(\omega) d\omega \quad (3.5)$$

which depends on the difference of the chemical shift isotropies $\delta = \omega_0^i - \omega_0^j$ and the width of the resonance Δ . The above equations are valid only in the static case, but one can consider that they work also in the case of fast- and slow- MAS. The reason is that by rotation, the time-dependent resonance frequencies of the interacting spins overlap each other just for a short time, during which the quasi-static approximation may be considered. From equation (3.3) it is obvious that besides the internuclear vector r_{ij} , the spin rate k_{ij} depends also on the probability $g_{ij}(0)$, which can be influenced by the 1H -coupling during the mixing time period and therefore it is influenced by the linewidth of the resonance lines. Therefore, the spin diffusion is stronger during the mixing time, in contrary to the believe that it is just a weak effect.

The solution of the problem related to the separation of the spin diffusion effect from the molecular exchange comes from the simple fact that while the molecular exchange is temperature dependent, the spin diffusion in a good approximation is not. Therefore, by cooling the sample at temperatures where we consider that the molecular exchange is "frozen" ($\tau_c \gg \tau_m$) and performing a typical exchange experiment we shall obtain a decay which provides information only about the spin diffusion, this one being the only process still active. In this way, the contribution of the spin diffusion to the signal decay can be easily subtracted from all the experiments recorded at higher temperatures than the one considered to have only the spin diffusion.

3.2 Kinetic parameters in Markov processes. Spin diffusion correction. Data normalization.

Let us consider again the typical 2D-exchange experiment, where the exchange spectrum is dependent of the mixing time τ_m . In the case of short mixing times, $\tau_m \ll \tau_c$, the spectrum will consist only of diagonal peaks, while for longer mixing times, $\tau_m \gg \tau_c$, also off-diagonal peaks appear. The 2D- exchange spectrum is given by the equation:

$$S(\omega_1, \omega_2, \tau_m) = \sum_{ij} P_{ij}(\tau_m) S_{ij}(\omega_1, \omega_2) \quad (3.6)$$

where i and j are the different frequencies with which a nucleus can precess. $S_{ij}(\omega_1, \omega_2)$ are the 2D-subspectra in the case that the nucleus was before the mixing time in the state j and after in the state i . The case $i=j$ means the absence of the exchange process or by mean of many individual processes the spins are back in the initial state. $P_{ij}(\tau_m)$ gives the fraction of spins which were before the mixing time in the state j and after the mixing time in the state i and it is a product between probability W_{ij} to find the spins in one of the two states and the probability P_j to find the spin before the mixing time in the state j . Considering the case of a stationary Markov process we have [Torchia82,Favre98]:

$$\frac{dW_{ij}(\tau_m)}{dt} = \sum_{k=1}^N k_{ik} W_{kj}(\tau_m) \quad (3.7)$$

with the initial condition $W_{ij}(0) = \delta_{ij}$. We shall consider the easiest case of a jump motion between N equivalent sites (any possible state in which we can find the considered spin), $P_j = 1/N$. In this case we obtain a relaxation matrix \bar{K} with the off-diagonal elements k_{hop} and $-(N-1)k_{hop}$ on the diagonal. The off-diagonal elements describe the probability of transition between two sites. We must consider also the rate k_{micro} of a nucleus to leave the state in which it is. Between these rates and the correlation time we have the following relations:

$$\begin{aligned} k_{micro} &= (N-1)k_{hop} \\ \tau_c &= \frac{P_j}{k_{hop}} = \frac{1}{Nk_{hop}} = \frac{N-1}{Nk_{micro}} \end{aligned} \quad (3.8)$$

The solution to equation (3.7) is [Favre98]:

$$W_{ij}(\tau_m) = \frac{1}{N} + \left(\delta_{ij} - \frac{1}{N}\right) e^{-Nk_{hop}\tau_m} = e^{-\frac{\tau_m}{\tau_c}} \delta_{ij} P_i + \left(1 - e^{-\frac{\tau_m}{\tau_c}}\right) \frac{1}{N} \quad (3.9)$$

$$P_{ij}(\tau_m) = W_{ij}(\tau_m) P_i = e^{-\frac{\tau_m}{\tau_c}} \delta_{ij} P_i + \left(1 - e^{-\frac{\tau_m}{\tau_c}}\right) P_i P_j \quad (3.10)$$

With these equations the probability $P_{ij}(\tau_m)$ can be described using the both rates, [Reichert00]:

$$P_{ij}(\tau_m) = \left[e^{\overline{K}\tau_m} \right]_{ij} P_j \quad (3.11)$$

In the case of a symmetric two-site jump we obtain after diagonalization and calculation of the eigenvalues of the exchange matrix \overline{K} :

$$P_{ij}(\tau_m) = \frac{1}{4} \begin{pmatrix} 1 + e^{-2k_{hop}\tau_m} & 1 - e^{-2k_{hop}\tau_m} \\ 1 - e^{-2k_{hop}\tau_m} & 1 + e^{-2k_{hop}\tau_m} \end{pmatrix} e^{-\frac{\tau_m}{T_1}} \quad (3.12)$$

A more complicated matrix must be used in the case of exchange involving more than two sites and when also the spin diffusion must be taken into account. Therefore, we should consider first a simple example: a three sites process (fig.3.1) were only the jump between the site 1 and 2 means an exchange process at a rate k_{ME} , the third one being a generalization of all other carbons in the sample and being connected with the first two only by spin diffusion with a rate k_{SD} .

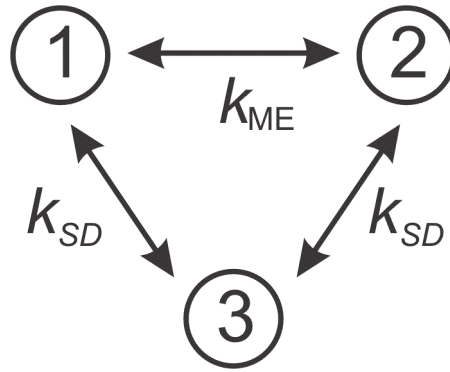


Fig.3.1 Schematic representation of a 3-sites exchange process. Only the first sites (1,2) are connected through a molecular reorientation process. The third site, represents all other carbons in the sample and are involved only in the spin diffusion process.

Following the approach given in literature [Krushelnitski99; Pascui02] we can write the exchange matrix \overline{K} like:

$$\stackrel{=}{K} = \begin{pmatrix} -k_{ME} - k_{SD} - \frac{1}{T_1} & k_{ME} & k_{SD} \\ k_{ME} & -k_{ME} - k_{SD} - \frac{1}{T_1} & k_{SD} \\ k_{SD} & k_{SD} & -2k_{SD} - \frac{1}{T_1} \end{pmatrix} \quad (3.13)$$

In this case the solution of the equation (3.7) becomes:

$$I^N(\tau_m) = \left(A^N + B^N e^{-3k_{SD}\tau_m} + C^N e^{-\left(k_{SD} + 2k_{ME}\right)\tau_m} \right) e^{-\frac{\tau_m}{T_1}} \quad (3.14)$$

where the parameters A^N, B^N, C^N depend on the mutual orientations of the CSA tensors of the carbons at the different sites. In the case of an amorphous sample these parameters do not provide any additional information. The fact that the spin diffusion is a process involving many sites, we actually have to consider that the term A^N might become very small and the other exponential must be replaced by a KWW function [Lindsey80; Cumbera93]:

$$I^N(\tau_m) = \left(B^N e^{-3\left(\frac{\tau_m}{\tau_{SD}}\right)^\beta} + C^N e^{-\left(\frac{\tau_m}{\tau_{SD}}\right)^\beta} e^{-\left(\frac{\tau_m}{\tau_c}\right)} \right) e^{-\left(\frac{\tau_m}{T_1}\right)} \quad (3.15)$$

where $\tau_c = \frac{1}{2k_{ME}}$, $\tau_{SD} = \frac{1}{k_{SD}}$, $0 < \beta < 1$. Usually β , which gives the width of the distribution of the

spin diffusion times, is between 0.6-0.7 and, therefore, we can approximate the term $e^{-3\left(\frac{\tau_m}{\tau_{SD}}\right)^\beta}$ by

$e^{-\left(\frac{\tau_m}{\tau_{SD}}\right)^\beta}$ in equation (3.15). Anyway the term 3 of the exponent arise from the arbitrary three-sites spin diffusion model that we chose. Then the equation (3.15) becomes:

$$I^N(\tau_m) = \left(B^N + C^N e^{-\left(\frac{\tau_m}{\tau_c}\right)} \right) e^{-\left(\frac{\tau_m}{\tau_{SD}}\right)^\beta} e^{-\left(\frac{\tau_m}{T_1}\right)} \quad (3.16)$$

Now, by running an experiment at lower temperatures where the molecular exchange is "frozen" we can obtain the rate of the spin diffusion process, which later allows us to subtract the spin diffusion effect from our exchange curves. After spin diffusion correction, we still have to remove also the effect of the T_1 relaxation. This is done by running in the same conditions (spin rate, temperature, etc.) a Torchia experiment [Torchia82] from which we obtain the values of the relaxation times. By replacing these values in equation (3.16) and multiplying by the term $\exp(\tau_m/T_1)$ we obtain exchange decays which provide information only about the correlation times of the molecular reorientation process:

$$I_{corrected}^N(\tau_m) = \left(B^N + C^N e^{-\left(\frac{\tau_m}{\tau_c}\right)} \right) \quad (3.17)$$

from which we can obtain the relative amplitude of the exchange component $a^N = C^N / (C^N + B^N)$ and the correlation time.

In the case of CODEX or normalized-trODESSA experiments (see chapter 2.3.4), due to the fact that we use the z -filter, there is no need to perform an additional Torchia experiment, while the T_1 correction is done internally by the fact that the "reference" spectrum is sensitive only to the relaxation process. In amorphous polymers, we expect also a distribution of the correlation times and not a single Debye process, therefore a KWW fitting function must be used. In the following we describe shortly how the spin diffusion and relaxation correction is done in a CODEX experiment.

The first mixing time in the CODEX experiment (or the so-called "exchange" part), is sensitive to molecular exchange, spin diffusion and relaxation, therefore the spectrum can be described with such an equation:

$$S^N(\tau_m, \tau_z) = \left(1 - a^N + a^N e^{-\left(\frac{\tau_m}{\tau_c}\right)^\beta} \right) e^{-\left(\frac{\tau_m}{\tau_{SD}}\right)^\beta} e^{-\left(\frac{\tau_m + \tau_z}{T_1}\right)} \quad (3.18)$$

The second part of the CODEX experiment, is sensitive only to T_1 relaxation and must be described like:

$$S_0^N(\tau_m, \tau_z) = e^{-\left(\frac{\tau_m + \tau_z}{T_1}\right)} \quad (3.19)$$

By dividing the equation (3.18) to (3.19) we obtain besides the T_1 correction also an internal normalization of the signal, that means that the CODEX decays from all the temperatures will start at the maximum intensity 1 and will decay in the limit case of infinite mixing time to zero. Then we can write the CODEX decay as:

$$\frac{S^N(\tau_m)}{S_0^N(\tau_m)} = \left(1 - a^N + a^N e^{-\left(\frac{\tau_m}{\tau_c}\right)^\beta} \right) e^{-\left(\frac{\tau_m}{\tau_{SD}}\right)^\beta} \quad (3.20)$$

For an experiment performed in the conditions described as above, the term for the spin diffusion

will be $\frac{S^{SD}(\tau_m)}{S_0^{SD}(\tau_m)} = e^{-\left(\frac{\tau_m}{\tau_{SD}}\right)^\beta}$ and after the spin diffusion correction the CODEX decay will obey the expression:

$$\frac{S(\tau_m)}{S_0(\tau_m)} = \left(\frac{S^N}{S_0^N} \right) / \left(\frac{S^{SD}}{S_0^{SD}} \right) = \left(1 - a^N + a^N e^{-\left(\frac{\tau_m}{\tau_c}\right)^\beta} \right) \quad (3.21)$$

where a can provide information about the mobile fraction or the number of sites. In the case of an exchange process involving only two sites (ex. DMS for a certain value of the recoupling period

NT_R at a mixing time $\tau_m > \tau_c$) $a \sim 0.5$, the highest possible value being 1 (no exchange) and the lowest 0 which would mean an exchange process involving an infinite number of sites (diffusion-like process).

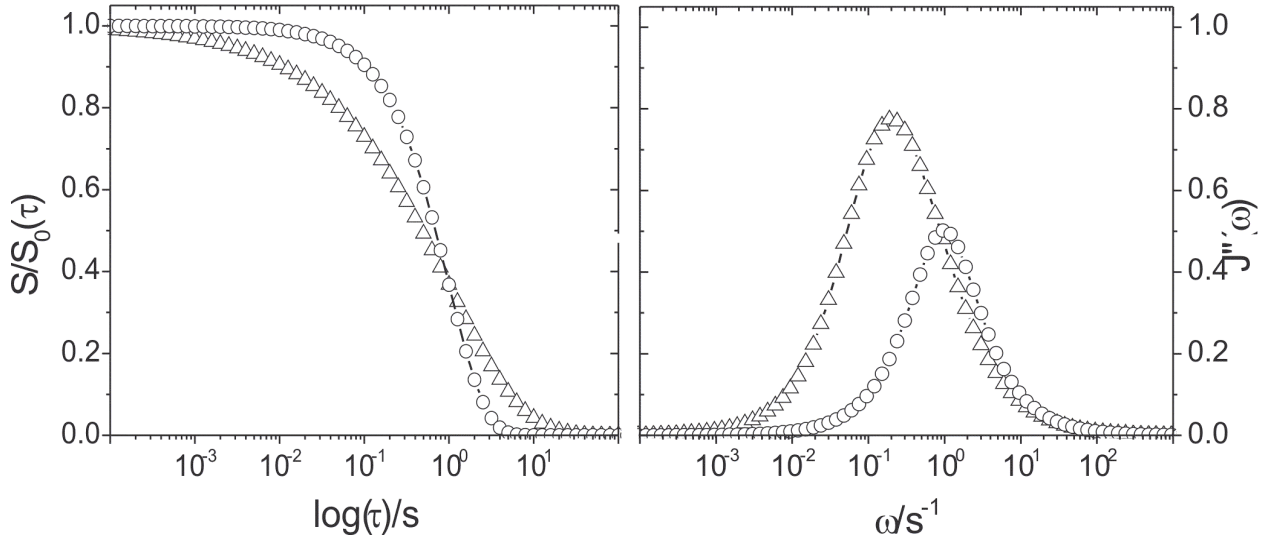


Fig.3.2 Difference between a single exponential (open circles) and a KWW function (open triangles) with $\beta = 0.7$ (left) and their correspondents in the frequency domain (right)

As we already mentioned, the parameter β is related to the existence of a distribution of correlation times, typical values for amorphous polymers being 0.5. In the case of a single exponential ($\beta = 1$) the spectral density is a Lorentzian line center around the frequency ν_{\max} with a full-width-at-half-maximum-height $\delta\nu$ of about 1.4 frequency decades. For $\beta < 1$, the maximum is shifted according to [Schröter98] :

$$\ln(2\pi\nu_{\max}\tau_c) = 0.60607(\beta - 1) \quad (3.22)$$

broadening the spectral density (fig.3.2). The ν_{\max} which we call it "frequency peak" will be plotted in the Arrhenius diagram. In NMR experiments we assumed a log-Gaussian distribution, and to correlate the values of β with the width of such a distribution we used the formula:

$$\frac{S}{S_0}(\tau_m, \tau_0, \delta\nu) = \int_{-\infty}^{\infty} \frac{1}{\sqrt{2\pi} \delta\nu} \exp\left[-\frac{\left(\ln\frac{\tau_c}{\tau_0}\right)^2}{2(\delta\nu)^2}\right] \exp\left(-\frac{\tau_m}{\tau_c}\right) d\ln\tau_c \quad (3.23)$$

The KWW curves for different β values describing the decays were fitted with the expression (3.23), this providing us the equivalent log-Gaussian distribution in the frequency domain ($\delta\nu$). In the next chapter, to show the existence of the distribution of correlation times, in the Arrhenius diagrams we shall plot the maximum frequency ν_{\max} and its distribution like vertical bars with the length $\delta\nu$.

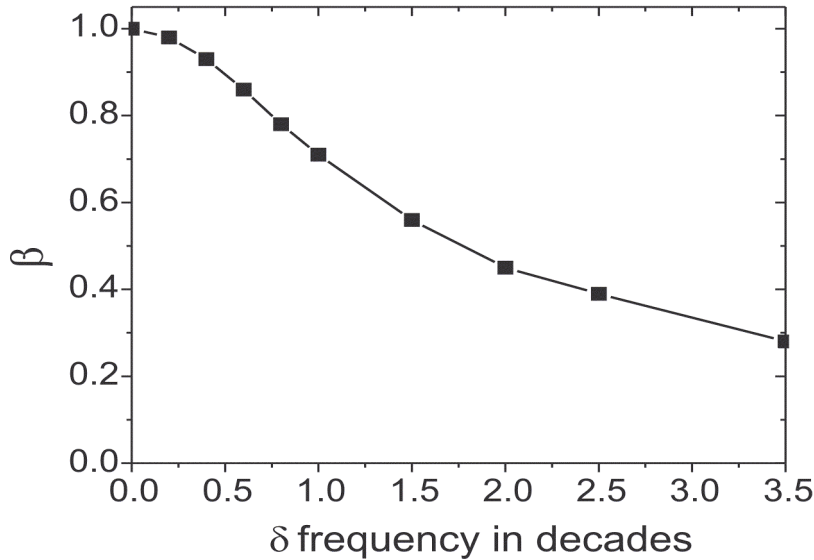


Fig.3.3 Correlation between the width of distribution of a KWW function and the equivalent width of a log-Gaussian distribution according to eq.(3.23)

A similar approach for correction of the experimental data was used also for trODESSA and PATROS experiments. Here due to the absence of the z -filter experiment, a Torchia experiment was performed to assure the proper correction of the data for the T_1 relaxation. For these types of experiments an artificial normalization was performed after the T_1 correction by fitting the data with an expression similar to (3.17) and then divided the experimental data with the sum $(B^N + C^N)$ obtained in the previous step. After that the spin diffusion correction and the fit procedure was similar with

that from the CODEX case. An similar approach to the CODEX was used in an attempt to obtain an internal normalization of the data for the trODESSA experiments. The trODESSA pulse sequence was modified by addition of a z -filter after the last $T_R/2$ delay. Again two experiments ("exchange" S and "reference" S_0) were recorded for each value of the desired mixing times. The results, similar to those from a CODEX experiment were plotted and compared with those from an usual trODESSA experiments (fig.3.4).

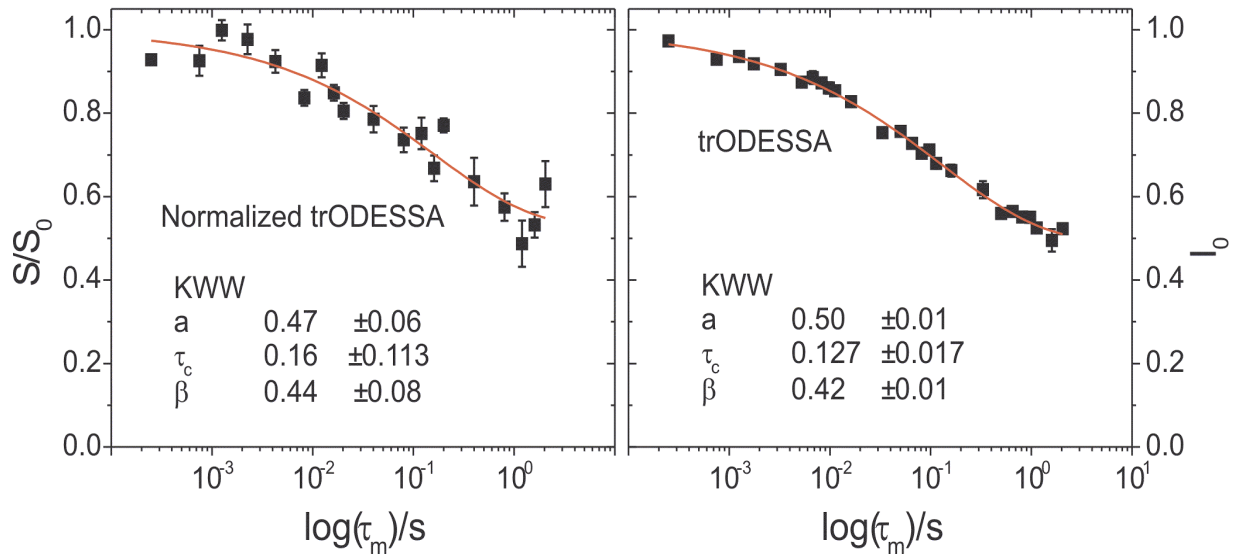


Fig.3.4 COO, PnBMA after correction for trODESSA (right) and normalized-trODESSA (left). Both experiments were recorded in the same condition and in the same experimental time (for more details see text).

The correlation time obtained from both types of experiments were identical, being an additional prove that the whole correction and fitting procedure was the right one. The plots from figure 3.4, were obtained in the same conditions, the total experimental time being the same. Due to the fact that two experiments must be acquired in the same experimental time, the signal-to-noise ratio in the plot showing normalized-trODESSA results is lower than for the simple trODESSA. One could ask now which are the criteria to choose between internal normalization and T_1 correction and the correction using an external Torchia experiment. In this work the signal-to-noise and the available experimental time were the criteria mostly used. One must bear in mind that using the z -filter in the trODESSA or CODEX experiments increases the length of the pulse sequence and therefore decreases the signal intensity due to T_2 relaxations. Also by adding another mixing time τ_z , for each desired value of the mixing time two experiments must be performed (exchange S and reference S_0) with the same number of acquisitions which doubles the total acquisition time. In the

same time the Torchia experiment provides a very good signal-to-noise ratio requesting a smaller number of acquisitions and therefore being a fast experiment. The disadvantages using the Torchia method come from the fact that in this case we have to perform a "computational normalization" which sometimes could be difficult.

Another way to extract the correlation times from the ODESSA/trODESSA exchange decays without the need for an external experiment to remove the T_1 effect was proposed by Favre et al. [Favre98]. The idea is to take the ratio of the combined intensities of all spinning sidebands excluding the center band and the integrated intensity of the entire spectrum to eliminate the exponential factor associated with the T_1 relaxation, was first applied for the EIS (*Exchange Induced Side bands*) experiments and then adjusted for the ODESSA/trODESSA methods. Therefore, instead of having a dependence of the intensity of a line of N -th order over the mixing time we will have a dependence of these ratios:

$$R_N^{ODESSA}(\tau_m) = \frac{(-1)^N I_N^{ODESSA}(\tau_m)}{\sum_N I_N^{ODESSA}(\tau_m)}$$

$$R_N^{trODESSA}(\tau_m) = \frac{I_N^{trODESSA}(\tau_m)}{\sum_N (-1)^N I_N^{trODESSA}(\tau_m)} \quad (3.24)$$

In this work, we preferred other correction methods despite the additional experimental time required, because ODESSA/trODESSA ratios (eq. (3.24)) contains in their denominators summations involving positive and negative peaks which would provide as result a small value. Also to apply this correction all ssb's must be recorded. Thus, the errors for correlation times obtained from ODESSA/trODESSA are expected to be large, if we consider also the influence of other factors like signal-to-noise, artifacts, etc.

Figure 3.5 shows a typical example for trODESSA decay before and after the spin diffusion correction. As one can see, without the spin diffusion correction one could think that the exchange process has a certain rate. After spin diffusion correction the correlation time of the detected process can change considerably as shown below.

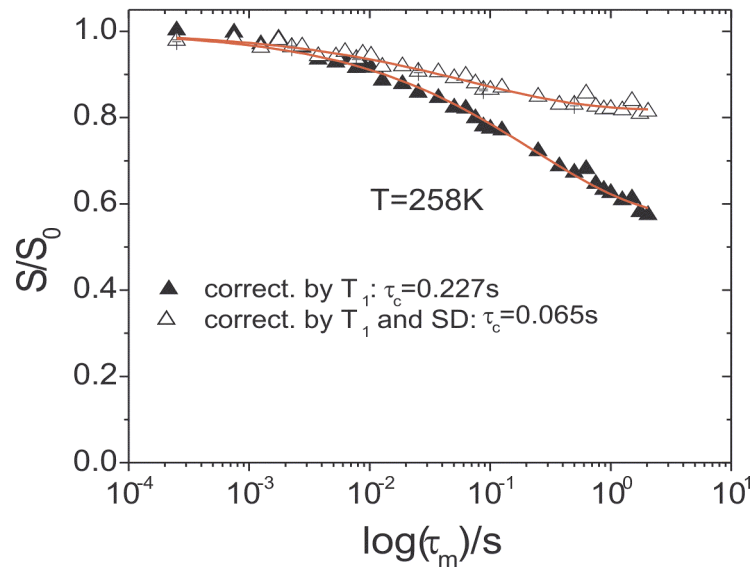


Fig.3.5 COO, PnHMA, in an trODESSA experiment
before and after spin diffusion correction

CHAPTER IV

This chapter presents the results obtained in the NMR investigation of the molecular dynamics in several types of polymers. The investigations were performed using the exchange experiments described in chapter II. The polymers investigated belong to the families of amorphous alkyl methacrylates and semicrystalline polymers. In the following, we refer to “topology of the exchange process” as jump angles, mobile fraction f_m and number of sites involved in the process.

4.1 Investigation of molecular exchange in poly-n-alkyl methacrylates.

From this family of amorphous polymers, PnBMA (poly-n-butylmethacrylate) and PnHMA (poly-n-hexylmethacrylate) were extensively investigated to obtain information about the molecular processes above and below their glass transition temperatures. The PnBMA sample was obtained from Polyscience Inc. and used as obtained. PnHMA was obtained from Dr. Maier (MPI Mainz) and used without further treatment. The glass temperatures, T_g , were determined by DSC (*differential scanning calorimetry*) using a temperature ramp of 10 K/min, as 254K for PnHMA and 298K for PnBMA. NMR experiments were performed on a VARIAN UNITY 200 spectrometer operating at 50.3 and 200.2 MHz for ^{13}C and ^1H , respectively, using a DOTY 7mm Super-Sonic VT CP-MAS probe and on a VARIAN INOVA 400 spectrometer operating at 100.5 and 399.8 MHz resonance frequencies for ^{13}C and ^1H , respectively, using a VARIAN 7mm VT CP-MAS probe with JACKOBSEN design. Standard constant amplitude cross-polarization (CP) and CW ^1H decoupling were applied in all experiments. Typical values of 1 ms for contact time (CP) were used together with $\frac{\pi}{2}$ pulses of 3.7 μs for ^1H , and 4.5 μs for ^{13}C . A temperature calibration, accounting for MAS heating, was performed before the experiments [Bielecki95]. The temperature was controlled with a standard temperature controller, the variations being less than 1°C. In these experiments typical spin rates of 2000 Hz were used both for trODESSA (at UNITY 200) and CODEX experiments (at INOVA 400), with a rotor stability better than 2 Hz. The spin rate was controlled by either a standard DOTY spin rate controller for UNITY 200 or the standard VARIAN MAS accessory on INOVA 400 spectrometer. In all experiments the rotor synchronization of the mixing time period

was achieved by converting the optical signal from the probe into a TTL signal and feed to the acquisition controller. For some experiments the built-in rotor synchronization facility of the spectrometer (INOVA 400) was used to obtain mixing times as short as $T_R/2$. The method is based on the existence of a high-frequency counter [Reichert,hab]. The “trigger“ signal (the optical signal which was converted in a TTL signal) starts the counter at the beginning of each rotation period. Before the first 90° pulse the counter is stopped and the time from the ”trigger“ is measured. The mixing time is applied and then the counter waits for the ”trigger“ before counting back to zero. After that the second 90° pulse is applied. This rotor-synchronization method is very simple but requires additional expensive hardware available for commercial spectrometers. For PnBMA and PnHMA, the recycle time was chosen to be 1 s and between 3200 and 5200 accumulations were necessary for both trODESSA and CODEX experiments to ensure an appropriate signal-to-noise ratio (and implicit smaller experimental error bars). A typical exchange experiment containing around 20 mixing times was performed in approximately 60 hours.

4.1.1 Exchange in PnBMA

Figure 4.1 shows the chemical structure of the monomeric units of PnBMA as well as the corresponding CP-MAS spectrum recorded on a 4.7 T magnet at a spin rate of $\nu_R = 2\text{kHz}$, at room temperature. Typical experiments regarding the COO group were performed using the trODESSA method while the results regarding the aliphatic groups were obtained from CODEX-type experiments (see figure 2.9 and the discussion in chapter II for more details). The symbol (*) in figure 4.1 marks the spinning sidebands of the COO line. The small signals at 100 ppm are originated from the spinning sidebands of the carbons from the main- and side- chain (#1, #2, #3). One may observe that for this spinning rate the COO lines are well resolved, and the existence of several spinning sidebands assures an optimal sensitivity of the trODESSA method regarding the molecular dynamics. Also we see that for the both CH_3 groups we get a superposition of the two lines, being impossible to distinguish them. The signals from the main chain carbons (lines #1 and #2) are well resolved, but the absence of the spinning sidebands at this spinning rate makes the application of trODESSA inefficient as discussed in chapter II. Therefore, after several attempts to use the PATROS to investigate the dynamics of these lines we decided that for the aliphatic carbons the CODEX method is more appropriate. Choosing between trODESSA and CODEX to investigate the dynamics of different lines in PnBMA (as well as in other samples) was made considering the width

of the CSA of the lines to be investigated, and the additional experimental time required by the CO-DEX sequence.

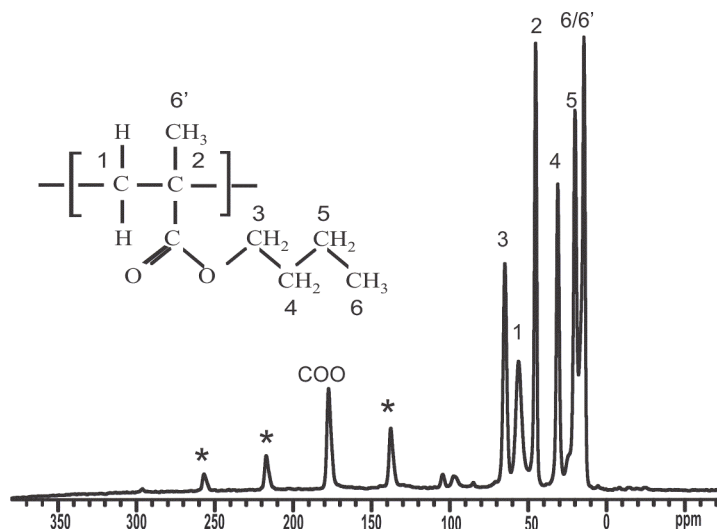


Fig.4.1 Chemical structure and CP-MAS spectrum of PnBMA

The experiments were performed at several temperatures, starting almost 50K below the glass transition temperature, up to 50K above T_g . The lowest temperature data was considered to contain only information about the spin diffusion process and was used for the spin diffusion correction procedure as described in the chapter III. To correct the data from the trODESSA experiments, additional T_1 measurements were required. The typical values of the spin-lattice relaxations obtained range between 8 s for COO to 0.35 s for the carbons of the side chain as one can see in appendix A. After obtaining the T_1 values, the T_1 -correction was done according the procedure described in the previous chapter. After both T_1 and spin diffusion corrections, the obtained experimental curves were fitted using a KWW function (see chapter 3.2).

The resulting decay curves are plotted in figure 4.2a for several temperatures. The β parameters obtained from the fitting procedure are smaller than those expected (0.5-0.7) from other experimental methods [Donth92], indicating a wider distribution of correlation times. The values obtained are given in the first table in appendix B together with the values obtained for the side and main chain.

It is evident that the molecular process, present in the decays at higher temperatures (above 300K), becomes slower approaching the glass transition temperature, and very slow below T_g . The signal-to-noise ratio was very good for these experiments, resulting in the small error bars in figure 4.2a. The correlation times observed range between 0.023 to 0.167 seconds for the respective temperatures (see Table 1 in appendix B).

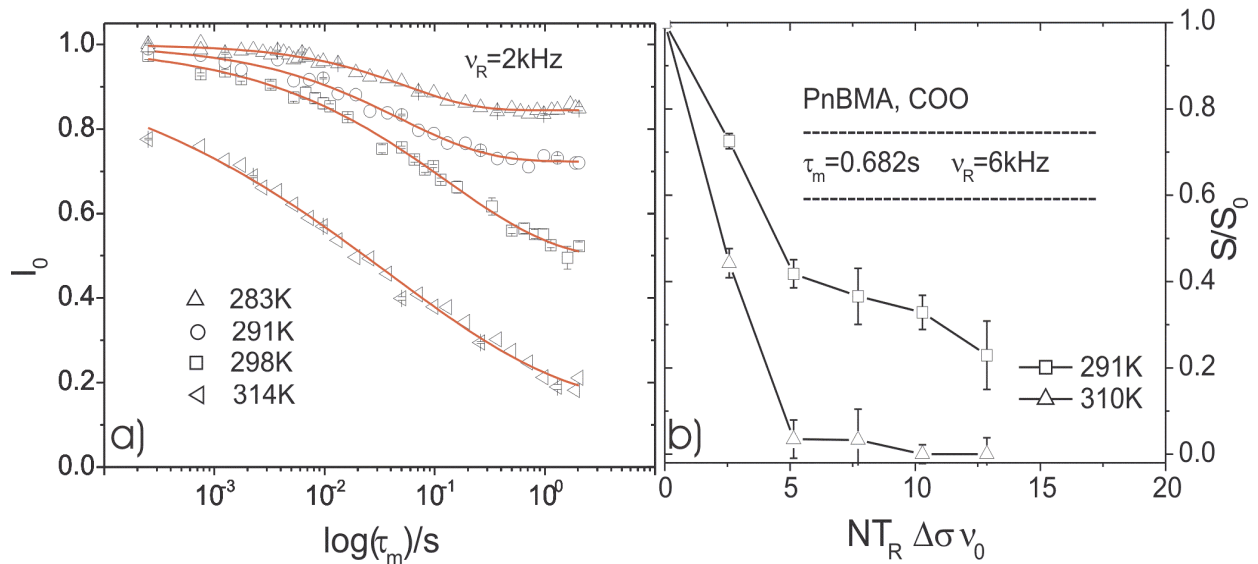


Fig.4.2 a) COO, PnBMA- *tr*ODESSA decays for several temperatures
 b) CODEX, NT_R -dependence experiments

The correlation times obtained from the fitting procedure were plotted after conversion using the formula given in eq. (3.22) in an Arrhenius diagram together with the data from the dielectric experiments. The β values were also converted using the procedure described in chapter III, to reveal the wide distribution character of the process and plotted in the Arrhenius diagram as vertical bars (fig. 4.3). Here the bars do not mean the error in the correlation times determination, rather the existence of a wide distribution of correlation times (see figure 3.3).

The curves in figure 4.2a provide only limited information about the topology of the exchange process. Some considerations about this could be made after running more experiments using the CODEX method (see figure 4.2b). As discussed in [Bonagamba01], CODEX NT_R -dependence curves obtained for PMMA revealed that the COO group exhibits an exchange process which is a mixture of flips and small-angle reorientations. After a closer inspection of the curves depicted in figure 4.2b, one may observe that the 310K curve decays fast reaching the plateau value close to zero, this being an indication about an exchange process involving an infinite number of sites, therefore a “diffusive-like motion”. This type of dynamics is common in amorphous polymers where jumps to random sites are likely to happen. A fast decay is usually related to a reorientation motion involving relatively large angles, while a slow decaying curve reveal the existence of a small-angle motion (see also figure 4.4b). The different behavior of the CODEX decays for the temperatures presented above, could be related to a change in the number of nuclei which participate to the motions described above, mobile fraction f_m , as described in chapter 2.5. More information about the percentage of nuclei performing flips, can be obtained only if CODEX experiments with very short

NT_R values are performed, which is not the case in figure 4.2b. From our experiments, we could conclude that the dominant process in figure 4.2b is the one related to small-angle reorientations or “twists”, the temperature increase affecting the mobile fraction or the number of sites involved. As we already mentioned, the a parameter from the trODESSA fit does not provide information about the number of sites or fraction of nuclei involved in the molecular process. The ratio S/S_0 is plotted as function of the recoupling period NT_R multiplied by the width of the CSA ($\Delta\sigma$) and the Larmor frequency ν_0 so that results from experiments at different spinning frequencies could be compared. The values of $\Delta\sigma$ were obtained using the Herzfeld-Berger method from experiments performed in slow-MAS regime (1 kHz). Typical values of 155 ppm for COO, 28 ppm for main chain #2 and 45 ppm for side chain #3 were found. The 310K data (fig. 4.2b), show an exchange process which in these conditions imply a diffusional motion (f_m has its maximal value). It is interesting to compare the asymptotic level for which the plateau is reached with the corresponding calculations. It is known from experiments on PMMA and PEMA [Kuebler96; Kuebler97; Kulik94; KSR94] that the carboxylic carbon performs a dynamics that can be characterized by a π -flip around the bond connecting the carboxyl carbon with the main-chain carbon #2 (“flip”) and a rotation by an angle $\delta\gamma$ of the main chain segment (“twist”) around the C-C main chain bond that adjusts for the violation of the local symmetry. Taking the tensor orientations and Euler angles from [Kulik94] and performing calculations as described in [Reichert97] yields an asymptotic intensity due to the flip of about 0.44, much bigger than the experimental value of 0.2 at low temperatures. In contrast, the result for the twist depends on the value of $\delta\gamma$ and yields 0.92 for $\delta\gamma=10^\circ$ and 0.80 for $\delta\gamma=20^\circ$. Thus, we assume that the contribution of the carboxyl carbon to the β process that can be separated from the α process at lower temperatures, is more likely a small-angle twist of the main chain, rather than the flip of the carboxyl group. At higher temperatures when the dynamics of the carboxyl carbon contributes to both the α as well as the β process, both motional models are likely to happen, as it was found for PMMA [Kulik94]. Therefore, the only conclusion that we can draw from both the value of the asymptotic trODESSA intensity as well as from the CODEX- NT_R dependence is that the process that we observe most likely involves a relatively small to medium-angle reorientation of the carboxyl carbon as shown in fig. 4.2b.

The results in figure 4.3 show that the correlation times obtained from the trODESSA decays of the COO group in PnBMA can not be assigned only to one of the traces in the glass transition. For temperatures around T_g , the results could indicate that the COO group is mainly active in the β relaxation process. This would mean that for these temperatures COO features the same molecular motion like the side chain carbons, namely, only by the local modes. With increasing temperature,

above T_g , we obtain a larger distribution of the correlation times for the COO, which may suggest that the processes presented here can act also for α transition. The limitations of the NMR techniques (see the accessible experimental window in fig. 4.3) makes the investigation of the molecular dynamics at higher temperatures (splitting region) difficult, if not impossible. Therefore, it is not possible to speculate about the implication of the COO dynamics in the glass transition close to the splitting region or in the a trace of the transition.

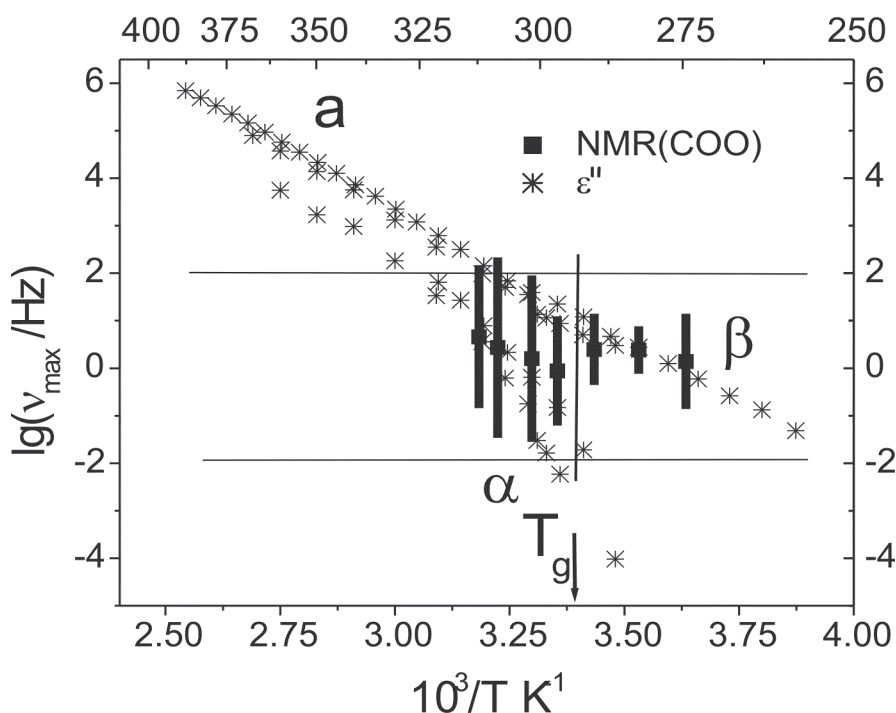


Fig.4.3 Arrhenius diagram of the COO, PnBMA.

The parallel horizontal lines represent the range of the NMR experimental window.

The vertical line marks the change in the dynamics of COO group.

To investigate the side and main chains, the trODESSA method could not be used due to the smaller CSA which would require lower spin rates to keep a good sensitivity (see chapter II) for the detection of exchange process. Therefore, the CODEX method was extensively used to investigate the dynamics of the side and main chains, whose ^{13}C CSA's are smaller than for the COO group. The experiments were performed on a 9.4 T magnet operating at a resonance frequency of 100 MHz for the carbon channel. Typical spin rate used was 2 kHz, higher spinning rates being used in the CODEX experiments in which the recoupling period NT_R was incremented. For the CODEX experiments involving a mixing time dependence, the recoupling period was chosen about 2 ms ($N=4$), so that the signal loss due to the increased length of the pulse sequence to be in acceptable range.

The exchange curves obtained for the main chain carbon (#2), corrected by spin diffusion using the procedure described in chapter III are presented in figure 4.4a. In this case the temperature chosen for the spin diffusion was 240K. The curves were fitted using a KWW function, which assumes the existence of a distribution of correlation times. The fit follows well the behavior of the experimental points, the possible errors of the fitting procedure could arise at very short mixing times, where the fitting curve falls below the experimental points. This led us to the idea that possibly two processes with different correlation times are involved [Reichert02] but further analysis of the data concluded that the experiments describe only one exchange process characterized by a wide distribution of correlation times. One may observe that at 333K, the decay is described by a single KWW function with an asymptotic plateau at $a=0.5$. This could mean an exchange process involving two sites, or an indication that the detected process entered the intermediate regime. The typical values of the correlation times obtained are in the order of several milliseconds. By decreasing the temperature the value of this parameter changes (see 315-303K curves) along with the corresponding correlation times. Close to the glass transition temperature (293K) the molecular dynamics is described by a long correlation time of 14.5 seconds. Due to the large errors found in the determining this value, we decided to omit this point. Information about a change in amplitude motion involved in the exchange process is provided also by the CODEX experiments performed for several recoupling periods for $\tau_m > \tau_c$, which would mean that the exchange process already took place (excepting the data at 293K for which the correlation time is much longer than the mixing time). The corresponding results are provided in the figure 4.4b.

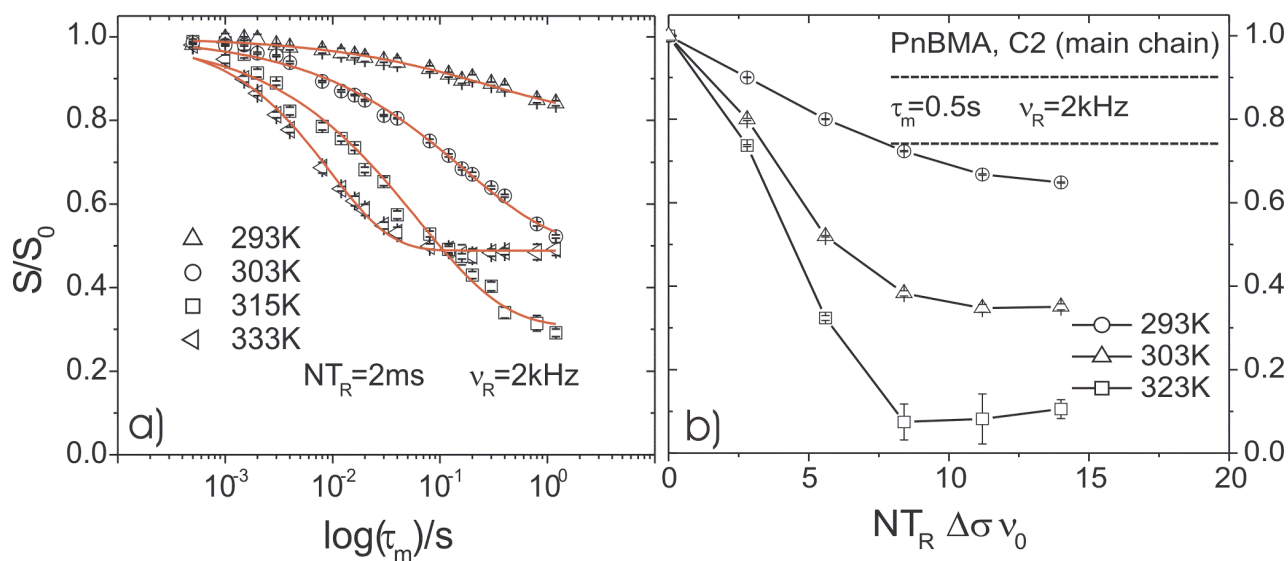


Fig.4.4 a) C2 (main chain), PnBMA- CODEX mixing time dependence

b) C2 (main chain), PnBMA- CODEX NT_R -dependence

CODEX NT_R dependence experiments in figure 4.4b show that a change in the amplitude of the motion is possible as suggested also by the mixing time dependence experiments. A closer inspection of figure 4.4b indicates that a change in amplitude of the motion is present for the 293K (small-angle, slow decay) and 323K (large-angle, fast decay) data. The fact that the asymptotic level is reached for 323K close to zero is an indication that we have to deal with a diffusive motion. Although, in this case the different asymptotic levels could come from the fact that the $\tau_m \gg \tau_c$ is not fulfilled for lower temperatures measurements. By comparing the curves from figure 4.4b with those from 4.2b one can see that the motion angle of the COO group is relatively larger than that of the main chain carbon. This could indicate that the “twist” observed at room temperature is related with the beginning of the α relaxation. The correlation times obtained from CODEX mixing time experiments are given in table 1 in appendix B. Using the equation (3.22) the correlation times were converted in the corresponding maximal frequency and then plotted in an Arrhenius diagram together with the results from the dielectric spectroscopy. The width of the distribution of the correlation times are plotted like vertical bars in figure 4.5.

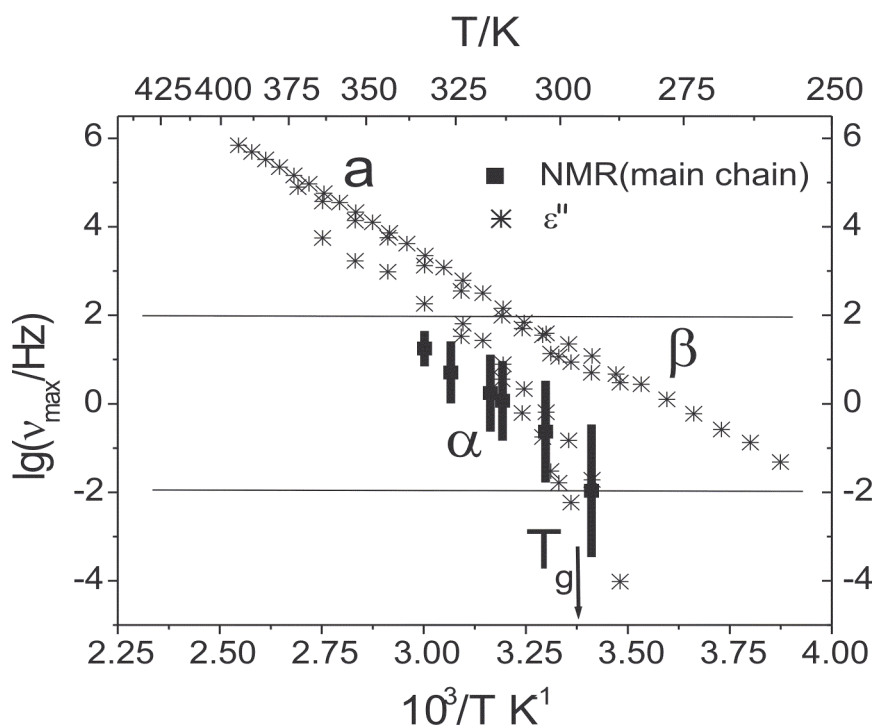


Fig.4.5 Arrhenius diagram for the PnBMA, main chain #2

Figure 4.5 shows that the correlation times determined using NMR methods for the carbon #2 (main chain) in PnBMA are in good agreement with those obtained from other methods. As expected, the molecular dynamics of the main chain contributes only to the α process of the glass transition, being a cooperative process as revealed by the calorimetric measurements. The vertical bars

from figure 4.5 shows that at temperatures below the glass transition we have a wide distribution of correlation times. Again, the experimental window for the NMR exchange experiments limits the investigation to the zone delimited by the horizontal lines in fig. 4.5.

Due to the similar width of the CSA, the same CODEX experiments were used to investigate both main and side chain. The results shown in figure 4.6a present the CODEX mixing time dependence decays for the side chain carbon (#4) for several temperatures. Similar data plots were obtained also for the carbon #3 in the side chain but due to the lower resolution (smaller signal-to-noise ratio) we present here the carbon #4 data. The data processing routine was the same like for the main chain: spin diffusion correction and then fit with a distribution function of KWW type. The spin diffusion temperature was chosen to be close to 240K. At this temperature the only process active remains the spin diffusion. Here also a recoupling time of 2 ms was used; additional CODEX experiments involving a dependence of the recoupling period for mixing times longer than the correlation times were also performed. The exchange curves for the carbon #4 (side chain) are presented in figure 4.6b. The solid lines are resulted after fitting with a single KWW function. It is obvious that the fit curves are in good agreement with the experimental points, the experimental errors (signal-to-noise ratio) are acceptable (see error bars in fig. 4.6). Larger experimental errors are to be expected for longer mixing times where the T_1 relaxation plays an important role. Experimental data for carbon #3 shows a similar tendency, but they exhibit larger experimental errors due to the relative smaller intensity of the line, however they still could be fitted in the same manner and the correlation times obtained are plotted in figure 4.7.

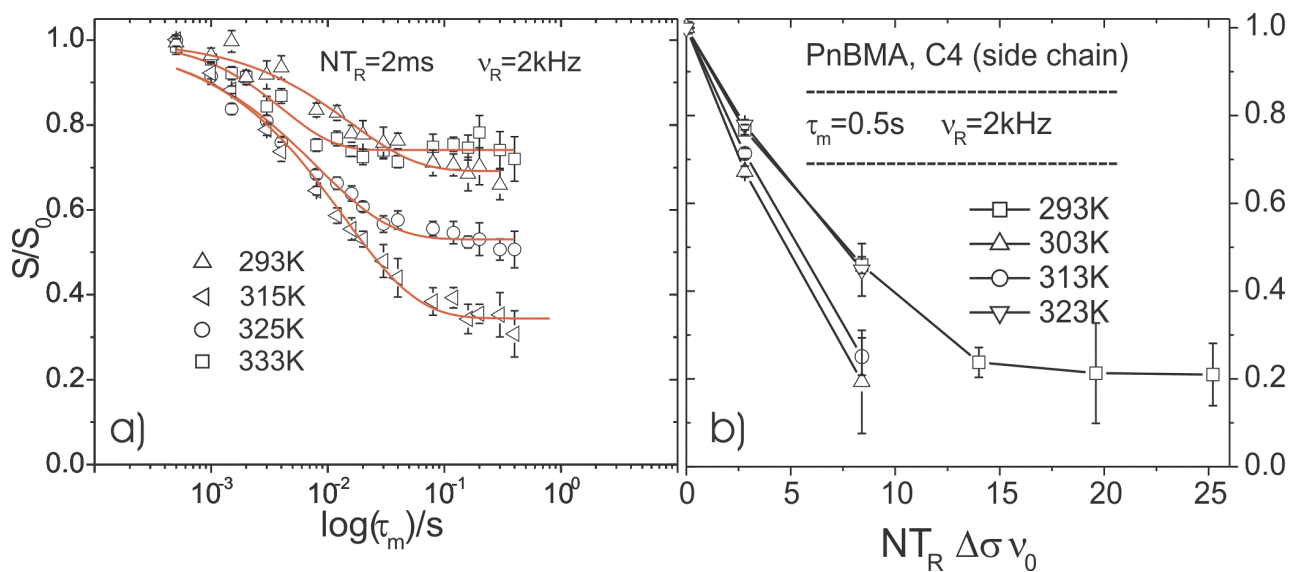


Fig.4.6 a) CODEX mixing time dependence for PnBMA, side chain (carbon #4)

b) CODEX NT_R -dependence for the side chain (carbon #4)

At closer look to the plots in figure 4.6a we can notice that a change in the temperature at which the experiments were performed is followed by a change of the asymptotic plateau of the exchange process while the correlation times change only slightly. The fact that for several temperatures the asymptotic plateau is reached at mixing times of several hundreds of milliseconds but for different α values allows us to speculate that for different temperatures, the amount of the spins active in the exchange process is changing. Also, figure 4.6a shows a dependence of the correlation times on the temperatures, this being an information that the observed effect is due only to molecular reorientations. A change in the fraction of mobile spins is observed also in the CODEX experiments which regards the dependence of the exchange on the recoupling period. Typical mixing times used for this type of experiments were of the order of 0.5 s. Carbon #3 and #4 behave in a similar manner (as one can see from the Arrhenius diagram, fig. 4.7) their molecular dynamics being almost identical (correlation times). The different values for which the asymptotic plateau is reached (fig. 4.6b) could come from a change in the number of sites involved in the exchange process from two to more, or could be explained by the fact that for some temperatures only fractions of the nuclei that can participate to the process (more probably) or by the conformational changes related to the main chain that can influence also the behavior of the side chains.

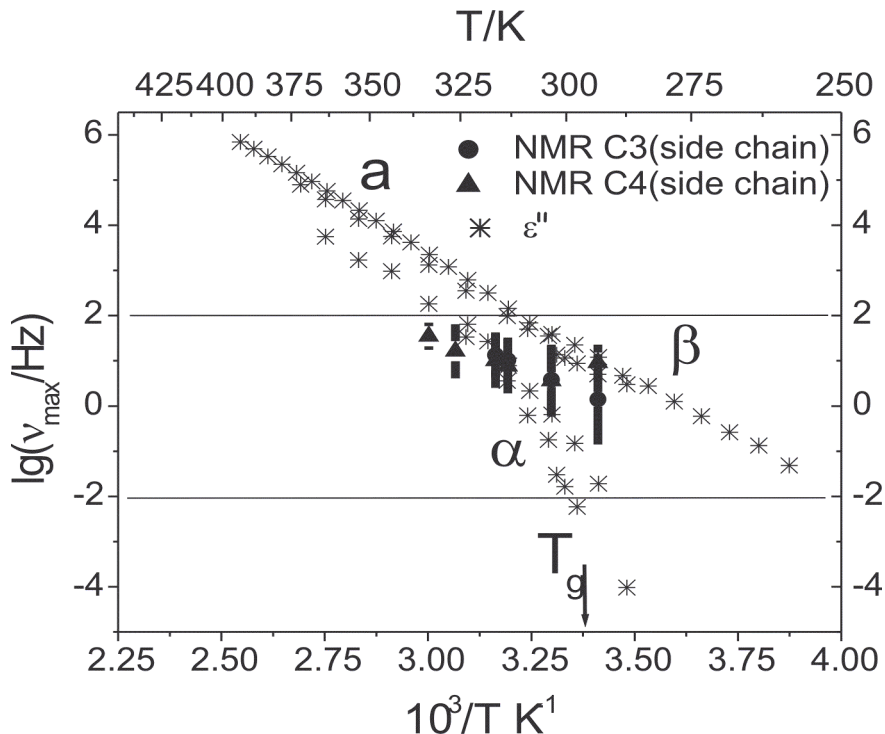


Fig.4.7 PnBMA, side chain #3 and #4, Arrhenius diagram

For further assumptions on this question, additional experiments performed with the 4-times-CODEX method would be required, but the limitation related to the finite experimental time have not made this possible. The correlation times and their distributions obtained from the KWW fit of the experimental data presented in figure 4.6 are plotted in an Arrhenius diagram together with the results from dielectric spectroscopy (fig. 4.7).

The Arrhenius diagram (fig. 4.7) shows the maximal peak frequency obtained from the corresponding correlation times of the side chains carbons #3 and #4 in the PnBMA. It is obvious that the carbon #3 participates at temperatures higher than T_g mainly to the α relaxation similar to the main chains. This behavior could be explained by the position of this carbon close to the main chain which will force it to execute similar reorientation motions. For temperatures closer to the glass transition the determined frequencies show that the carbon #3 (side chain) could participate also to the β relaxation as expected for a side chain unit. The side chain unit #4 performs almost the same type of motion like carbon #3. For temperatures above the glass transition they participate in the α relaxation while close to T_g we observe a process which contributes to the β relaxation. The additional degree of freedom as compared to the carbon #3 could be the cause of a stronger contribution of the #4 side chain unit to the Johari-Goldstein process. These results show that close or even below the glass transition temperature we detect the effect of both relaxation processes. This could indicate that in this temperature range the chain twists are associated with the α relaxation.

4.1.2 Investigation of exchange processes in PnHMA

The second member of the poly-methacrylates family which was used in these investigations is the PnHMA. The typical CP-MAS spectrum recorded at a spinning rate of 3000 Hz, 273K, on a spectrometer operating at a resonance frequency of 100 MHz for the ^{13}C channel is given in figure 4.8. As one can observe in figure 4.8, the COO group due to the larger CSA is well separated from the aliphatic lines (side and main chain). At this spinning rate, the COO produces several spinning sidebands (*), while the increased length of the side chain makes the spectrum crowded in the region from 0 to 70 ppm. As in the case of PnBMA, to investigate the dynamics of the COO, the trODESSA method was preferred, while for the side and main chain CODEX experiments with mixing-time and recoupling period dependence were recorded.

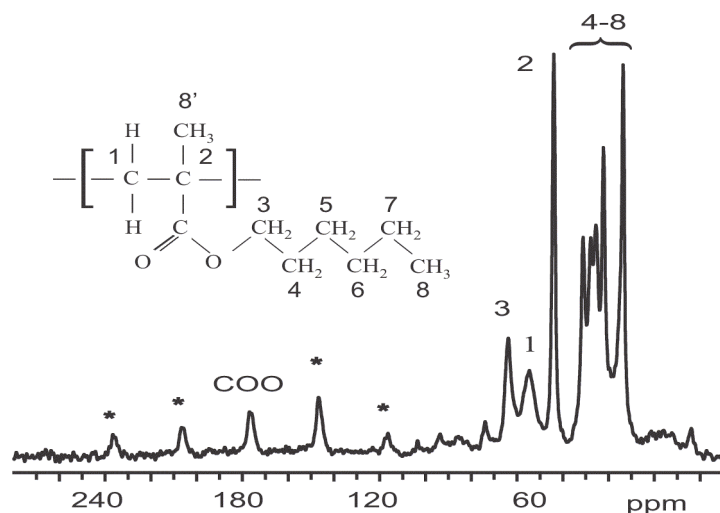


Fig.4.8 CP-MAS spectrum of PnHMA recorded at $\nu_R = 3\text{kHz}$, $\nu_0 = 100\text{MHz}$

The experimental conditions described in the case of PnBMA are valid also for the PnHMA. Some of the results obtained with trODESSA on the COO group are presented in figure 4.9. The decays in the plot in figure 4.9a are artificially normalized as described in chapter III, while the CODEX data are normalized during the acquisition.

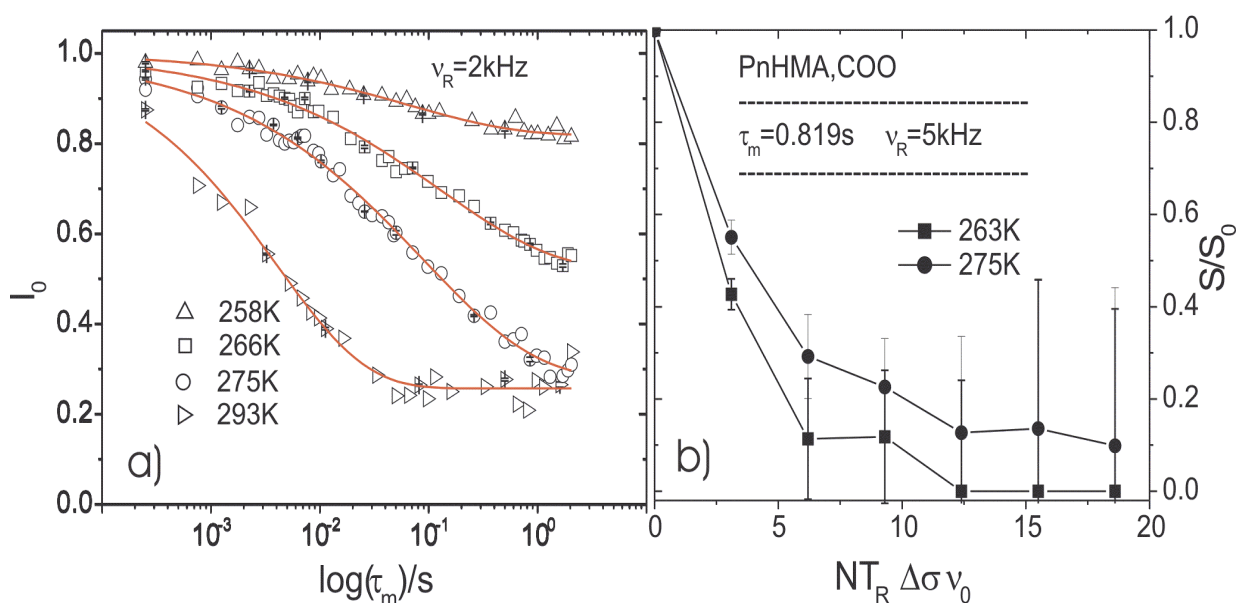


Fig.4.9 a) COO, PnHMA, trODESSA decays

b) CODEX NT_R dependence experiments

As for the COO in the PnBMA, the trODESSA decays show a strong dependence on the temperature with the fastest correlation time obtained at room temperature. The β parameters obtained

from fitting with a stretched exponential of KWW type are in the range of expected values for this polymer and probes the existence of a wide distribution of correlation times. The correlation times obtained from fitting with a KWW function are summarized in table 2 in appendix B together with those from the side and main chain. The results obtained running CODEX NT_R -dependence experiments are presented in the figure 4.9b. The decays show that the detected exchange process involves jumps between an infinite number of sites, therefore a diffusive motion. The results are similar to those obtained for the COO, PnBMA.

The values of β are correlated with the shift of the maximum and the width of the spectral density and the results which quantify the dynamic process are plotted in the Arrhenius diagram as vertical bars with length $\delta\nu$ centered around $\delta\nu_0$ (fig. 4.10).

With the help of the conversion equation given in chapter III, the maximal peak frequencies are obtained from the correlation times resulted from the trODESSA decays and plotted in an Arrhenius diagram together with the data provided by Prof. Donth group, obtained from other methods (DSC, dielectric spectroscopy and mechanical relaxation).

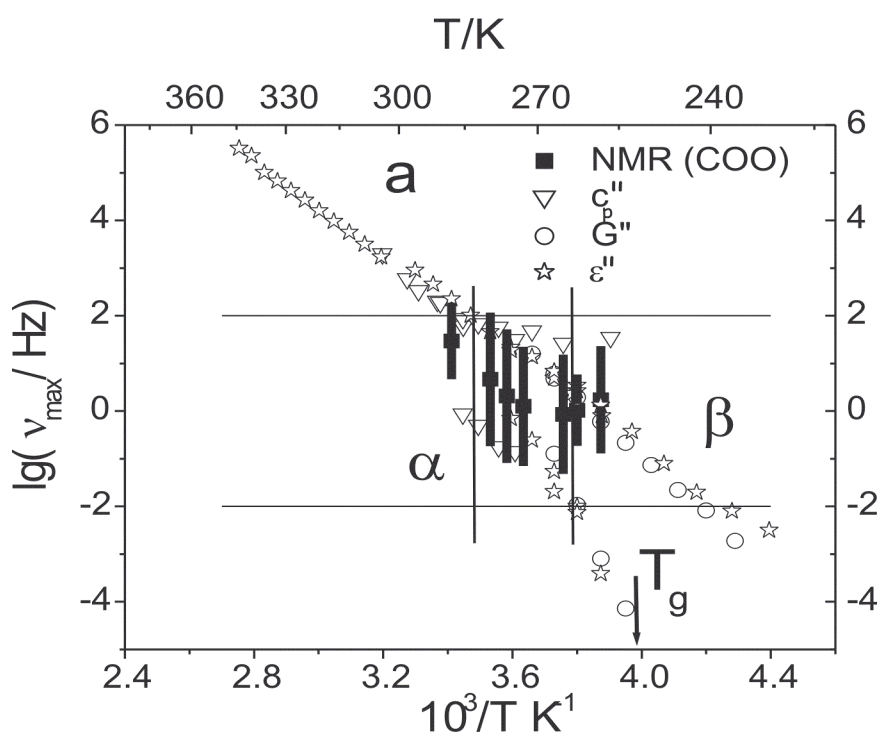


Fig.4.10 COO, PnHMA, Arrhenius diagram.

Vertical thin lines show 3 motional regimes of the molecular dynamic.

The results reveal the existence of three motional regimes in the dynamics of the COO group. For temperatures close to T_g , the dynamics of the carboxyl is mostly related with the secondary β

relaxation. With increasing the temperature, 266K, both α and β processes contribute to the dynamic of COO group. This could mean that the exchange process detected at these temperatures is a merging of 2 separate processes which accounts for α and β relaxations, but the actual investigations can not tell apart the different processes in the COO exchange data [Pascui02]. At room temperature the detected dynamics contributes again only to one process $\{\alpha a\}$. The vertical bars at lower temperatures accounts for a wide distribution of correlation times which could suggest that the effect observed in the calorimetric measurements in this region is related to the dynamics of the COO group.

The existence of 2 separate processes in PnHMA was the aim of carefully data analysis of the exchange data obtained from CODEX experiments for the main chain carbon #2. The experiments were performed with a recoupling period of 2 ms, at a spinning rate of 2 kHz. The corrected CODEX decays after spin diffusion correction are presented in figure 4.11a. The fact that the only temperature for which the CODEX decay reached the plateau (286K) at a asymptotic value close to 0.75 made us to keep this value fixed also for the other temperatures.

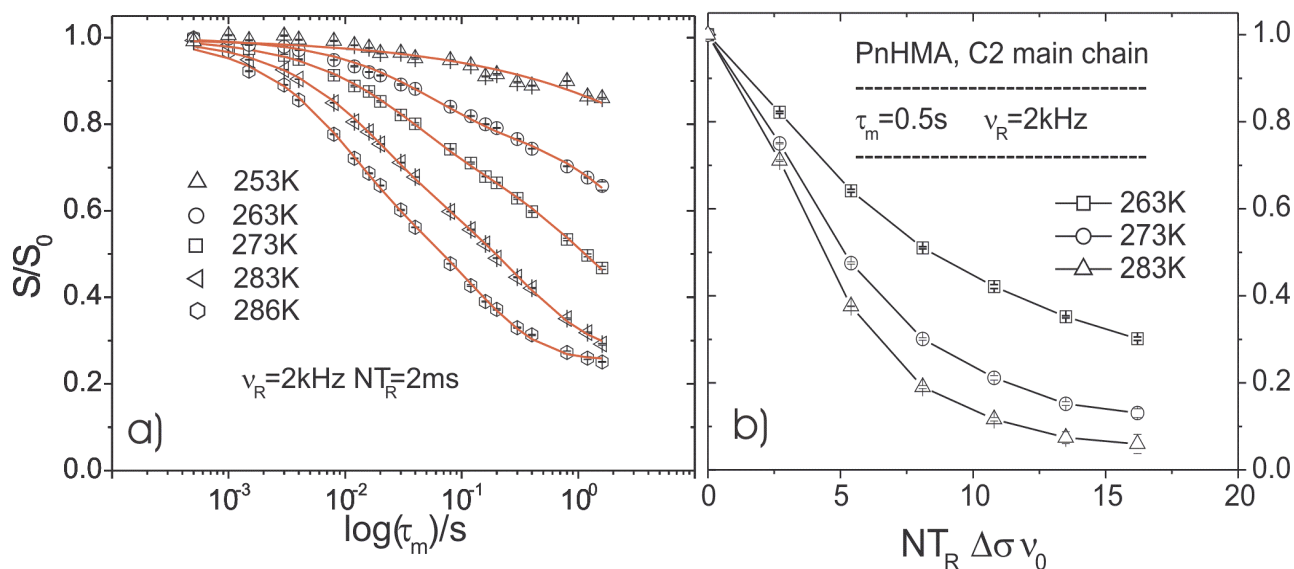


Fig.4.11 a) PnHMA, main chain #2, CODEX mixing time dependence experiments
 b) CODEX NT_R -dependence experiments

The systematic deviations of the fitting curves from the experimental points obtained after fitting the data with one stretched exponential and visualized in deviation plots in figure 4.12, made us try to fit the obtained data using two KWW functions. The very good signal-to-noise ratio obtained in the NMR experiments (see small error bars in figure 4.11) made this possible. The curves presented here were fitted with the exception of that at 253K with two stretched exponential. The

fitting procedure revealed the existence of two dynamic processes which are revealed by the CODEX curves. The two component processes are characterized by correlation times ranging from 0.009 s for short and 0.11 s for long component at 286K to 0.05 s and respectively 6.8 s at 263K. For the long component the determined β values were in the expected range of 0.5-0.7 while for the short component larger values are obtained. The different asymptotic values in figure 4.11a are most likely related with changes in the mobile fraction of nuclei involved in the exchange process. Figure 4.11b shows some of the results obtained in the CODEX experiments performed by incrementing the recoupling period NT_R for a mixing time of 0.5 s. Again, one can see that the motion of the main chain involves smaller angles than for the COO group. Also for the main chain in Pn-HMA, the behavior of the CODEX NT_R curves indicate an exchange between infinite number of sites (283K).

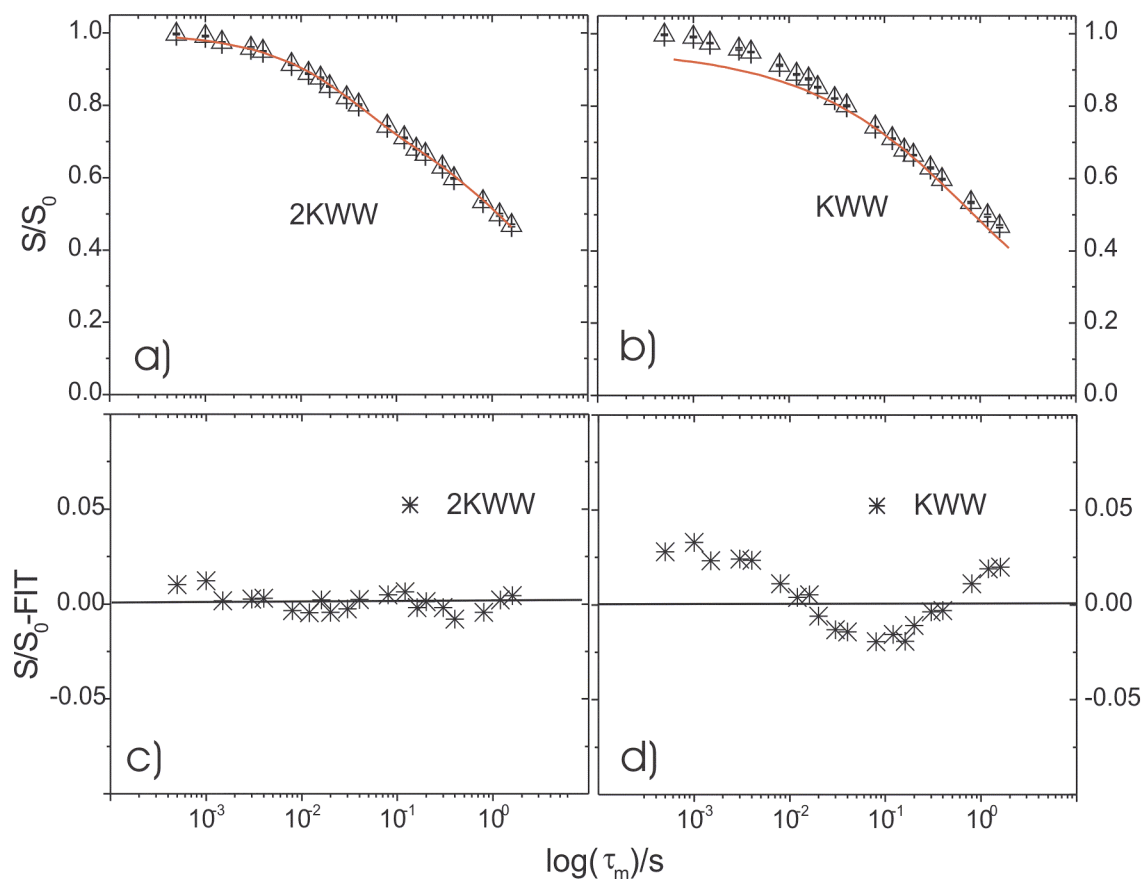


Fig.4.12 Deviation plots for main chain carbon #2 data at 283K

- a) fitting with two stretched exponential function
- b) fitting with only one KWW function
- c) deviation of the experimental points from the 2KWW fit curve
- d) deviation of the experimental points from the KWW fit curve

Figure 4.12 shows a comparison between the exchange data at 283K fitted with one KWW (b) and a two components KWW function (a) and their respective deviation from the experimental points. It is clear that the experimental points are better described with a two component KWW function, a single KWW function could not reproduce the data within the error margin. The fact that the experimental points are not scattered makes us to attribute the failure of the single KWW function to cover the initial part of the decay (fig. 4.12b) to the existence of a secondary process. Also the points in the lower part of the decay are better described by a two component KWW function. In figure 4.12 (c and d) we can see the deviation plots which mark the deviation of the fitting curve from the experimental points. Similar deviation plots were made for each temperature and helped us decide which one of the models to use. For the lowest temperature, 253K, surprisingly the best fit was obtained using a single KWW function which could be explain by the fact that close to the glass transition temperature the dynamics of the main chain is different. The result was a point on the α trace in Arrhenius diagram, but with a distribution spanned across several frequency decades.

The correlation times obtained from fitting were plotted in the activation diagram with the help of their corresponding frequencies, the resulted Arrhenius diagram being showed in figure 4.13. As one may notice, the NMR data match those obtained from the dielectric spectroscopy and HCS.

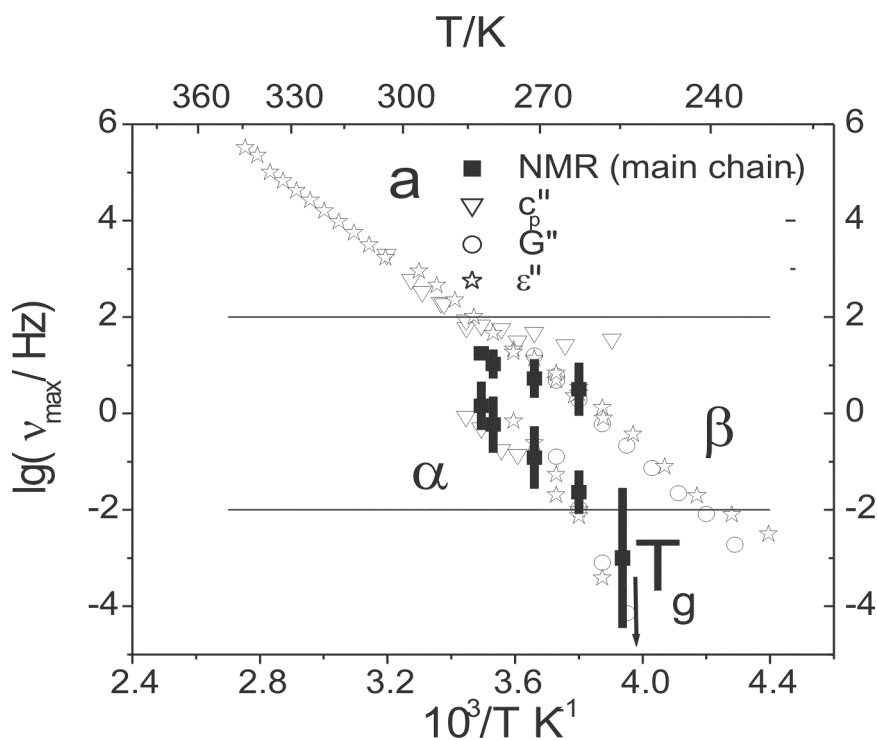


Fig.4.13 Arrhenius diagram for the main chain carbon #2 in PnHMA

There is a good agreement between data originated from different experimental methods. The plot shows that at low temperatures the only process which contributes to the dynamics of the main chain is the α process. With increasing the temperature, a second process occurs which contributes to the Johari-Goldstein type process. The separation of the two processes coming from their different nature and correlation times is well observed. By further increasing the temperature, the dynamics becomes very fast for both components.

A necessary step further was to investigate how the increased length of the side chain may influence the dynamics of the functional group contained within. We saw that, as compared to the main chain of PnBMA, the main chain groups in PnHMA participate to both α, β relaxations, while the carbon #2 in the main chain of PnBMA contributes only to the α process.

The investigations regarding the side chain groups, were performed in the same experimental conditions as those for the main chain. Again, CODEX experiments were performed for both mixing time dependence and NT_R dependence. Experiments for which the mixing time was varied were performed with a 2 ms recoupling period. The resulted experimental data were corrected by spin diffusion and then fitted with a stretched exponential of KWW type. Some of the decay curves are given in figure 4.14a. For the PnHMA we restricted our investigations of the side chain dynamics to the functional group #3 (see fig. 4.8) due to the poor resolution of the other lines (not well separated).

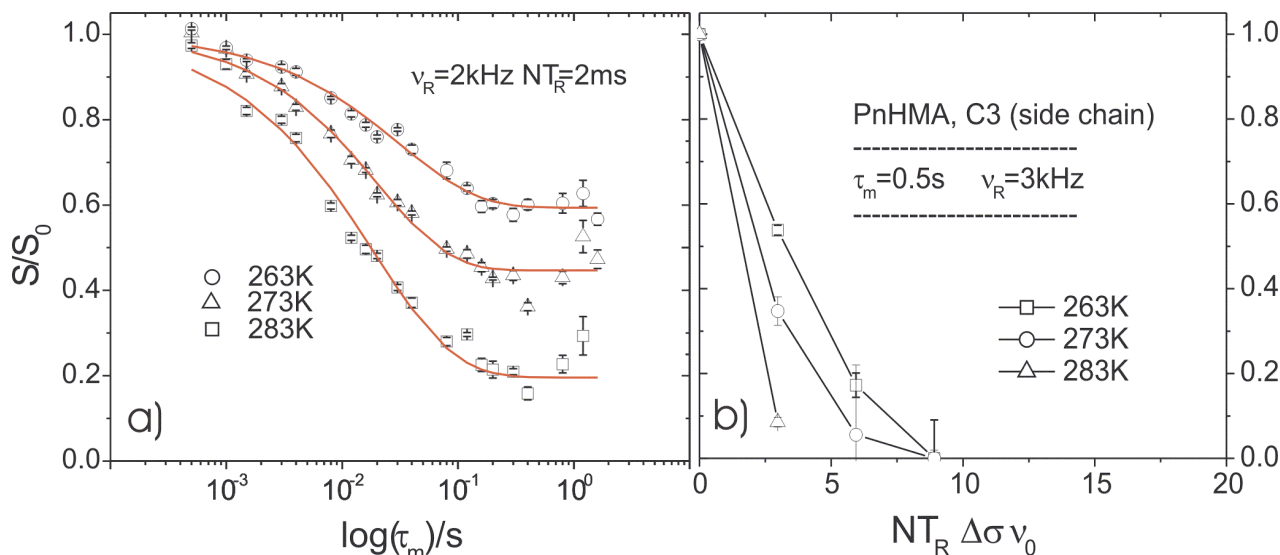


Fig.4.14 a) Side chain (carbon #3), PnHMA- CODEX mixing time decays (2 kHz)

b) CODEX NT_R -dependence experiments (3 kHz)

The increasing error bars at mixing times larger than hundred milliseconds is due to the effect of the T_1 relaxation which for this functional group is around 0.35 seconds at room temperature (see appendix A). This effect of the T_1 relaxation regards only the decrease of line intensity in spectrum which will show in the smaller signal-to-noise ratio and does not influence the correlation times showed here. We recall here the information that the z -filter used in the CODEX pulse sequence allows us to make an internal normalization and T_1 correction of the obtained data

Due to the fact that the CODEX NT_R dependence experiments were performed at a spinning rate of 3 kHz it is hard to correlate the results from figure 4.14b with those from 4.14a. Usually, for CODEX experiments performed with the same rotation frequency, one can correlate the position of point from the NT_R dependence for a certain mixing time with the position of the point at the same mixing time in the CODEX mixing time dependence decay performed with the same recoupling period. The necessary conditions are: the same rotation frequency in both experiments and the value of the mixing time chosen in the NT_R dependence experiment has to fulfill $\tau_m \gg \tau_c$.

However, the decays in the 4.14b indicate a change in the topology as revealed also from the mixing time dependence results, which is sufficient for a qualitative description of the effect. The correlation time which describes this process, $\tau_c = 0.020s$, is an indication of a relatively fast motion. A 10° change in the sample temperature is bringing also a change in the time scale and in the mobile fraction and angle of the process. The fastest process was recorded at 286K where the exchange happens in 0.009 s. The values for the β parameter of the KWW fit function, vary between 0.64 for lower temperatures up to 0.82 for the 286K data. Some attempts to fit the data for the side chain with a KWW function similar to the one used for the main chain were done, but the deviation plots and the whole behavior of the fit parameters lead us to the conclusion that the best fitting model to use is the one involving a single stretched exponential like the one used for the COO group. Also the fact that for all temperatures the plateau was reached, not only that show the change in the number of spins active in the process, but also made the fitting procedure more accurate in this case. The small intensity of the line in the spectrum makes the investigation of the topology difficult for large recoupling periods where large number of π pulses are required (figure 4.14b). An increase in the number of pulses is usually followed by a decrease of the intensity of the signal due to the T_2 relaxation, and this should be avoided here. Therefore, considering only the behavior of the first experimental points we can say that a change in the angle of the motion is observed as expected from the CODEX experiments with the mixing time dependence. Again the obtained informations from the resulted correlation times was compared to the data acquired by other physical methods and plotted in an activation energy diagram (figure 4.15).

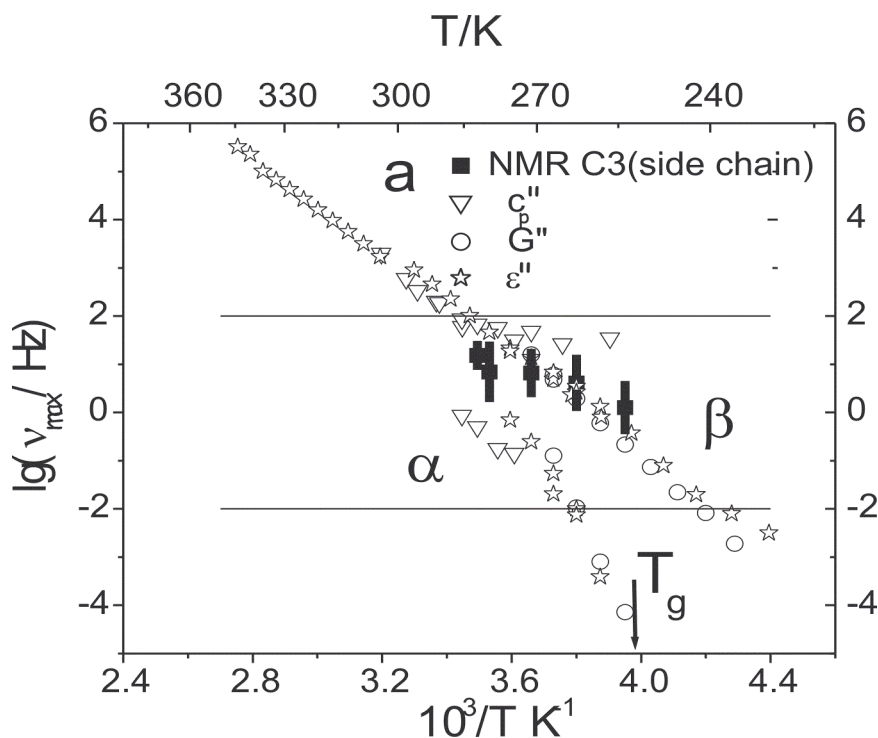


Fig.4.15 Arrhenius diagram of the side chain carbon #3 in PnHMA

This allow us to make some considerations about the reorientation motions in PnHMA. While the main chain execute two type of processes, well separated on the time scale of their correlation times, the COO group which is in the close vicinity of the main chain carbon #2 shows only one re-orientation process which is characterized by a wide distribution of correlation times and which contributes for higher temperatures to both α, β processes as the main chain. Increasing the distance to the main chain the functional groups of the side chain, despite their additional degrees of freedom tends to execute their own type of motions which are namely those of the β relaxation. It would be interesting to study the effect of the main chain motion on the CH_3 close to them, but the spectrum presented in the figure 4.8 shows that it is impossible to tell apart the two CH_3 groups despite their different position in the monomer unit. 1D-MAS exchange experiments performed on PnBMA and PnHMA from the family of amorphous methacrylates have shown that the same functional groups behave different in the two types of polymers. Despite the existent conception that the increased number of carbons in the side chains of the methacrylates does not influence too much the behavior of the polymers during the glass transition [Donth92], we were able to observe a completely different behavior of the polymers. In PnBMA the COO group was found to participate for $T > T_g$ to both α and β relaxation, while for $T_g \geq T$ only to β relaxation. In PnHMA, the same functional group of COO has a similar behavior: for lower temperatures it participates only to β relaxation, then to both

processes and for higher temperatures again only to α relaxation. In the same time in PnBMA, the main chain (#2) participates for all temperatures only to α process, while in the PnHMA, the same main chain (#2) contributes in the same time to both relaxations, its molecular dynamic being described by two independent processes. As to the side chains groups (#3 and #4) in PnBMA their molecular dynamic is described by three regions: for $T_g \geq T$ they are contributing only to β relaxation, then for a small temperature interval to both relaxations and for $T > T_g$ only to α process. In PnHMA, the side chains contribute only to β relaxation as expected, but from CODEX NT_R dependence experiments we can conclude that the topology of the exchange in this group is changing with the temperature.

4.2 Investigation of exchange processes in semicrystalline polymers

Another important part of this work was dedicated to the study of the molecular dynamics in semicrystalline polymers. The semicrystalline polymers are characterized by the existence of an amorphous and a crystalline phase. The crystalline phase allows the investigation of these polymers with the aid of X-ray scattering techniques, yielding relatively sharp reflections (but broader than in the case of low molar mass crystals) while the amorphous phase produces just a broad halo in the scattering pattern due to their disorder structure [KSR94].

Some of these polymers have a helical chain structure of the crystallites. The helices are classified as m_n helices, where m represents the number of structural repeat units per repeat structure of the helix and n is the corresponding number of turns around the helix axis. For example a 7_2 helix, like is the case in poly(4-methyl-1-pentene) in form I, would mean that the n -th and the $n+7$ -th units have the same orientation but are separated by 2 turns of the helix, that is, a displacement by 2 helix pitches along the helix axis. In the case of a typical helix, its projection on a perpendicular plane to the chain axis have m -fold rotation symmetry around its center. In this case a translation of the chain by one repeat unit, combined with a rotation of the chain by $360^\circ n/m$ reproduces the structure.

From this type of semicrystalline polymers we have investigated the poly(4-methyl-1-pentene) (70% crystallinity) or shortly P4M1P. This polymer has a wide range of applications due to its optical and electrical properties, low bulk density, high chemical resistance, and high permeability to gases [HWS97]. The densities of its crystalline and amorphous phases are very close to each other conferring a high degree of optical transparency. At room temperature, the crystalline

phase is slightly less dense than that of the amorphous phase. Melting point of 518K and glass transition around 318K are reported in the literature for the crystalline P4M1P [Lopez92]. From the mechanical studies was found that at least two major relaxation processes exist in this polymer: one around 293-323K and the other around 378-408K [deRosa97]. It is generally assumed that the transition around 318K is the glass transition, and the process at 408K being associated with the onset of motions within the crystalline regions [HWS97].

In the case of isotactic poly(4-methyl-1-pentene) or i-P4M1P which was investigated here, the existence of five crystalline forms is recognized. In this work we were interested only in the forms I and III of the polymer for which the helical structure is well known. Form I of the polymer is characterized by a $7/2$ helical conformation packed in tetragonal unit cell. Slight deviations from the uniform $7/2$ helix have been suggested by a refinement of the crystal structure of form I [Kusanagi78], according to this, chains are slightly distorted and packed in the space group $P4b2$. Form III is characterized by a tetragonal unit cell with chains in $4/1$ helical conformation, packed in the $I4_1$ space group [Takayanagi67]. The helical structure of both forms I and III are presented in figure 4.16.

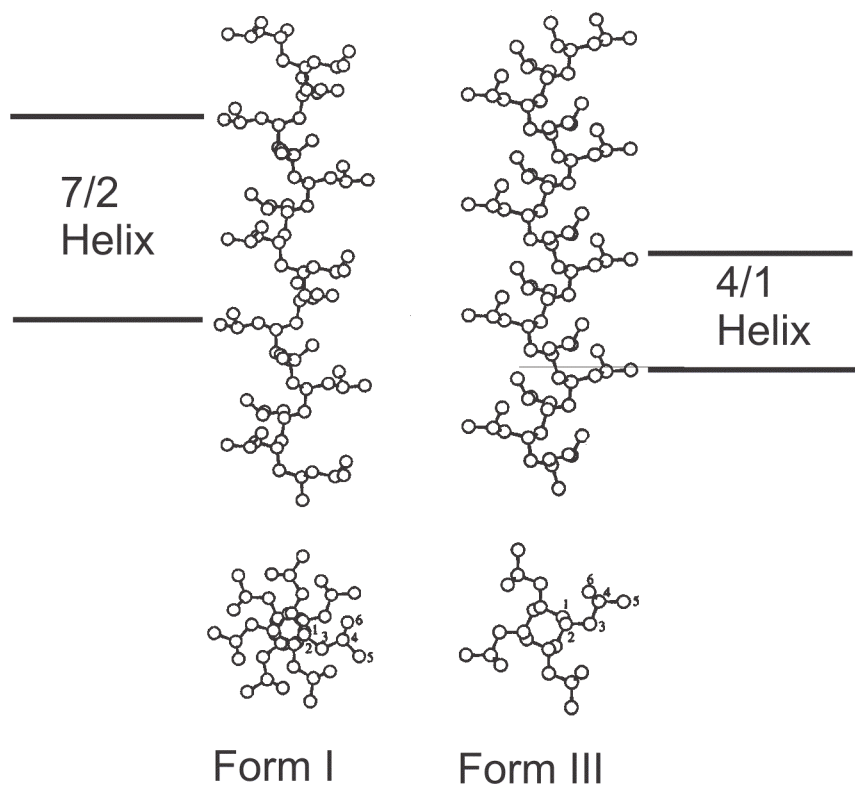


Fig.4.16 Helical structures of P4M1P in form I and III.

i-P4M1P with an average molecular weight (Mw) of 180,000 was purchased from Poly Science Co. Ltd. Initially, form III was obtained by crystallization into semi-dilute toluene solution (0.25wt%)[Miyoshi02]. Form I was obtained from form III via a crystal-crystal transformation. Both samples were provided by Dr. T. Miyoshi (AIST, Tsukuba, Japan), who was directly involved in the experimental part and the simulations performed on these samples. Solid-state NMR measurements were conducted on a Varian INOVA 400 spectrometer. ^{13}C carrier frequency is 100.5 MHz and a standard VARIAN 7 mm VT-CP-MAS probe was used in the experiments. The 90° pulse of ^1H and ^{13}C are 3.5-3.8 and 4.1-4.5 μs , respectively. The cross-polarization time and recycling time were set to 1 ms and 2 s, respectively. The spinning frequency was set to 3 (for simple CP-MAS and CODEX mixing time dependence experiments) and 5.5 kHz (for CODEX NT_R dependence experiments).

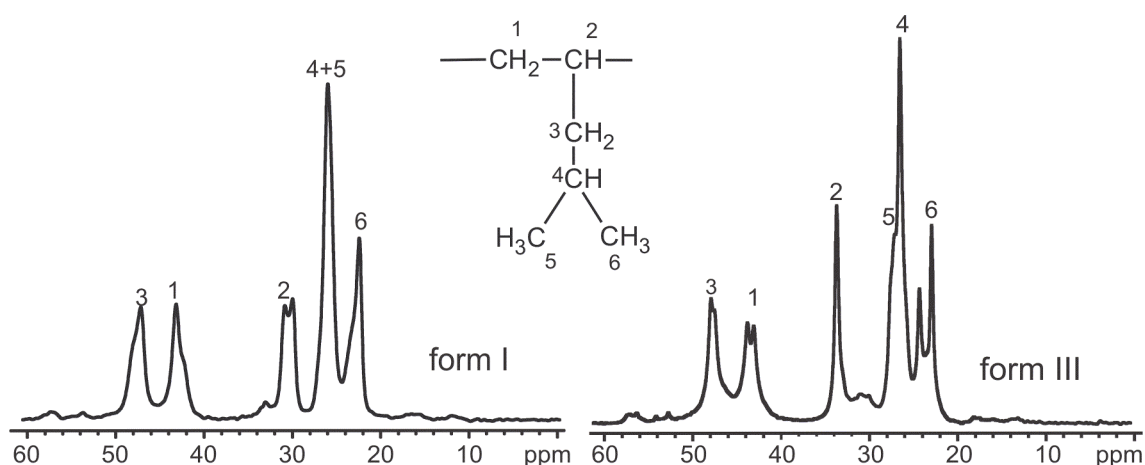


Fig.4.17 Chemical structure and line assignment of *i*-P4M1P in form I and III

Typical CP-MAS spectra at a spinning rate of 3 kHz are presented in figure 4.17. The resonances of the backbone methylene carbon #1 show a split for all forms of the polymer (for form I the small hump of the line), while the side chain #3 shows the split only in some of the five forms of P4M1P. In form I the resonance of the backbone methine carbon #2 is also split in a doublet at 29.63 and 30.85 ppm which, despite the small difference, it is assumed to be a conformational effect and not a packing effect. According to the refinement of the crystal structure in form I, the chains assume a helical conformation slightly distorted from the uniform $7/2$ helix (figure 4.18) with succession of the torsion angles ...TGT'G'T"G"... instead of $(TG)_n$ [deRosa97].

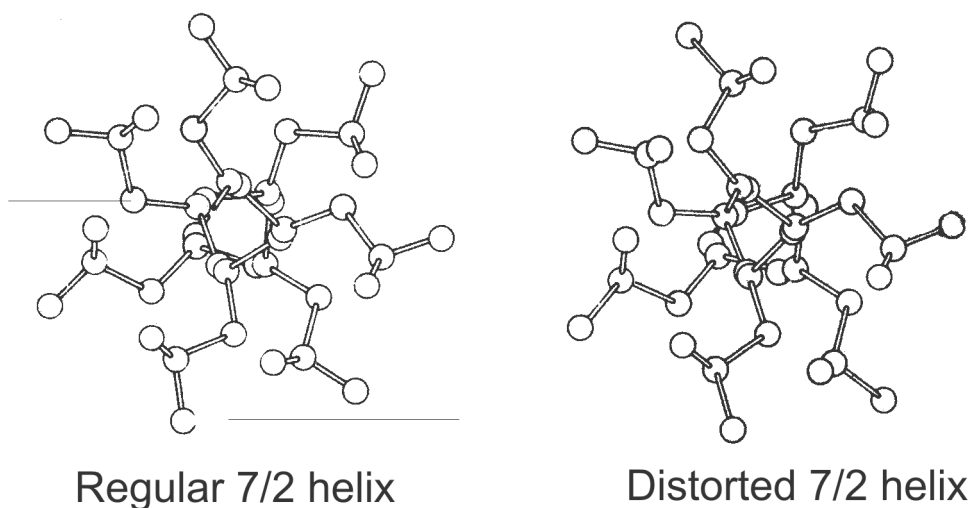


Fig.4.18 Representation of regular (left) and distorted (right) 7/2 helices for *i*-P4M1P form I

The small hump at about 30 ppm in the CP-MAS spectrum of form III at room temperature (fig. 4.17) is attributed to the amorphous part of the polymer. The small signal presented in the CP-MAS spectrum of form I in the region close to 32 ppm is a residual signal resulted from the transformation of form III in form I at temperature above 318K. After heating at higher temperatures for several hours the residual signal completely disappeared. The presence of two distinct resonances separated by approximately 3 ppm for the methyl carbons #5 and #6 indicates that the methyls belonging to the monomeric unit are non-equivalent; this being explained on the basis of the γ -*gauche* shielding interaction and of the conformations of polymer chains and lateral groups. The methyl carbons #5 and #6 have the same methine carbon #2 in the γ -position, but for both 7/2 and 4/1 helical conformations of forms I and III, #2 is in *gauche* arrangement with respect to the methyl #6 and *trans* arrangement for methyl #5. The small differences in the resonances from forms I and III were attributed to a deviation of the torsion angles (the angle between the bonds) in the helical 7/2 conformation of the form I [deRosa97]. The study cited in the above reference has shown that a deviation of the torsion angles between 12-15° from the exact values of 60° and 180° expected for 7/2 helix in form I, and 22°-26° for the 4/1 helix of form III, is responsible for the small γ -*gauche* shielding effect of -2, -2.5 ppm as compared with the expected value of -5 ppm. For the resonances #4, #5, and #6 which do not depend on the torsion angles of the main chain, chemical shifts at nearly the same values were observed. For form III the resonances of methyls #5 and #6 are split in doublets, this splitting being attributed to packing effects. This effect is also responsible for the small splitting, 1-2 ppm of the methyl resonances for all forms. Figure 4.19 shows different packing possibilities for the form I 7/2 helix and form III, 4/1 helix of *i*-P4M1P.

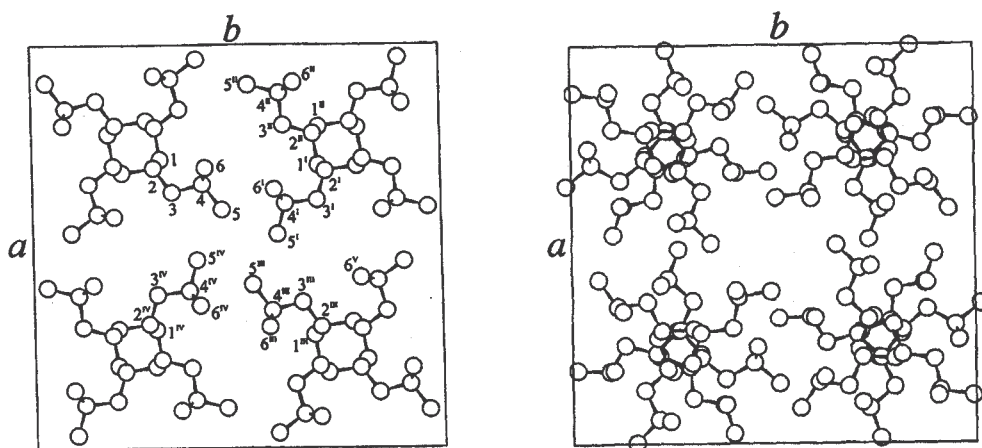


Fig.4.19 Models of the packing, in the *ab* projection, of *i*-P4M1P form I (right) in the 7/2 helix of space group *P4b2* and form III (left) in the 4/1 helix of group *I4₁* ([deRosa95])

The experiments involving detection of the exchange process were performed using the CODEX pulse sequence with the *z*-filter. Typical 1024 accumulations were used in the experiments regarding the mixing time dependence, which accounts for 22-24 hours of total experimental time. In the mixing time dependence experiments, a recoupling period of 2 ms ($N=6$) was used at a spinning rate of 3 kHz. Again a CODEX experiment was performed at low temperature where the spin diffusion is the only active process, in this case 258K. The mixing time dependence of the main chain carbon #2 of form I is presented in figure 4.20a.

The plots (fig. 4.20a) show that at relative high temperature (355K) a fast exchange process with a correlation time of 0.019 s is detected. The curves were fitted again using a stretched exponential of KWW type, with distribution widths (β) ranging from 0.46 at room temperature to 0.80 at 355K. The asymptotic plateau is reached at the highest temperature at 0.33 which would account for an exchange process involving a three sites jump. Considering the 7/2 helical structure of the *i*-P4M1P in form I a jump angle of 102° would be expected in the case of a uniform helical structure and in the case that all possible sites are involved in the exchange, a plateau close to $1/7=0.14$ should be reached. This is here not the case because we are detecting only jumps from site *i* to site *j* ($i \rightarrow j, j \rightarrow i$) or *k* ($i \rightarrow k, k \rightarrow i \rightarrow j$). By decreasing the temperature the exchange becomes slower and at room temperature we obtain a correlation time of the order of tens of seconds and a broad distribution. Similar data were acquired also for the side chains, the mixing time dependence of the methylene #3 are shown in figure 4.20b.

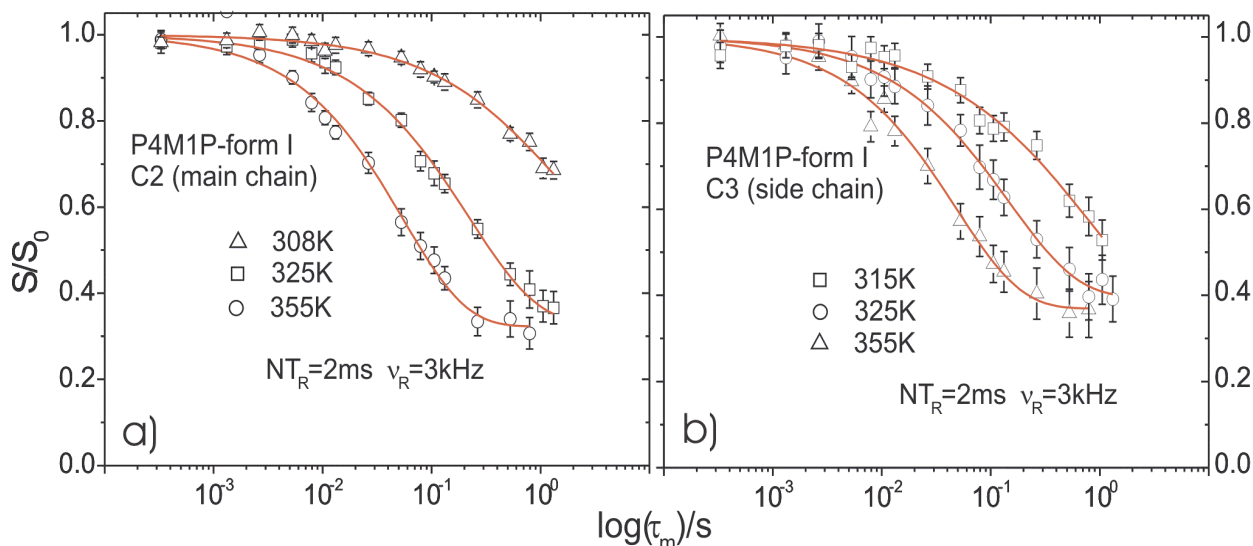


Fig.4.20 CODEX mixing time dependence of *i*-P4M1P form I

a) main chain carbon #2

b) side chain carbon #3

The results presented in figure 4.20b show a behavior similar to the methine carbons in the main chain. At higher temperature an exchange process characterized by a correlation time of 0.017 s is detected and the plateau is reached for $S/S_0 = 0.3$. Also the width of the distribution is similar to the main chain, values of β between 0.81 and 0.51 being observed, which would mean a distribution width between 0.75-1.59 frequency decades. As for the main chain, the decrease of the temperature does not change significantly the characteristics of the exchange process, which becomes only slower. Also the methylene #1 from the main chain was investigated and the results are presented in table 1 in appendix C together with those for the other carbons for both form I and III.

In order to get information about the activation energy of the process in *i*-P4M1P in form I the correlation times obtained from the CODEX mixing time dependence were converted using the equation (3.22) and plotted in an Arrhenius diagram. Again the vertical bars are not error bars but the width of the distribution of the correlation times which describe the exchange process. As expected from the similar correlation times obtained for main and side chain also the Arrhenius diagrams are similar, in figure 4.22 we present only the data from the methine group from the main chain.

An identical approach was followed also to investigate the dynamic of *i*-P4M1P in form III, for which a helical 4/1 structure is assumed. This would imply 90° jump motions of the helix. The CODEX mixing time dependence experiments were performed at 3 kHz in similar conditions like in the case of form I. Figure 4.21a shows some of the exchange decays obtained for the methine group of the main chain in form III, after the spin diffusion correction. As one may notice, the asymptotic

plateau is reached at 0.5 which would account for a two-sites jump motion or would indicate that most of the nuclei participate in the process (large mobile fraction). The curves were fitted like for form I with a KWW stretched exponential, the shortest correlation time obtained being 0.02 s at 313K. With decreasing the temperature the exchange becomes slower but again no additional change in the topology is observed. The β values obtained from fitting with a KWW function are smaller than for the form I, which would mean a wider distribution of the correlation times.

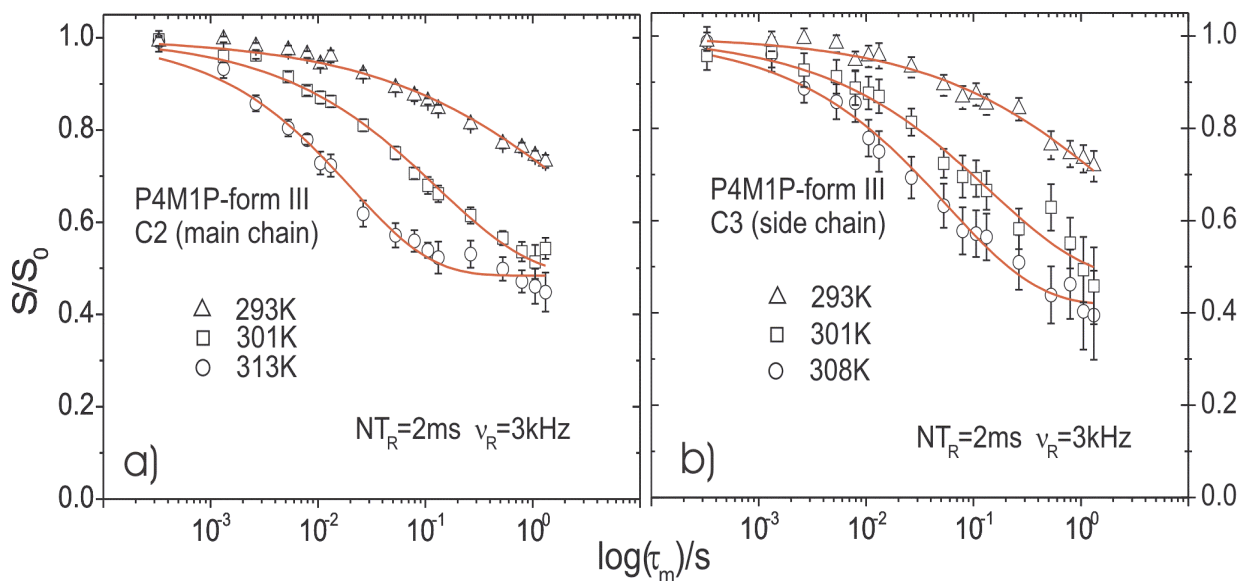


Fig.4.21 CODEX decays P4M1P form III.

a) main chain carbon #2

b) side chain carbon #3

As for the form I, a similar behavior of both side and main chains is detected. Figure 4.21b shows some of the decay curves obtained from the CODEX experiments for the methylene group #3 in the side chain. In this case slightly larger value of 0.42 for the asymptotic plateau is achieved at 308K. The small difference can not be automatically related to a change in the topology. For further analysis additional experiments and simulations must be performed. As we mentioned before, for a better understanding of the topology of the exchange process, CODEX experiments in which the recoupling period is arrayed must be performed. Additionally the knowledge of the orientation of the CSA tensors is necessary to be able to perform simulations from which by comparison with the CODEX results information about the topology of the process can be obtained. Before presenting these types of experiments, we have to mention that also for the side chain #3 group, the distribution width is broader than in the form I. Investigations at higher temperatures for the form III

were not performed due to the fact that by heating the sample above 318K, i-P4M1P in form I is obtained.

The correlation times obtained from CODEX experiments for both form I and III are converted to the corresponding maximal frequencies using the formula presented in chapter III. Because similar behavior of the side and main chains were detected for both forms of the polymer we present in figure 4.22 only the Arrhenius plots for the methine groups in the main chain (carbon #2). The plots were used to determine the activation energies of the detected processes. For the main chain of i-P4M1P in form I an activation energy of 95 KJ/mol was obtained while for the sample in the form III a larger activation energy of 210 KJ/mol was calculated.

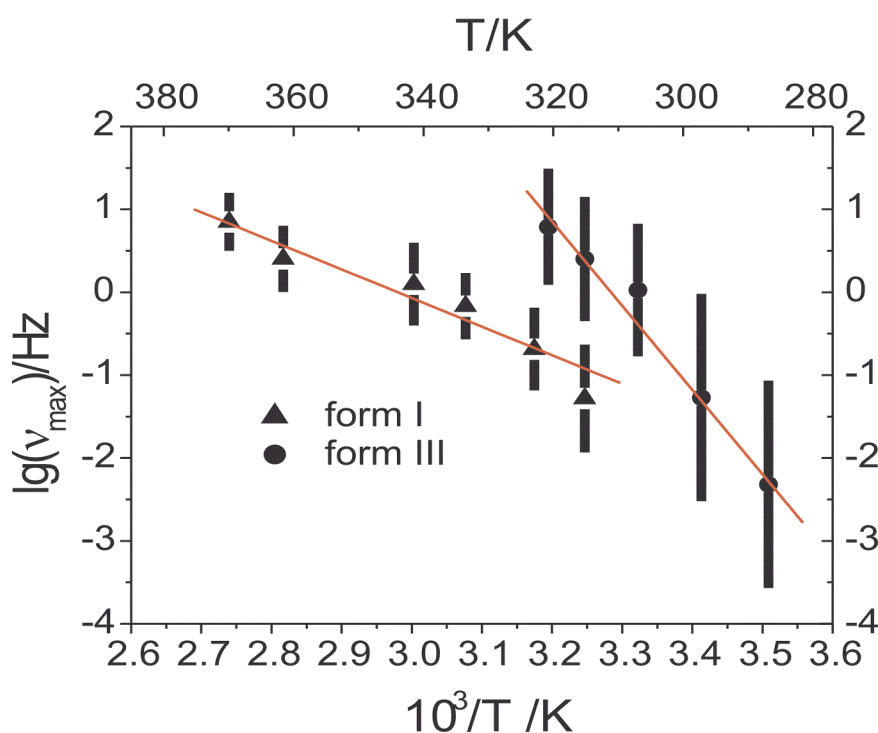


Fig.4.22 Arrhenius diagram of i-P4M1P in form I and III

This difference between E_a values of forms I and III could be related to segmental mobilities in amorphous and interphase regions. It is well known [HWS97, KSR94] that in semicrystalline polymers the chains can extend from crystalline to the amorphous region of the polymer. In this case the motion in the crystalline part will require a certain mobility in the amorphous phase. One may consider that the large amplitude motions in the crystalline phase are highly related to the segmental motions in the amorphous phase, namely helical jumps are allowed when the amorphous phase is very mobile. This would imply that helical jumps are likely to happen only when we are above T_g . However, our results suggest that the large amplitude motion is possible to occur also

below or close to T_g . However, motions in the crystallites below T_g are highly restricted by the immobility of the amorphous regions. Therefore, we attribute the large difference in activation energy between the two forms to the segmental mobilities in the amorphous or interphase regions. The correlation times and their distribution widths for side and main chains of i-P4M1P in form I and III are given in table 1,2 respectively in appendix C.

For further investigations of the topology of the exchange process in i-P4M1P, additional experiments and simulations were performed. We mentioned in the previous chapters that by running CODEX experiments with a recoupling period dependence (NT_R) for a mixing time $\tau_m > \tau_c$ we can obtain informations about the topology of the dynamic processes in polymers. Additionally, if simulations are performed and their results are correlated with those obtained from the exchange experiments a complex overview of the dynamic processes in the investigated polymers can be achieved. Running simulation implies the knowledge of the CSA tensor values and orientations for each functional group in the sample. To obtain these information, besides the already discussed Herzfeld-Berger method [Herzfeld80] several methods are available. In our case we used a new method developed recently by K. Schmidt-Rohr & co. [KSR02]. The method, named SUPER (*separation of powder-patterns by effortless recoupling*) was developed starting from the method created in early 90's by Tycko & co. [Tycko89]. The SUPER has the advantage of being easy to implement for MAS probes able to run at spinning rates between 2.5 and 5 kHz, with a decoupling power up to 80 kHz. For both forms of i-P4M1P SUPER experiments were performed the CSA tensor values are given in table 2 in appendix C.

As we mentioned, besides the values of the CSA tensors also the knowledge of their orientations is required to be able to perform the simulations. In this work we assumed a similar orientation of the CSA tensors to those assumed in [KSR94] for the PE (see fig. 4.23): σ_{11} axis is assigned to the direction parallel to the H-H vector and thus perpendicular to the C-C-C plane, the σ_{22} axis to the direction parallel to the H-C-H angle bisector and σ_{33} to the direction parallel to the molecular chain axis (orthogonal to the H-C-H plane) [Kuwabara00]. We need to recall that the motion in semicrystalline polymers featuring a helical conformation is usually described as a translation motion from one site to its neighbors and at the same time a rotation around the central axis of the helix, as shown schematically in figure 4.23.

The simulations (more properly calculation of the CODEX decays for different recoupling periods) involve the relative orientation change of the CSA tensors in the molecular frame (MF) which here was chosen to be the fixed to the helix axis. Usually to calculate the change of the CSA tensor orientations from the principal axis system (PAS) to the molecular frame (MF), the following formula is used:

$$\sigma^{MF} = R^{-1}(\alpha, \beta, \gamma) \begin{bmatrix} \sigma_x & & \\ & \sigma_y & \\ & & \sigma_z \end{bmatrix} R(\alpha, \beta, \gamma)$$

where the arguments of the rotation matrix $R(\alpha, \beta, \gamma)$ are the Euler angles. (α, β) are the polar coordinates of the rotation axis in PAS, while γ denotes the rotation angle around the molecular axis which in the case of helical jumps in i-P4M1P form I and III can be $n \times 102.8^\circ$ and $n \times 90^\circ$, respectively.

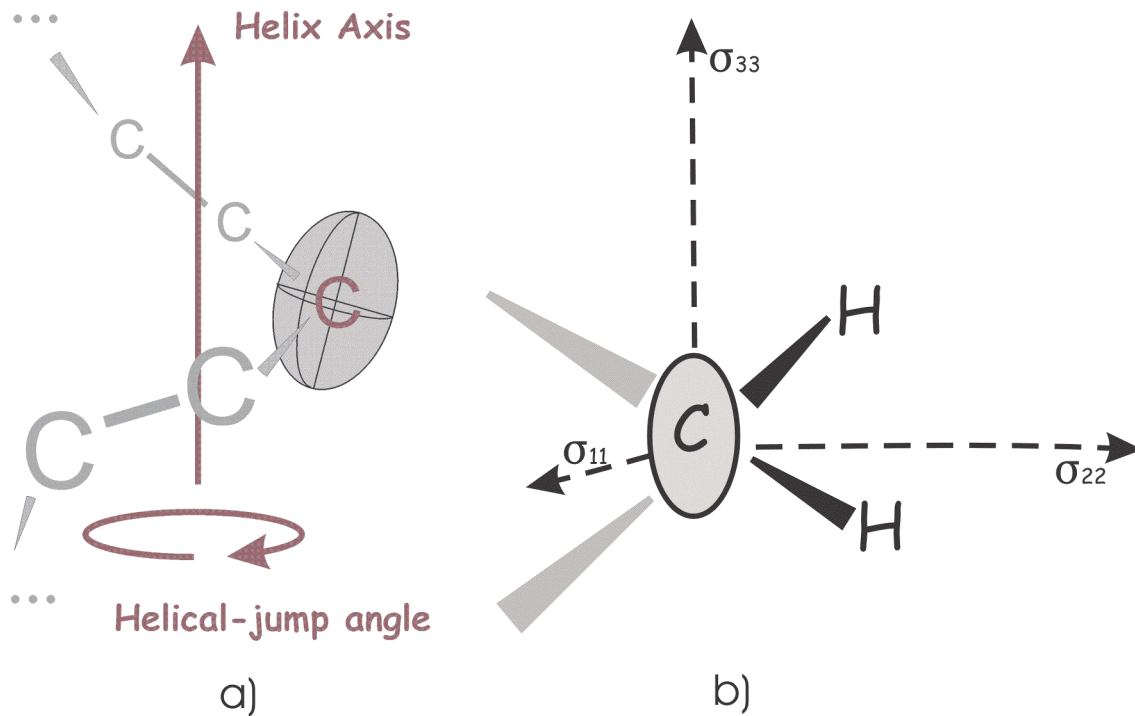


Fig.4.23 a) Typical helical motion in semicrystalline polymers
b) CSA tensor orientations for CH_2 groups

Considering that the PAS is described by the coordinate axis $(X^{PAS}, Y^{PAS}, Z^{PAS})$ and MF by (X^{MF}, Y^{MF}, Z^{MF}) , then the polar coordinates (β, α) describe the orientation of Z^{MF} in PAS, and $(\beta, \pi - \gamma)$ the orientation of Z^{PAS} in the molecular frame (MF) [KSR94]. Data obtained from X-ray investigations [Miyoshi02] were used to obtain the values of the Euler angles α, β, γ . For i-P4M1P in form I, assuming a uniform 7/2 helical configuration these would be $(80.6^\circ, 41.2^\circ)$ with a jump

angle of 102.8° according to the X-ray findings [Kusanasagi78]. Considering the distorted $7/2$ helix and knowing the positions of the atoms from the X-ray data and the assumed orientation of the CSA tensors in MF, angles were calculated for the each jump involving successive sites. In our simulations we assumed, considering also the data from CODEX experiments, that the only possible jumps are to the nearest neighbors. For form I this would mean successive jumps from first site to the second one and so on (1->2, 2->3, 3->4, 4->5, 5->6, 6->7, 7->1) with different jump angles (121.7° , 83.5° , 93.2° , 145.0° , 96.3° , 71.8° , 108.5°) that eventually would account for a 720° rotation around the helix axis. The simulated jumps for all the sites are plotted in figure 4.24.

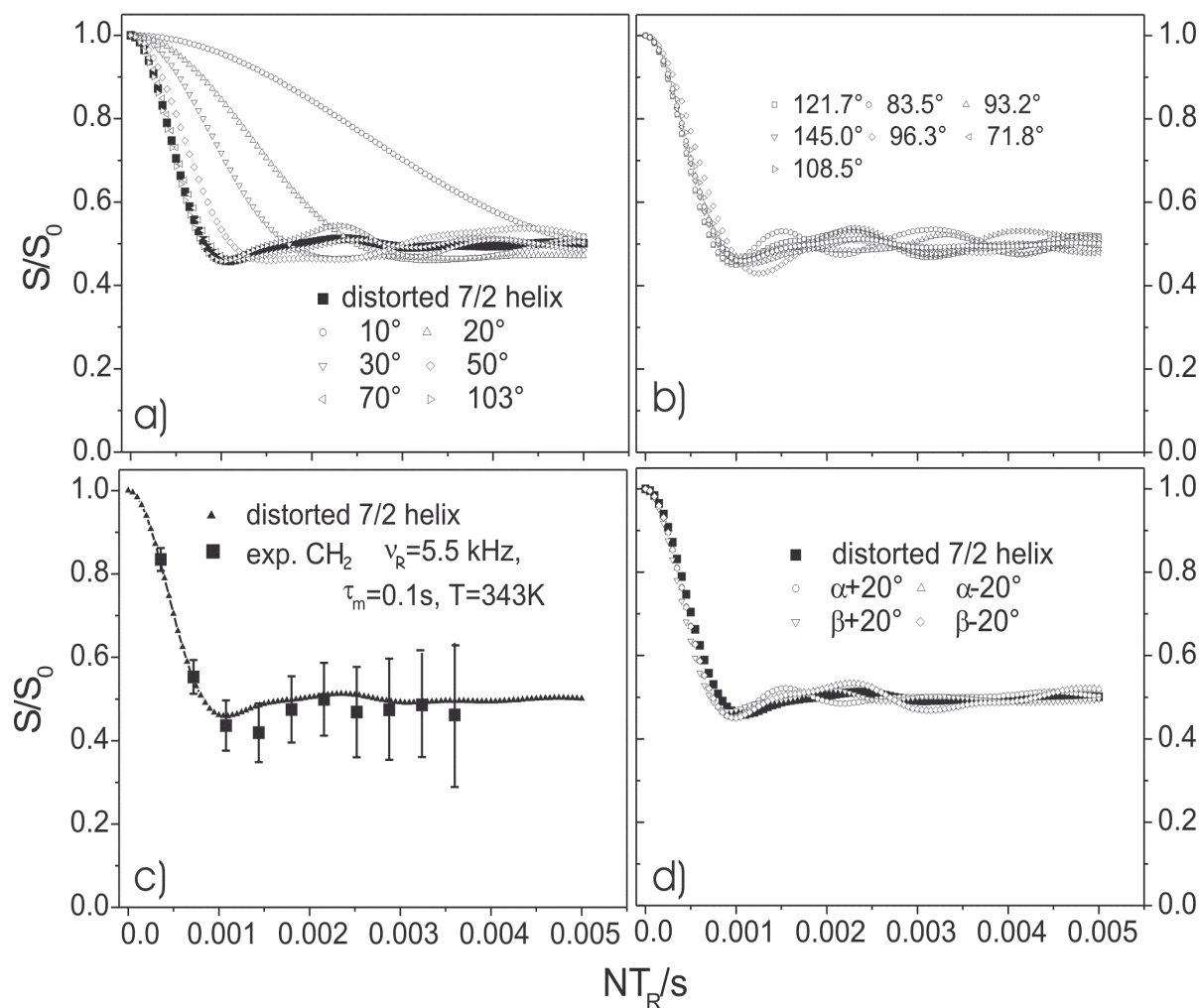


Fig.4.24 Simulated jumps for P4MIP form I

- a) different jump angles and jump for the distorted $7/2$ helix
- b) simulated curves for all possible two-site jumps
- c) experimental points and simulated jump for $7/2$ distorted helix
- d) influence of the deviations of the Euler angles

Figure 4.24b shows the individual two-site jumps possible for a disordered 7/2 helix structure according to the data from the X-ray experiments. The experimental points (fig. 4.24c) were obtained from CODEX NT_R -dependence performed at a spinning rate of 5.5 kHz at 343K and shows the behavior of the main chain #1 group for a mixing time of 0.107 s. It is obvious that the simulated averaged jump for a disordered 7/2 helix describes well the points from the experimental data. For a better understanding of the topology, simulations were performed also to obtain the possible behavior of the CODEX decays for different jump angles. The results obtained are showed in figure 4.24a.

The black squares in the figure 4.24a represents the averaged jump for a disordered 7/2 helix and it is seen that has almost the same behavior like the simulated curve which describes a two-site motion with a 103° jump angle. This would mean that the assumed model of motion in the i-P4M1P form I is in agreement with the expected 102.8° jump angle expected for a uniform 7/2 helical motion. The small differences between the discussed curves are coming from the structural deviations of the polymer from the uniform 7/2 helix structure. In the figure 4.24d it is shown how deviations up to 20° from the assumed value of the Euler angles influences the shape of the decay curves. The black squares line represents the averaged motion for disordered 7/2 helical motion. The results presented here, show that together with the X-ray investigations, NMR exchange methods can offer a detailed view about the dynamic in the i-P4M1P form I featuring a disordered 7/2 helix.

The same procedure was used for further investigate the reorientation motions in form III of the polymer. Considering the uniform 4/1 helical structure [deRosa95] of the i-P4M1P in form III, identical values of the α , β Euler angles (111.6° , 47.8°) were assumed from the X-ray data for all possible sites. First successive jumps from one site to its neighbors (1->2, 2->3, 3->4, 4->1) were assumed which would account for a jump angle of 90° .

The simulated curves features almost the same behavior for all jumps, as expected for a 4/1 uniform helix. The experimental points obtained from CODEX experiments performed at a spinning rate of 5.5 kHz and a mixing time 0.1 s are plotted at the bottom together with the simulated decay curve for the average 90° jump. There is a good agreement of the experimental data with the simulated ones. Also a more complicated motion was assumed, which besides 90° jumps between neighboring sites could involve also jumps with larger angles to different sites. Figure 4.25b shows the simulated curves involving direct jumps from 1-th site to site 1,2,3 and 4. Here it is also evident that despite the fact that the jumps are done with an increased angle the curves show a similar behavior, excepting the 1->1 jump which shows a completely different one. The black points in figure 4.25b represent an averaged motion featuring all possible jumps but considering that only fractions of the total number of spins in site 1 can participate to different jumps (1 for 1->2 jump, 1/2 for 1->3 jump, 1/4 for 1->4 jump and 1/8 to 1->1 jump). We can say that for i-P4M1P in form III the

typical dynamic is a 90° jump between adjacent sites, even that jumps to further sites may also be possible.

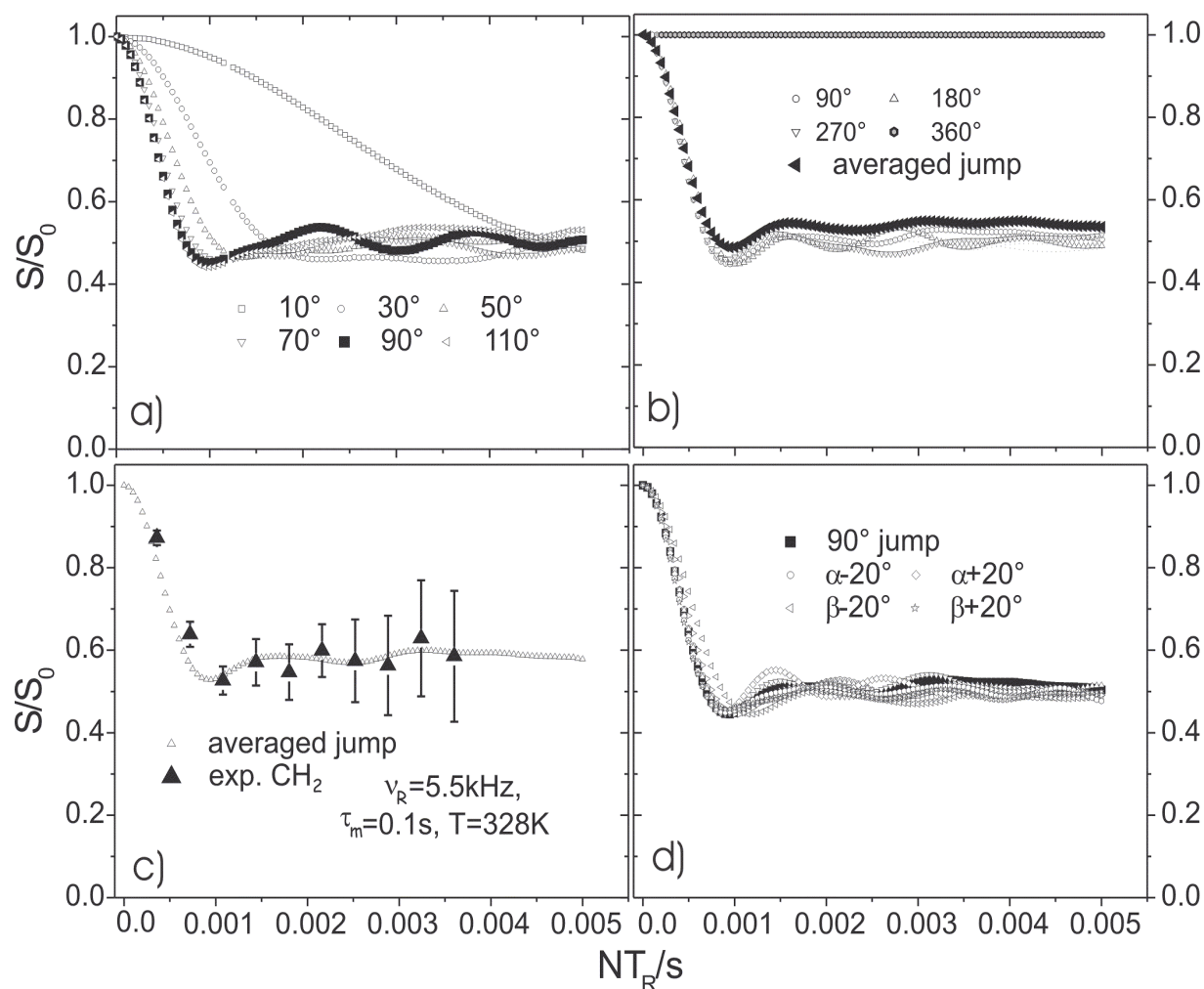


Fig.4.25 Simulated possible jumps and experimental points for *i*-P4M1P form III.

- a) simulated curves for different jumps angles
- b) jumps involving 90° , 180° , 270° and 360° angles together with their average
- c) experimental points and the averaged jump
- d) effect of the deviation from the assumed values of the Euler angles

Like for the *i*-P4M1P in form I simulations regarding jumps with different angles were performed also for the form III. The results are shown in figure 4.25a. The black squares represent a 90° jump between site 1 and 2 (1- \rightarrow 2). It is again obvious that the simulations and the experimental results are in good agreement showing an exchange process involving two-site jumps. Deviations up to 20° from the considered values for the orientation angles were taken into account also for form III, the results obtained from the simulation are presented in the figure 4.25d. They show that

deviations up to 20° of the true CSA tensors orientations from the considered values does not influence too much the behavior of the CODEX decay.

The simulations and the experimental results presented here are in full agreement with the classical image of the motion for a semicrystalline polymer with a helical structure: we speak about a rotation around the helix axis with a $360^\circ n/m$ angle and in the same time a shift by one repeat unit which moves the chain between equivalent positions in the crystallite. We have shown that for i-P4M1P in form I reorientations processes specific to the disordered $7/2$ helix structure are present, their jump angle being close to 103° . For the sample in form III an exchange process with jump angles of 90° was revealed, which comes from the shift of the chains between the adjacent positions in crystallite. The existence of jumps with larger angles than 90° could not be excluded (in this case the asymptotic value for which the plateau is reached in CODEX experiments would be smaller than 0.5), though these involves only fractions of the population spins.

Conclusions

The correlation between the macroscopic properties of the polymers and their relaxation behaviors, and therefore their properties on the molecular level, plays an important role in physics nowadays. In this work were presented several recently developed 1D-MAS NMR exchange experiments which try to answer these questions. During this project, it was demonstrated that exchange NMR experiments are, together with the DSC, dielectric spectroscopy, mechanical relaxation, among the most important methods for obtaining informations about the behavior of polymers close to the glass transition.

Bearing in mind these facts, several 1D-MAS NMR experiments like simple dynamic MAS exchange experiments, ODESSA/trODESSA, PATROS and CODEX were extensively used to characterize the dynamics found in some amorphous polymers from the poly-methacrylates family, and semicrystalline polymers with specific helical structure. In order to obtain the correct informations about the correlation times of the dynamic processes detected, it was shown that corrections of the acquired data by spin diffusion (SD) and T_1 relaxation are necessary. It was known that in non-spinning experiments, spin diffusion is weak due to the different CSA orientations of the interacting spins and the consequently different resonance frequencies. In MAS experiments, however, the resonance frequencies become time dependent and occasionally match each other during the course of a MAS-rotation period, leading in turn to a much enhanced spin diffusion rate. Therefore the spin diffusion correction is a "must" for each spectroscopist which uses NMR MAS exchange experiments to characterize the dynamic processes detected in the investigated sample. It was demonstrated in the course of this project that neglecting the spin diffusion effect, which is present starting with mixing times of several hundreds of ms can change the value of the correlation time with more than an order of magnitude. Also it was shown that by using the so called z -filter in experiments like trODESSA or CODEX the T_1 relaxation correction is done together with an "internal" normalization of the acquired data. However, the additional mixing time which plays the role of a z -filter increases the total length of the pulse sequence and therefore the effect of the T_2 relaxation which is responsible for the reduction of the signal intensity. Moreover, the additional mixing time doubles the acquisition time required to acquire experimental data with a reasonable signal-to-noise ratio. Therefore the experimentalist must take into account the advantages and disadvantages of using an internal T_1 correction and normalization as compared with the external ones. As we observed, sometimes the small intensity of a particular NMR signal makes us to avoid using the z -filter, and

therefore independent experiments must be used to eliminate the T_1 relaxation effect from the exchange decays.

The investigations concerning the dynamics of the amorphous polymers from the methacrylates family in a temperature range close to their glass transition temperature T_g , have revealed that the increasing number of carbons in the alkyl side chains substantially modifies the behavior of the polymers. The assignment of all relaxation processes was done using results from other investigations (dielectric spectroscopy, DSC, HCS, etc.), therefore results obtained from NMR exchange experiments were closely correlated with those from other methods.

Experiments performed on the PnBMA have revealed that the main chain carbons contribute only to the α relaxation. Experimental data fitted with a stretched exponential of KWW type, have provided information about correlation times of the dynamic process and in some cases about the jump angle of the motion. At a closer inspection of the resulting Arrhenius diagrams, one may observe that the wide distribution of correlation times for the main chain span across several frequency decades. At the same time the investigations of the side chains in this polymer show that they contribute at temperatures higher than the glass transition temperature only to α relaxation, while close to T_g , the side chains can participate to both α, β relaxations. By further decreasing the temperature, one observes that the secondary β relaxation is the one who describes the dynamic process from the side chains. Like in the case of the main chains, the detected correlation times have a wide distribution, especially at lower temperatures. A similar behavior was detected also for the dynamic of the COO group, which at higher temperatures can participate to both α, β relaxations, and for temperatures lower than T_g , the only active process remains in our experimental window the Johari-Goldstein type relaxation.

The next question in this investigation was to see how the increase length of the side chain may affect the general behavior of the polymer in an temperature interval close to T_g . Experiments performed on PnHMA, from the same family of methacrylates, have shown that beside the well known effect of shifting the T_g to lower temperatures (“internal softening”), the additional alkyl groups in the side chain change also the behavior of the polymer during a temperature interval close to T_g . CODEX experiments performed on PnHMA, have revealed that the dynamics of the main chains is governed by two processes which can be easily told apart for a specific temperature range. The correlation times of the two detected processes, characterized by a wide distribution, fall exactly on top of the α and β relaxations detected from DK, DSC, and other methods. That in fact means that the dynamics of the main chain in PnHMA, is responsible for both traces in the Arrhenius diagram. The accuracy of the experimental data resulted from CODEX mixing time

dependence experiments, have made possible an adequate fitting procedure which made evident the coexistence of the two exchange processes in the exchange decays. Additional CODEX experiments in which the recoupling period NT_R was varied, have shown that the number of sites or the fraction of the spins who participate in the exchange process changes with the temperature. Considering the results obtained for the COO dynamic in PnBMA, also in PnHMA was expected that the carboxyl group could participate to both relaxation processes. Indeed, the Arrhenius diagram resulted from plotting the correlation times of the detected process in the trODESSA experiments shows a large distribution of correlation times which makes evident the contribution of COO dynamic to both α and β relaxations. As expected, the side chain dynamics is only responsible for the β relaxation. Good agreement between the NMR results and those provided by other methods (DK, DSC, MR, etc.) is observed.

NMR investigations performed on PnBMA and PnHMA have shown that the increased number of carbons in the side chains strongly influences the behavior of the polymer during the glass transition. COO groups in both PnBMA and PnHMA participate to both α and β relaxations; this could be the reason why from the dielectric measurements one may think that the increasing number of alkyl groups in the side chains does not change to much the behavior of the chain. 1D-MAS NMR exchange experiments demonstrate that in reality side chains in the PnBMA participate to both α and β relaxation as the COO groups, while in the PnHMA, functional groups from the side chain contribute only to the secondary β relaxation. Also, a difference in the behavior of these two polymers has been observed also in the main chains. In PnBMA, the main chains participate only to α relaxation while the main chains of the PnHMA show for several temperatures a dynamic that can be described only by two different processes: one which participates to α relaxation and another one which participates only to β relaxation. In the case of the PnHMA a dynamic heterogeneity was found: the side chains have a separate dynamics characterized by changes in the amplitude of the motion which counts for the β relaxation, while the main chains are active in both relaxations.

This work demonstrates that NMR exchange methods are among the few ones which can easily assign different traces of the relaxation processes to different functional groups in polymers. During this project it was remarked that the dynamics of the COO group as resulted from DK and DSC measurements can not be assigned as dynamics of the entire polymer, main and side chain usually having different ways to contribute to the relaxation processes.

In another part of this project the dynamics of semicrystalline polymers like i-P4M1P in forms I and III was investigated. It was demonstrated that using CODEX mixing time dependence experiments, information about the correlation times of the exchange processes in polymers with 7/2 and 4/1 helical structure can be obtained. These correlation times, after plotting in an Arrhenius

diagram, provide us information about the activation energy of helical jump motions in polymers with helical structure. Moreover, the found values for the activation energies, are in agreement with those obtained from other methods. It was found that in both forms I and III of i-P4M1P, the dynamics of the main and side chains is characterized by similar correlation times. That means that as contrary to the amorphous polymers investigated, in the i-P4M1P the side chain is strongly coupled to the main chain. CODEX experiments in which the recoupling period was incremented, together with simulations performed, have provided a detailed overview of the topology (jump angles, number of sites, mobile fractions) of the exchange processes active in i-P4M1P. For accurate simulations of the detected process, a good correlation between NMR and X-ray spectroscopy and other experimental techniques must exist. Information obtained from X-ray spectroscopy proved to be vital in the simulations performed, which together with the experimental results from CODEX measurements have revealed that the form I of i-P4M1P is packed within a $7/2$ helix, as suggested from X-ray data. Additional, from simple CP-MAS experiments it was easy to observe the difference between packing effects and γ -shielding. The simulations for form I of i-P4M1P have demonstrated that variation from the standard torsion angles in a $7/2$ helix structure are possible. Typical averaged jump angle found was to be close to 102° which is expected in a uniform $7/2$ helix. Investigations concerning the dynamics in form III of i-P4M1P have revealed that the main part of the exchange is made by 90° jumps between the equivalent sites of the helix but also jumps with larger angles: 180° , 270° and 360° are possible.

The results presented in the frame of this project, have shown that NMR exchange experiments, especially 1D-MAS techniques, are among the important methods available for study of dynamic in polymers nowadays. Generally, the results provided by NMR methods have proved to be in good agreement and complementary with those obtained from other experimental methods. Sometimes, the slightly different results obtained, originate in different probe mechanism chosen in different methods. We have seen here that it is not correct to assign the dynamic of COO obtained from dielectric spectroscopy to the entire dynamic of the polymers from methacrylate family.

1D-MAS NMR experiments and their complementary simulations can be and have been successfully used to gain informations about the dynamics in various polymers and compounds. These experiments can be used also to study the dynamics in more complicated substances like large biopolymers. Work in this direction is on the way. Due to the fact that the probe in NMR methods is the nuclear spin, actually any substance may be investigated using NMR techniques. Moreover, the easy implementation of the methods described in this work, make the application of 1D-MAS exchange experiments suitable for any sample containing $1/2$ - nuclear spins. 1D-MAS NMR exchange methods described here, can be used on any MAS capable spectrometer without special demands for the hardware.

References:

- [Abragam61] Abragam A., *The principle of nuclear magnetism*, Oxford Univ. Press, Oxford, 1961
- [Adam65] Adam G., Gibbs J.H., *J. Chem. Phys.*, 43, 139 (1965)
- [Antzukin94] Antzukin O. N., Song Z., Feng X., Levitt M.H., *J. Chem. Phys.* 100, 130-140 (1994)
- [Antzukin95] Antzukin O.N., Shekar S.C., Levitt M.H., *J. Magn. Reson.*, A115, 7-19 (1995)
- [Beiner96] Beiner M., Korus J., Lockwenz H., Schröter K., Donth E., *Macromolecules*, 29, 5183-5189 (1996)
- [Beiner99] Beiner M., Schröter K., Hempel E., Reissig S., Donth E., *Macromolecules* 32, 6278-6282 (1999)
- [Beiner01] Beiner M., *Macromolecules Rapid Communication* , 22, 869-895 (2001)
- [Bielecki95] Bielecki A., [D.P. Burum, *J. Magn. Reson.* A116, 215-220 (1995)
- [Bonaga01] Bonagamba T.J., Becker-Guides F., deAzevedo E.R., Schmidt-Rohr K., *J. Polym. Science: Part B: Polym. Phys.*, vol 39, 2445-2453 (2001)
- [Cumbreira93] Cumbreira F.L., Sanchez -BajoF., Guiberteau F., Solier J.D., *J. of Material Science* 28, 5387-5396 (1993)
- [deAzevedo99] deAzevedo E.R., Hu W.-G., Bonagamba T.J., Schmidt-Rohr K., *J. Am. Chem. Soc.* 121, 8411-8412 (1999)
- [deAzevedo00] deAzevedo E.R., Hu W.-G., Bonagamba T.J., Schmidt-Rohr K., *J. Chem. Phys.* 112, 19 (2000)
- [deRosa97] deRosa C., Capitani D., Cosco S., *Macromolecules* 30, 8322-8331 (1997)
- [DeLacroix92] DeLacroix S.F., Titmann J.J., Hagemeyer A., Spiess H.W., *J. Magn. Reson.*, 42, 390-394 (1992)
- [Dixon82] Dixon W.T., *J. Chem. Phys.*, 77, 1800-1809 (1982)
Dixon W.T., Schaefer J, Sefcik M.D., Stejskal E.O., McKay R.A., *J. Magn. Reson.*, 49, 341-345 (1982)
- [Doi88] Doi M., Edwards S.F., *The theory of polymers dynamics*, Oxford Univ. Press 1988
- [Donth92] Donth E.-J., *Relaxation and thermodynamics in polymers*, Akademie Verlag, 1992
- [Donth01] Donth E., Huth H., Beiner M., *J. Phys.:Condens. Matter*, 13, L451-L462 (2001)
- [Ediger96] Ediger M.D., Angell C. A., Nagel S.R., *J. Phys. Chem.*, 100, 13200-13211 (1996)
- [Ernst87] Ernst R.R., Bodenhausen G., Wokaun A., *Principles of Nuclear Magnetic Resonance in One and Two Dimensions*, Oxford Univ. Press, Oxford 1987
- [Favre98] Favre D.E., Schaefer D.J., Chmelka B.F., *J. Magn. Reson.*, 134, 261-279 (1998)
- [Flory88] Flory P.J., *Statistical mechanics of chain molecules*, Oxford Univ. Press 1988

- [Gerar96] Gerardy-Montouillout V., Malveau C., Tekely P., Olender Z., Luz Z., J. Magn. Reson., A123, 7-15 (1996)
- [Guillon89] Guillon T., Schaeffer J., J. Magn. Reson., 81, 196 (1989)
- [Haarer95] Haarer D., Spiess H.W., *Spektroskopie amorpher und kristalliner Festkörper*, Steinkopff/Darmstadt 1995
- [Hagem89] Hagemeyer A., Schmidt-Rofr K., Spiess H.W., Adv. Magn. Reson., 13, 85-130 (1989)
- [Heijboer82] J. Heijboer, M. Pineri. In *Nonmetallic Materials and Composites of Low Temperatures 2*; Hartwig, G., Evans, D., Eds.; Plenum Press: New York, 1982
- [Herzfeld80] J. Herzfeld and A.E. Berger, J. Chem. Phys. 73, 6021-6030 (1980)
- [HWS97] Reddy S., Desai P., Abhiraman A.S., Beckham H.W., Kulik A.S., Spiess H.W., Macromolecules, 30, 3293-3301 (1997)
- [Jeener79] Jeener J., Meier B.H., Bachmann P., Ernst R.R., J. Chem. Phys., 71, 4546-4553 (1979)
- [Johari70] Johari G.P., Goldstein M., J. Chem. Phys., 53, 2372 (1970)
- [Kolbert90] Kolbert A.C., Griffin R.G., J. Chem. Phys., 166, 87-91 (1990)
- [Krush99] Krushelnitsky A., Reichert D., Hempel G., Fedotov V., Schneider H., Yagodina L., Shulga A., J. Magn. Reson., 138, 244-255 (1999)
- [KSR94] Schmidt-Rohr K., Spiess H.W., *Multidimensional solid-state NMR and polymers*, Academic Press 1994
- [KSR99] Hu W.-G., Schmidt-Rohr K., Acta Polymerica, 50, 271-285 (1999)
- [KSR02] Liu S-F., Mao J-D., Schmidt-Rohr K., J. Magn. Reson., 155, 15-28 (2002)
Schmidt-Rohr K., de Azevedo E.R., Bonagamba T.J., Enc. of N. Magn. Reson., vol. 9, 633-642 (2002)
- [Kuebler96] Kuebler S.C., Heuer A., Spiess H.W., Macromolecules, 29, 7089-7096 (1996)
- [Kuebler97] Kuebler S.C., Schaefer D.J., Boeffel C., Pawelzik U., Spiess H.W., Macromolecules, 30, 6597-6609 (1997)
- [Kudlik94] Kudlik A.S., Beckham H.W., Schmidt-Rohr K., Radloff D., Pawelczik U., Boeffel C., Spiess H.W., Macromolecules, 27, 4746-4754 (1994)
- [Kusa78] Kusanasagi H., Takase M., Chatani Y., Tadokoro H., J. Polym. Sci.: Polymer Physics Edition, 16, 131-142 (1978)
- [Kuwabara00] Kuwabara K., Kaji H., Tsuji M., Horii F., Macromolecules, 33, 7093-7100 (2000)
- [Lindsey80] Lindsey C.P., Patterson G.D., J. Chem. Phys., 73(7), 3348-3357 (1980)
- [Lopez92] Lopez L.C., Wilkes G.L., Stricklen P.M., White S.A., J. Macromol. Sci., Rev. Macromol. Chem. Phys., C32, 301 (1992)

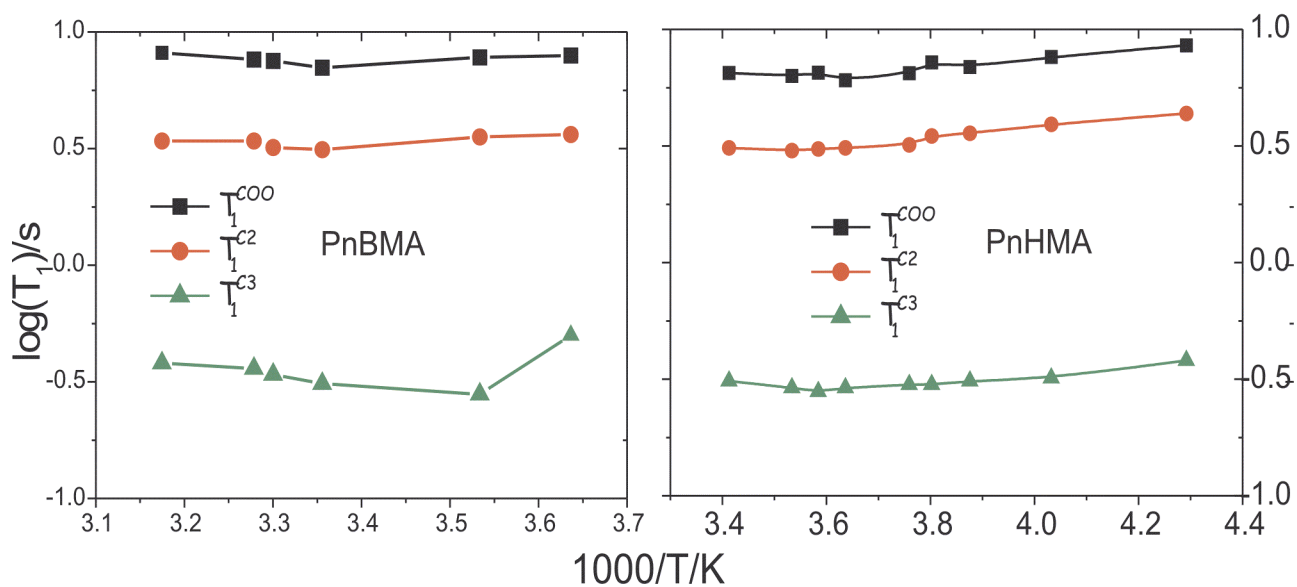
- [Luz92] Luz Z., Poupko R., Alexander S., J. Chem. Phys., 32, 145-160 (1992)
- [Luz02] Luz Z., Tekely P., Reichert D., accepted in Progress in NMR Spectroscopy
- [Mehring76] Mehring M., *High-Resolution NMR in solids*, in NMR Basic Principles and Progress, Vol.11, Springer, Berlin 1976
- [Miyoshi02] Miyoshi T., Hayashi S., Imashiro F., Kaito A., Macromolecules, 35, 2624-2632 (2002)
- [Miyoshi02] Miyoshi T., Pascui O., Reichert D., Macromolecules, 35, 7178-7181 (2002)
- [Munk89] Munk P., *Introduction to macromolecular science*, John Wiley & Sons, Singapore 1989
- [Pines72] Pines A., Gibby M.G., Waugh J.S., J. Chem. Phys., 56, 1776-1777 (1972)
- [Pines73] Pines A., Gibby M.G., Waugh J.S., J. Chem. Phys., 59, 569-590 (1973)
- [Pascui02] Pascui O., Reichert D., Beiner M., accepted in Macromolecules
- [Raleigh88] Raleigh D.P., Olejniczak E.T., Griffin R.G., J. Chem. Phys., 89, 1333-1350 (1988)
- [Reichert97] Reichert D., Zimmermann H., Tekely P., Poupko R., Luz Z., J. Magn. Reson., 125, 245 (1997)
- [Reichert99] Reichert D., Hempel G., Zimmermann H., Tekely P., Poupko R., Luz Z., Favre D.E., Chmelka B.F., Appl. Magn. Reson., 17, 315-327 (1999)
- [Reichert,hab] Reichert D., *Untersuchungen zur molekularen und spin-dynamik in organischen festkörpern mittels 2D- und 1D-MAS-NMR-methoden*, kumulative habilitationsschrift Halle/Saale 1999
- [Reichert00] D. Reichert, G. Hempel, H. Zimmermann, H. Schneider, Z. Luz, Solid State NMR, 18, 17-36 (2000)
- [Reichert00] Reichert D., Hempel G., Luz Z., Tekely P., Schneider H., J. Magn. Reson., 146, 311-320 (2000)
- [Reichert01] Reichert D., Bonagamba T.J., Schmidt-Rohr K., J. Magn. Reson., 150,1 (2001)
- [Reichert02] Reichert D., Pascui O., Beiner M., Macromol. Symp. 184, 175-181 (2002)
- [Takaya67] Takayanagi M., Kawasaki N., J. Macromol. Sci.-Phys. B1, 741 (1967)
- [Torchia78] Torchia D.A., J. Magn. Reson., 30, 613-616 (1978)
- [Torchi82] Torchia A.D., Szabo A., J. Magn. Reson., 49, 107-121 (1982)
- [Tycko92] Tycko R., Dabbagh G., Isr. J. Chem., 32, 179-184 (1992)
- [Suwelack80] Suwelack D., Rothwell W.P., Waugh J.S., S J. Chem. Phys., 73, 2559-2569 (1980)
- [Schmidt86] A. Schmidt, S.O. Smith, D.P. Raleigh, J.E. Roberts, R.G. Griffin and S. Vega, J. Chem. Phys. 85, 4248-4253 (1986)
- [Schwarzl90] Schwarzl F.R., *Polymer-mechanik. Struktur und mechanisches Verhalten von Polymeren.*, Springer-Verlag, 1990

[Schroter98] Schroter K., Unger R., Reissig S., Garwe F., Kahle S., Beiner M., Donth E., *Macromolecules* 31, 8966-8972 (1998)

[Williams66] Williams G., *Trans. Faraday Soc.*2, 1966

Appendix A

Information regarding the T_1 relaxation times for the COO, C2 (main chain) and C3 (side chain) in PnBMA and PnHMA were obtained using the Torchia experiment as described in the reference [Torchia78] for a spinning rate of 2kHz. The experiments were performed on a UNITY spectrometer featuring a resonance frequency of 50 MHz for ^{13}C channel. The results obtained are presented in the following figure.



T_1 relaxation times for COO, C2 and C3 carbons in PnBMA (left) and PnHMA (right)

Appendix B

Table 1. Correlation times and the width of their distribution obtained from the fitting for PnBMA

T/K	τ_c/s				β			
	COO	C2	C3	C4	COO	C2	C3	C4
264			0.160±0.060				0.75±0.17	
275	0.082±0.166				0.46±0.06			
283	0.054±0.004				0.69±0.05			
291	0.048±0.006				0.54±0.06			
293		14.692±7.345	0.081±0.011	0.016±0.02		0.35±0.01	0.45±0.03	0.75±0.08
298	0.127±0.018				0.42±0.04			
303	0.064±0.016	0.673±0.054	0.032±0.002	0.033±0.001	0.28±0.04	0.41±0.01	0.56±0.04	0.54±0.04
310	0.037±0.009	0.136±0.008	0.015±0.001		0.260.04±	0.48±0.02	0.68±0.06	
315	0.023±0.007	0.095±0.010	0.010±0.001	0.013±0.001	0.35±0.05	0.52±0.02	0.72±0.05	0.67±0.05
325		0.032±0.002		0.008±0.0009		0.59±0.03		0.67±0.06
333		0.009±0.0004		0.004±0.0005		0.77±0.03		0.85±0.15

Table 2. Correlation times and distribution width of the exchange process detected in PnHMA

T/K	COO		C2		C3	
	τ_c/s	β	τ_c/s	β	τ_c^*/s	β^*
253			68.78±21.53	0.37±0.13		
258	0.064±0.013	0.43±0.07				0.102±0.052
263	0.117±0.029	0.57±0.12	6.8±1.35	0.73±0.08	0.051±0.005	0.67±0.03
266	0.13±0.017	0.41±0.03				
273			1.3±0.050	0.59±0.02	0.033±0.002	0.78±0.03
275	0.088±0.008	0.41±0.02				
279	0.052±0.006	0.36±0.03				
283	0.023±0.002	0.36±0.02	0.271±0.005	0.64±0.02	0.015±0.001	0.87±0.05
286			0.112±0.003	0.68±0.03	0.009±0.001	0.96±0.06
293	0.004±0.001	0.52±0.10				

Appendix C

Table 1. Correlation times and their distribution width for the exchange processes detected in form I of i-P4M1P.

T/K	C1		C2		C3	
	τ_C/s	β	τ_C/s	β	τ_C/s	β
293	10.18±3.723	0.57±0.09	12.324±4.854	0.46±0.07		
308	1.372±0.289	0.65±0.03	1.242±0.168	0.64±0.02	1.572±0.578	0.51±0.04
315	0.399±0.044	0.67±0.03	0.350±0.031	0.70±0.02	0.556±0.044	0.58±0.03
325	0.168±0.014	0.72±0.02	0.180±0.008	0.74±0.02	0.146±0.014	0.68±0.03
333	0.112±0.010	0.70±0.04	0.106±0.007	0.70±0.03	0.090±0.004	0.72±0.02
355	0.058±0.004	0.69±0.03	0.054±0.006	0.74±0.05	0.048±0.005	0.72±0.04
365	0.015±0.003	0.90±0.11	0.019±0.003	0.80±0.14	0.017±0.001	0.81±0.07

Table 2. Correlation times and their distribution width for form III of i-P4M1P.

T/K	C1		C2		C3	
	τ_C/s	β	τ_C/s	β	τ_C/s	β
285			23.734±7.911	0.40±0.08	21.68±13.040	0.40±0.08
293	4.729±1.543	0.36±0.04	2.069±0.237	0.40±0.02	1.768±0.183	0.44±0.02
301	0.166±0.018	0.50±0.03	0.112±0.006	0.52±0.01	0.142±0.055	0.47±0.05
308	0.043±0.006	0.59±0.05	0.048±0.006	0.55±0.03	0.057±0.009	0.51±0.03
313	0.021±0.002	0.66±0.06	0.020±0.002	0.58±0.04	0.036±0.005	0.58±0.04

Table 3. CSA tensors for i-P4M1P in form I and III, as obtained from the SUPER experiments. The estimated error is ±3 ppm

	form I				form III			
	C1	C2	C3	C6	C1	C2	C3	C6
σ_{11}/ppm	63	43	65	34	63	43	68	34.8
σ_{22}/ppm	40	27	49	35	43	33	48	25.8
σ_{33}/ppm	22	17	23	6	21	22	24	4.8

Zusammenfassung

Die Untersuchung von Struktur (Orientierungen, molekulare Abstände) und Dynamik (molekulare Beweglichkeiten) in organischen Festkörpern und Polymeren ist ein Beitrag zum grundsätzlichen Verständnis molekularer Prozesse und zur Korrelation mit makroskopischen Eigenschaften und Funktionalitäten. Während in der Vergangenheit meistens die Struktur untersucht wurde, steht jetzt die Dynamik in Mittelpunkt. Von besonderem Interesse sind langsame Prozesse, die für die makroskopische Anwendungseigenschaften der Stoffe von Bedeutung sind.

Geeignete experimentelle Methoden zur Untersuchung dieser langsamen Bewegungen sind die Methoden der dielektrischen (DR) und mechanischen Relaxation (MR) sowie neu entwickelte Methoden wie der Wärmekapazitätsspektroskopie (WKS). Alle diese Methoden liefern aber keine detaillierten molekularen Informationen, weil die Ankopplung der äußeren mechanischen Beanspruchung bei der MR und der Wärme wellen bei der WKS an die molekulare Struktur nicht völlig verstanden ist. Die dielektrische Relaxation beobachtet die Reaktion eines molekularen elektrischen Dipolmomentes auf ein angelegtes elektrisches Wechselfeld. Weil dieses elektrische Dipolmoment eine bestimmte Position in Molekül hat, liefern die erhaltenen Daten weitestgehend nur Informationen über diesen Teil des Moleküls. Die DR Methode ist anwendbar nur für Stoffe, die ein elektrisches Dipolmoment besetzen.

Im Gegensatz dazu bietet die NMR die Möglichkeit, detaillierte Aussagen zu verschiedenen molekularen Strukturen zu machen. Das geschieht durch selektive Isotopenanreicherung von Atomen mit geringer natürlicher Isotopenhäufigkeit oder durch die intrinsische spektrale Selektivität der NMR Spektren (MAS-Spektren). Die vorliegende Arbeit beinhaltet die Darstellung von MAS Methoden, welche die Detektion von dynamischen Prozessen durch die Modulation der anisotropen chemischen Verschiebung ermöglichen. Einige relativ neu entwickelte 1D-MAS Methoden wie trODESSA (time-reversed One Dimensional Spectroscopy by Spinning Sidebands Alternation) und CODEX (Centerband Only Detection of Exchange) sind hier detailliert zusammen mit ihren Aussagemöglichkeiten dargestellt. Diese 1D-MAS Methoden liefern Informationen über die Struktur und Dynamik der verschiedenen Gruppen in amorphen Polymeren (Poly(n-alkyl Methakrylaten)) und teilkristallinen Polymeren (Poly-4-methyl-1-pentene).

Die Untersuchungen an PnBMA (Poly-n Butylmethakrylat) haben gezeigt, daß die Hauptkette nur an die α Relaxation teilnimmt. Die Anpassung der experimentellen Daten liefert Informationen über die Korrelationszeiten des dynamischen Prozess und im beschränkten Maße auch über die Topologie der molekularen Prozesse. Die erhaltenen Korrelationszeiten werden zusammen mit den Daten

von DR, MR, WKS im Arrhenius Diagramm diskutiert. Man erkennt daß, die Korrelationszeiten der Hauptkette über einige Frequenzdekaden verteilt sind. Die Korrelationszeiten der Seitenkette haben gezeigt, daß diese für $T > T_g$ nur an der α Relaxation beteiligt ist, während sie für Temperaturen in der Nähe von T_g sowohl zur β als auch zur β Relaxationen beiträgt. Für tiefere Temperaturen bleibt die Johari-Goldstein Relaxation der einzige aktive Prozess. Die Untersuchungen an die COO Gruppe in PnBMA zeigen, daß diese für $T > T_g$ an beide Prozessen beteiligt ist bzw. für tiefere Temperaturen nur an der β Relaxation.

Es wurde gezeigt, daß eine verlängerte Seitenkette (Poly-n Hexamethylmethakrylat, PnHMA) eine wichtige Rolle für das dynamische Verhalten des Polymer spielt. CODEX Experimente beweisen daß, die Hauptkette hier an zwei molekularen Prozessen beteiligt ist (Relaxationen). Auch in diesem Fall ist eine breite Verteilung der Korrelationszeiten vorhanden. Die experimentelle Daten wurden im Fall der Hauptkette mit einer zwei komponentigen Kohlrausch-William-Watson (KWW) Funktion angepaßt.

In PnHMA die Seitenkette nimmt, wie erwartet, nur an der β Relaxation teil. Die COO Gruppe zeigt fast dieselbe Tendenz wie für PnBMA: für tieferen Temperaturen die β Relaxation, dann beides (α und β) und für höhere Temperaturen nur die $\{\alpha_a\}$ Relaxation. Alle NMR Resultaten zeigen eine gute Korrelation mit denen von DR, MR, WKS. Diese Arbeit zeigt, daß die Dynamik des elektrische Dipolmoment (hier die COO Gruppe) nicht auf das ganze Molekül übertragen werden kann.

1D-MAS NMR Methoden (CODEX) zeigen, daß im Fall des teilkristallinen Polymeres P4M1P in Kristallstruktur Form I eine gestörte $7/2$ Helix Struktur vorhanden ist, wie aus Röntgen Daten vermutet wird. In Form III kristallisiert dieses Polymer als $4/1$ Helix Struktur. Die Korrelationszeiten zeigen, daß Haupt- und Seitenkette dieselbe Dynamik haben. Aktivationsenergien von 95 KJ/Mol für Form I und 210KJ/Mol für Form III ergeben sich aus dem Arrhenius Diagramm. Die E_a Differenz wird als Einfluß den amorphen Bereiche diskutiert. Die Simulationen den NMR Daten zeigen, daß für Form III des P4M1P, eine Dynamik mit einem 90° Sprungwinkel vorhanden ist, obwohl auch Bewegungen mit Sprungwinkeln von 180° , 270° und 360° möglich sind. Für Form I besteht die Dynamik aus Sprüngen von ein "Site" zum Nachbarn mit verschiedenen Winkeln, die eine gestörte $7/2$ Helix beweisen.

Diese Arbeit zeigt, daß die 1D-MAS NMR Methoden für die Untersuchung von langsame Dynamik in Polymeren geeignet sind. Die Methoden sind auch für andere Substanzen wie Biopolymere (Proteine, etc.) anwendbar.

Lebenslauf

Angaben zur Person

Name, Vorname: Pascui, Ovidiu Florin
Akad. Grad: M. Sc.
Geburtsdatum: 29.8.1976
Geburtsort: Oradea, Rumänien
Nationalität: Rumäner
Wohnort: 06108 Halle/Saale, Leitergasse 5
Familienstand: verheiratet

Schulischer Bildungsgang

1982-1990: Scoala Generala, Alesd
1990-1994: Liceul Teoretic Alexandru Roman, Alesd
1994: Abitur

Universitärer Bildungsgang

1994-1998: Physikstudium, Babes-Bolyai Universität Cluj-Napoca, Rumänien
1998: Diplomarbeit, Prof. V. Znamirovski, zum Thema:
Absorption of uranium in green algae, in different conditions of magnetic fields
1998-1999: Magister, Babes-Bolyai University of Cluj-Napoca, Rumänien
1999: Dissertation, Prof. A. Briguet, Universite Claude-Bernard Lyon1, Frankreich
zum Thema: *L'imagerie MRI dans les milieux quasi-solides*
Seit 1999: BAT O/IIa 1/2 Stelle, FB Physik, Prof. H. Schneider Martin-Luther
Universität Halle-Wittenberg

Erklärung

Hiermit erkläre ich an Eides statt, daß ich die vorliegende Arbeit selbständig und ohne fremde Hilfe verfaßt und nur die angegebenen Quellen und Hilfsmittel verwendet habe. Ergebnisse aus anderen wissenschaftlichen Arbeiten wurden als solche gekennzeichnet. Diese Arbeit wurde bisher weder im In- noch im Ausland in gleicher oder ähnlicher Form in einem Prüfungsverfahren vorgelegt.

Halle, im Dezember 2002

Aknowledgement

This work was supported by the Deutsche Forschungsgemeinschaft **DFG** in the framework of the Sonderforschungsbereich **SFB 418**. The following persons, to whom I would like to thank were directly or indirectly involved in this project.

First, I would like to thank Prof. Schneider who accepted me in his group (in Martin Luther University) making possible the realization of this project.

A big, special THANK YOU goes to Detlef, who was my direct supervisor during these years. He managed to transfer his dedication and interest on this project to me, on very short time, transforming my work on 1D-MAS NMR exchange methods on a permanent challenge.

I would also like to thank :

Heike, Manfred and Günther who were always ready to help me and to make sure that my stay in Halle is a pleasant one. Bike tours, trekking and barbecue-parties were always a welcomed change.

Alexey, for fruitful discussions about slow dynamics problems.

Miyoshi-san for his help in running experiments on the i-P4M1P sample and for putting at my disposal his simulations results on this sample; I hope we can continue this collaboration also in the future.

Mario for his help for the understanding of the complicated processes in glass transition region in polymers and his special contributions to this project.

Karin, for making Halle my second home and for help related to the extraprofessional problems.

Andrea for a pleasant atmosphere in the office, her help with the German-language related parts. Also for granting me with unrestricted access to her goodies.

Maxim for interesting discussions about computers, books and SF movies and beers.

Finally, I would like to thank my wife, for her support during this time and for her understanding (especially related to the fact that sometimes week-end means more work to do and less free time and relaxing).

LONG LIVE LINUX!

